Doctoral theses at NTNU, 2024:261

Nitesh Godara

Hydrodynamic rainfall-runoff modelling for flash floods in small and steep catchments

Doctoral thesis

NTNU
Norwegian University of Science and Technology
Thesis for the Degree of Philosophiae Doctor
Faculty of Engineering
Department of Civil and Environmental Engineering

NTNU
Norwegian University of Science and Technology

Nitesh Godara

Hydrodynamic rainfall-runoff modelling for flash floods in small and steep catchments

Thesis for the Degree of Philosophiae Doctor

Trondheim, June 2024

Norwegian University of Science and Technology
Faculty of Engineering
Department of Civil and Environmental Engineering

NTNU
Norwegian University of
Science and Technology

NTNU
Norwegian University of Science and Technology

Thesis for the Degree of Philosophiae Doctor

Faculty of Engineering
Department of Civil and Environmental Engineering

ISBN 978-82-326-8114-3 (printed ver.)
ISBN 978-82-326-8113-6 (electronic ver.)
ISSN 1503-8181 (printed ver.)
ISSN 2703-8084 (online ver.)

Doctoral theses at NTNU, 2024:261

Printed by NTNU Grafisk senter

Preface

This PhD thesis has been submitted to the Norwegian University of Science and Technology (NTNU) as a part of partial fulfillment of the requirements for the degree of Philosophiae Doctor (PhD). The research work was conducted within the Department of Civil and Environmental Engineering, Faculty of Engineering, under the guidance of Professor Oddbjørn Bruland as the main supervisor and Professor Knut Tore Alfredsen as the co-supervisor. This thesis is written as a part of the project World of Wild Waters (WoWW), project number 949203100, which falls under the umbrella of NTNU's Digital Transformation initiative.

This dissertation is the outcome of a four-year PhD program, presented as a compilation of three research articles published in international journals. The main text, spanning 44 pages, outlines the main methods, results, discussions, and conclusions related to the topic, establishing a coherent link and storyline among the published articles. The first article titled "Simulation of flash flood peaks in a small and steep catchment using rain-on-grid technique" is published in the Journal of Flood Risk Management. The second article titled "Modelling Flash Floods Driven by Rain-on-Snow Events Using Rain-on-Grid Technique in the Hydrodynamic Model TELEMAC-2D" is published in Water. The third and last article titled "Comparison of two hydrodynamic models for their rain-on-grid technique to simulate flash floods in steep catchment" is published in Frontiers in Water. The individual articles are included in the appendices.

In presenting this work, I aspire to add a meaningful voice to academic discourse and provide a resource for those engaged in similar pursuits. This thesis is not merely a compilation of findings; it is a testament to the collective wisdom of scholars, mentors, and experiences that have shaped my academic journey. This PhD journey has taught me valuable lessons both professionally and personally.

I worked with unfamiliar codes and programming languages such as R, Python, Fortran, computer software and models, such as Bluekenue, Telemac-2D, Linux etc. I also gained more experience with programs that I was already familiar with.

Throughout my doctoral journey, I came to understand that facing challenges is inherent to the process, and it's crucial to acknowledge and celebrate even the smallest victories to maintain a sense of balance amidst the demanding nature of completing a PhD. Through my thesis work, I also discovered that it is important to interact and brainstorm with others to accomplish any professional task. Participating in discussions that arise from diverse opinions or approaches,and constructive criticism can be both time consuming and challenging to manage. But I firmly believe that such interactions have not only helped me avoid errors but have also contributed to enhance clarity in my work. Therefore, this preface is a humble expression of gratitude to all those who have played a part in shaping this work and enriching my academic journey.

Acknowledgments

I would like to express my deepest gratitude to my supervisors, Professor Oddbjørn Bruland and Professor Knut Tore Alfredsen, for their unwavering support, invaluable guidance and constructive feedback throughout the entire journey of my PhD. I particularly appreciate their encouragement and belief in me, which served as a constant source of motivation throughout my PhD journey. Their mentorship has been instrumental in shaping both the direction and quality of this research.

I am also thankful to the Department of Civil and Environmental Engineering at NTNU for creating the supportive academic atmosphere that was crucial for the successful completion of my doctoral studies. The resources and facilities made available here have been integral to the accomplishment of this research and my contribution to the Digital Transformation's WoWW project. I extend my heartfelt gratitude to my six fellow PhDs in the same project —Michal, Adina, Gebray, Shafaq, Amanda, and Silius— for being alongside throughout our doctoral journeys. Their presence made me feel supported and understood during the challenges of PhD life. Our regular meetings and collaborative brainstorming sessions were invaluable in navigating the complexities of our project.

My sincere thanks go to my colleagues and fellow researchers in Vassbygget who have contributed to stimulating discussions and provided a collaborative atmosphere that has enhanced the overall research experience. I am deeply grateful to my office mates, whose camaraderie and lightheartedness created an enjoyable atmosphere that motivated me to come to the office every day. Special thanks to my table tennis fellows for our unwavering and sometimes mean but fun sessions at 16:00 every single day, which provided not only a break but also a much-needed dose of fun physical exercise. I extend my appreciation to these colleagues with whom I also shared many enriching lunchtime discussions. These

conversations, spanning a wide range of topics, allowed me to delve into different cultures, mindsets, and opinions, thereby broadening my understanding and knowledge in various domains. I would like to express my heartfelt gratitude to each one of these individuals (listed in alphabetical order): Ana, Behnam, Bulat, Elhadi, Kevin, Mahdi, Mahmoud, Maren, Michal, Mulibirhan, Nils, Prasanna, Raffa, Rizza, Shams, Spyros, Subhojit, Theo, Thea, and Vincent. Your friendship, support, and shared experiences have enriched my academic journey in countless ways, and I am truly fortunate to have had you as my colleagues during this PhD.

I am deeply grateful to my family and friends for their enduring encouragement, understanding, and patience throughout this challenging yet rewarding academic journey. Their support has been my pillar of strength, sustaining me through the highs and lows. I want to acknowledge my niece Raavi, whose boundless energy and infectious joy brought light to even the most stressful days of the doctoral life.

Lastly, I want to express my gratitude to all those who, in one way or another, have been part of this academic journey. Your support, whether big or small, has played a crucial role in the completion of this PhD thesis.

Nitesh Godara

Abstract

Global warming and climate change lead to more frequent and extreme weather events. These include sudden and intense rainfall and rising temperatures which cause flash floods. In steep terrains, flash floods with high-flow velocities lead to erosion and sedimentation with potential disastrous changes of flood path. Flash floods caused by heavy rainfall with snowmelt contribution due to sudden rise in temperature (rain-on-snow events) have become common in autumn and winter in snow-covered Nordic catchments. These events have caused widespread damage, closure of roads and bridges and landslides leading to evacuations in affected areas. Therefore, the analysis of such flood types becomes more important in terms of inundation area, water depths and flow-velocities to identify critical locations in a catchment.

Hydrological and hydraulic models are usually used to simulate flash floods. But most of the traditional hydrological models only give output as a hydrograph but do not represent the consequences such as velocity, water depth, sheer stress etc. at any point or region in the catchment. So, the flood hydrograph from a traditional hydrologic model must be combined with a hydraulic model for downstream consequences. In the traditional method of manual coupling, the output from the hydrologic model is used as input and set as input boundary condition in the hydraulic models. This method of manual coupling requires the separate calibration of two models which makes it a time-consuming process. Sometimes due to many tributaries, more than one boundary condition is required and it is difficult to decide where to set the input boundary conditions in the hydraulic model. In addition to this, there is always some residual flow along the river from the catchment or the water from small tributaries, which is difficult to estimate and add in the hydraulic model calculations. In small and steep catchments, the inflow contribution from every section of the water course can be important to determine where critical

conditions may arise.

To overcome these challenges and the hassle of manual coupling of the two models, the direct rainfall method (DRM) also known as rain-on-grid (RoG) technique was tested in this research work. Primarily, TELEMAC-2D, a Hydrodynamic Rainfall-Runoff (HDRR) model, with Curve Number (CN) infiltration method, was used for this purpose in a study site of 10.5 km^2 steep catchment located in western Norway. Spatially distributed precipitation data with a resolution of 1km by 1km was used as input instead of point precipitation data to reduce the uncertainties related to precipitation distribution over the catchment. Since TELEMAC-2D is an open source toolbox, it was possible to make changes in the source code ourselves and implement spatially distributed precipitation as input.

Since TELEMAC-2D doesn't have a snow routine, initially only those peak flow events were simulated which were induced by rainfall without any contribution from snowmelt. Seven such events were simulated and a sensitivity analysis was conducted for the parameters such as the CN values, size of mesh elements, roughness and antecedent moisture conditions (AMC) in the catchment. In addition, a 200-year design flood was simulated to show the potential damages in the catchment. The study explored the benefits and limitations of the approach through a comprehensive description of model construction, calibration, and sensitivity analysis. The results showed that calibrated models can satisfactorily reproduce peak flows and produce relevant information about water velocities and inundation. Since, floods can reach even more extreme levels when snowmelt combines with the surface runoff generated by rainfall events. When rain falls on an existing snowpack in addition to the sudden increase in temperature, it is known as a rain-on-snow (RoS) event. These events can result into destructive flash floods due to the sudden melting of snow combined with the extreme rainfall.

Hence, in the next part of the thesis work, the contribution and effect of snowmelt in flash floods were analysed. The hydrological model HBV was used to find out the portions of snow and rain from the raw precipitation data and to calculate the snowmelt. The sum of snowmelt and rain calculated from HBV, which eventually contributes to flash floods, was used as the input precipitation in TELEMAC-2D for HDRR modelling. The results showed the importance of including snowmelt for distributed runoff generation and how the combination of hydrological and hydraulic models allows to extract flow hydrographs anywhere in the catchment. It is also possible to extract the flow velocities and water depth at each time-step showing the critical points in the catchment in terms of flooding. The RoG technique works particularly good for single peak events, but not for floods with long-duration sustained flow and which are generated by multiple rainfall storms. The results indicated a need for implementation of time-varying CN values or another

infiltration model with a time-varying infiltration rate for such multi-storm floods.

Therefore, another HDRR model HEC-RAS 2D with the Green-Ampt Redistribution (GAR) infiltration method was tested and compared with TELEMAC-2D for its RoG technique. CN method was applied in both the models to simulate two single storm events up to 20 hours duration. NSE and R^2 for the models ranged from 0.70 to 0.90 and from 0.93 to 0.95. Moreover, the two models were compared for the calibration process, computational time, mesh size and shape, model availability in general, as well as for the results including inundated areas, water depths and velocity of water after a flood event. In addition, The GAR method was applied in HEC-RAS 2D for a multi-peak flood event with sustained flow between the peaks, but the results showed that even this method was unable to reproduce all the peaks of the flood event. Therefore a sensitivity analysis of the GAR parameters was done to understand why GAR method could not reproduce the multi-storm flood. The sensitivity analysis showed that the results are not very sensitive to the two GAR parameters which are responsible to influence the flow of the later peaks.

Neither of the HDRR models could reproduce such multi-storm long duration floods because of the fact that both the HDRR models permanently lose the infiltrated water out of the model domain which usually contribute as the return flow to the river which is mainly the reason for the sustained flow between the multiple storms and for a gradual recession limb of a flow hydrograph. However, neither of the models incorporate a return flow algorithm. Hence, the HDRR models should only be used if it is sure that the infiltrated water goes to the deep base flow where there is no chance of subsurface return flow, or they should be used only for short-duration single storm floods.

Potential follow up to this research work can be to implement a subsurface flow module or the contribution of return flow in the fully integrated hydrologic- hydrodynamic RoG models. This enhancement would enable these models to effectively handle both short and long duration floods. Moreover, a snow routine can also be implemented in the HDRR models which eliminates the need of a separate model to calculate snow storage and snowmelt in the catchment.

Contents

List of Tables

List of Figures

Abbreviations

List of the abbreviations in alphabetic order:

- **AMC**- Antecedent moisture conditions
- **CN**- Curve Number
- **DRM**- Direct Rainfall Method
- **DTM**- Digital Terrain Model
- **GA**- Green-Ampt
- **GAR**- Green-Ampt Redistribution
- **HDRRM**- Hydrodynamic Rainfall- Runoff Model/Modelling
- **HR2D**- HEC-RAS 2D
- **NSE**- Nash–Sutcliffe Efficiency
- **RoG**- Rain-on-Grid
- **RoS**- Rain-on-Snow
- **T2D**- TELEMAC-2D

Chapter 1

Introduction

1.1 Background

The occurrence of natural hazards and extreme events is on the rise worldwide, which can be attributed to factors such as changing weather patterns and climate conditions, urbanization, land use, and infrastructure development. Examples of such extreme events include temperature and precipitation extremes, flash floods, droughts, floods, and landslides (Seneviratne et al. 2021). These events are expected to increase in future causing even more fatalities, economic and environmental losses (Modrick and Georgakakos 2015; Zhang et al. 2021).

From 2008 to 2017, floods have killed approximately 5,000 people per year on average and continue to be the most frequent and destructive calamity in the world (CRED 2022b). A publication by the UN Economic and Social Commission for Asia and the Pacific (ESCAP 2023) indicates that in 2022, floods emerged as the deadliest natural disaster, comprising 74.4% of disaster events in the region and accounting for 88.4% of total fatalities worldwide. The Central European floods and subsequent landslides in July 2022 were one of the most expensive disasters, costing the German economy 40 billion US dollars (CRED 2022a). Furthermore, natural disasters are expected to increase the reported direct losses from the current $195 billion to $234 billion a year by 2040 (Barattieri et al. 2023).

Vormoor et al. (2015) studied flood trends in 211 norwegian catchments for periods from 1962- to 2012, 1972 to 2012, and 198 to 2012. They found a 20% to 40% increase in design flood estimates for rivers impacted by rain floods and smaller rivers responding quickly to heavy rainfall events. This implies a corresponding increase in estimated design flood discharge. One of the examples of flash floods,

generated by heavy rainfall in a small catchment, is the flash flood in village Utvik in July 2017 (Bruland 2020), which is explored in detail in the next section, also explaining how this flash flood event is related to this doctoral study.

Flash floods don't usually come alone. They lead to bedrock erosion (Swanston 1974) due to high stream power and shear stresses, sediment deposition (Johnson et al. 2010), and debris flow (Sandersen et al. 1997). Unusual heavy rain and flash flood events can cause debris slides and landslide events in wet periods. Whereas, in dry periods, snowmelt at higher altitudes that infiltrates the ground can lead to landslides, especially along steep and small rivers (Heyerdahl and Høydal 2017). Due to the large volume and velocity of debris flow, it can result in severe social and economic losses, and sometimes may lead to fatalities. The magnitude of floods can reach an even more extreme level when the snowmelt adds to the surface runoff generated by rainfall events. When it starts to rain on an existing snowpack due to a sudden increase in air temperature, it is called a rain-on-snow (RoS) event (Pall et al. 2019). Such events can usually result in destructive flash floods because of the sudden melting of the snow in combination to the extreme rainfall.

An increase in the frequency and intensity of strong precipitation events has been observed in Norway since 1957 (Dyrrdal et al. 2012). Surfleet and Tullos (2013) have indicated a decreased frequency of high flow RoS in low and middle altitudes while increased frequency of the same in high altitudes due to increasing temperatures. The number of days with heavy rainfall and the intensity of rainfall during these days are likely to increase in the future especially in the winter season, leading to more RoS events (Dyrrdal et al. 2012) by the end of this century (Hanssen-Bauer et al. 2017). According to Roald (2019), early autumn snowfalls are a frequent occurrence in Vestlandet (West Norway), followed by rapidly rising temperatures and intense snowmelt. This phenomenon is commonly observed in rivers in coastal areas in western and central Norway.

1.2 Flash flood in Utvik

Utvik is a small village in Vestlandet county in the western part of Norway that has around 400 inhabitants. The Storelva River, whose origin is in the glacier up in the mountain at 1553 masl and oulet in the fjord, passes through the centre of the village. Storelva is a steep river with a mean gradient of 12% and a maximum gradient of 18% and have a catchment area of 25 km^2.

On 24 July 2017, the water in the Storelva River increased from less than 1 m^3/s to extreme volumes in a mere 4 hours. It started to rain heavily at 4 am and continued to rain until around 2 pm with varied intensities (Bruland 2020). The extreme rainfall in the upper part of the catchment in the morning increased the flow rapidly

in the river, leading to the change in the river path (Figure 1.1) at several locations. This sudden increase in river flow resulted in flash flood along with debris flow (Figure 1.2) which led to damaged buildings, farmlands and terrain in the area. Power lines and underground cables were destroyed because of the flash flood and landslides on mountainous terrain above the fjord, leaving huge gaps in the landscape.

Figure 1.1: *Changed path of the river during the flash flood. Source: tv2.no.*

Figure 1.2: *Debris and damage in Utvik during the flash flood. Source: tv2.no.*

After being inundated with water from heavy rain and flooding, residents of Utvik were forced to spend several days without access to fresh water in their houses. In addition to destroying the local bridges and roads (Figure 1.3) leading to in and out of the village, the gaps in the landscape left the village isolated which made it much more challenging for rescue and repair teams to reach to the devastated areas. The village was receiving supplies of food and fresh water by boats. Total cost of the damages after the Utvik flood was estimated to be 7 million euros for private property damages and 5 million euros for repairing the roads (Sunnmørsposten 2017).

Figure 1.3: *One of the damaged roads and bridge in the village. Source: tv2.no.*

1.3 World of Wild Water (WoWW) project

After the Utvik flood, a multidisciplinary project, called World of Wild Waters (WoWW) was started. The main aim of the project is to create a holistic understanding of causes and effects of natural hazards by creating immersive user experience based on real data, realistic scenarios and simulations. Experienced stakeholders, planners, decision makers and emergency agencies can base their preventive and emergency measures on this to save lives and property. In this way, they can move the focus from repair to mitigation investments to save direct and indirect socio-economic losses. The project aims to bring together the knowledge of physical and statistical behaviors of natural hazards and the knowledge of digital storytelling and human behavior.

This project includes everything from meteorological, hydrological and geotechnical conditions to the effect of human influence through constructions and infrastructure elements influenced by or influencing the development of a natural hazards. WoWW project consists of five work packages (WP) and seven PhDs from various departments (Figure 1.4). This PhD along with two other PhDs, comes under WP2 and the aim is to create realistic flood simulations through hydrological and hydraulic modelling. WP2 aims to combine hydrological distributed and hydraulic 2D models to dynamically simulate the water flow, water levels, water ways, water forces, erosion and deposition of masses along any given watercourse. The challenge is to create realistic simulations with poor or no calibration data as well as to compromise between the speed and accuracy of these simulations for different purposes based on amount and quality of input information available from WP1.

Figure 1.4: *World of Wild Water (WoWW) project and its work packages.*

WP1 aims to simulate realistic extreme meteorological events with realistic spatial and temporal dependencies. These are vital inputs to the hydrologic simulation models and therefore for the conditional risks and realistic series of events that develop into natural hazards. PhD in WP1 is from mathematics and statistics field. WP3 from geotechnical engineering, aims to model and visualize run-out flow landslides of quick clay. WP4 from the Department of Electronic Systems, aims to develop serious gamification of natural hazards by creating Virtual Reality experience as well as digital storytelling and human behavior to create immersive user experiences. It enables the shift from a passive user to an active and engaged participant feeling a higher degree of affiliation to the content by triggering more of their senses. WP5 from the psychology department aims to explore the meth-

odology for human-simulation interaction developed by previous work packages. It aims for understanding human behavior in digital story telling of natural hazards, defining how the most realistic user experience interaction can be achieved through virtual reality and ensuring that the design of the gamification elements fosters decision-making.

1.4 Hydrologic and hydrodynamic models

River systems as well as flash floods are usually simulated using hydrologic and hydrodynamic models. Hydrological modelling consists of the part of the hydrological cycle (Chow et al. 1988) in which water reaches the ground in various forms of precipitation and then into a river. Typical output from a hydrological model is a hydrograph (graph between discharge and time) typically at the outlet of the catchment. Whereas the hydrodynamic, also known as hydraulic modelling, consists of modelling the flow inside the river to find hydraulic characteristics such as water depth, flow velocity, shear stress, erosion, submerged area, and sedimentation (Chow 1988). The output from hydrological models is normally used as the boundary condition at upstream locations in the hydraulic models.

1.4.1 Hydrologic models

Hydrologic processes are difficult to estimate because of their non-linearity and highly complex relationships among different parameters (Yoosefdoost et al. 2022). The hydrologic processes depend on many parameters such as precipitation, temperature, relative humidity, wind speed, solar radiations, evapotranspiration, vegetation, soil characteristics, land use, land cover etc. which makes it even more complex and difficult to get a reliable relationship among all parameters (Beven 2012). The processes involved in the movement of water in a hydrological system are quite complex because precipitation in the form of rain or snow does not flow directly into the river channels. Instead, it follows various pathways and undergoes different transfers before reaching the catchment's outlet. Hydrological models are used to simulate these transfers of water from precipitation to discharges. These models can be either lumped, where the entire basin is considered as a single unit, or distributed (Devia et al. 2015), where the basin is divided into small, interconnected unit elements (usually less than 1 hectare) and all the processes are modeled and routed into each other.

1.4.2 Hydrodynamic models

The complexity of hydraulic or hydrodynamic models is even more than that of hydrologic models. These models are based on the St. Venant shallow-water equations, which are the hydrodynamic equations used to simulate the water flow (Novak et al. 2018). These equations are solved by connecting unitary elements

to each other (referred to as a mesh in the case of 2D models), creating a detailed representation of rivers where water flow is driven by physical laws. Unit elements can be 1D, 2D (horizontal) or 3D, depending on the model requirements (Glock et al. 2019). A hydraulic model is considered closed when it includes limit conditions at all of its extremities, which drive its behavior. This means that every element that comprises the model requires an input condition. Furthermore, all models must have an initial condition from which they can evolve with the application of limit conditions.

1.4.3 Integration of models and Rain-on-grid modelling

Usually, the two types of models discussed above are integrated manually, where the output of a hydrologic model is used as input to the hydraulic model (Grimaldi et al. 2019). This manual integration is usually more time-consuming because of separate calibration of the two models (Li et al. 2021). Traditional hydrological models typically only provide hydrographs as output, without presenting information on the resulting consequences, such as velocity, water depth, and shear stress at specific points or regions of the catchment. Whereas, to evaluate flood damages, the hydraulic models require a hydrograph generated from a hydrologic model as an input boundary condition. In situations where a river has many tributaries, multiple boundary conditions may be required to correctly estimate the flood zones. However, determining where to set this input boundary condition in the hydraulic model can also be a challenge. Furthermore, there is typically some residual flow along the river from the catchment or small tributaries that can be challenging to estimate and incorporate into hydraulic model calculations.

Therefore, this thesis work uses the DRM- direct rainfall method (Hall 2015), also known as the rain-on-grid (RoG) technique, to address the aforementioned challenges and to avoid the need for manual coupling of the two model types. With this approach, the input rainfall is applied directly to the grid cells of a 2D hydraulic model, eliminating the need for a separate hydrological model. RoG technique offers the advantages of both hydrologic and hydrodynamic models by allowing the extraction of a hydrograph at any point within the catchment. This approach also enables determining the consequences of floods throughout the catchment. Such information can aid in identifying critical flood locations within the catchment.

To maximize the effectiveness of the RoG technique, spatially varied precipitation can be used as input. Spatial variations in rainfall significantly influence catchment hydrological responses by affecting runoff generation, infiltration, soil moisture and streamflow, including the timing and magnitude of peak discharges and localized flooding. Moreover, models that consider spatial rainfall patterns are better at identifying critical flood-prone areas within a catchment, offering an advantage

over using constant rainfall inputs which can oversimplify and underestimate the catchment's response (Khosh Bin Ghomash et al. 2022). This enhanced understanding aids in flood risk management and planning, ensuring more resilient and adaptive strategies.

1.5 Aims and objectives of the thesis

This PhD work focuses on flash flood analysis in small and steep snow-covered catchments. The main purpose of the study is to identify the most suitable technique for flash floods in such mountainous catchments. In particular, the study aims to achieve the following objectives:

- To simulate flash floods and analyze the response of small and steep catchments in terms of both the hydrological and hydraulic characteristics such as hydrograph, water velocities and inundated areas .
- To check the suitability of the open-source hydrodynamic model TELEMAC-2D for hydrodynamic rainfall-runoff (HDRR) modelling.
- To identify and simulate the contribution of snowmelt and/or Rain-on-Snow events which may lead to more intense flash floods and consequences of such events.
- To identify advantages and limitations of the tested HDRR models and used infiltration methods for flash flood simulations in small and steep catchments.

Chapter 2

Materials and methods

2.1 Study site and input dataset

It is a significant challenge to find a small and steep catchment with measurements and data available for the modelling purposes. The area chosen for this study is one of the few catchments that has a fully operational gauge station inside it. In addition, it is a small and steep catchment that has the potential for disastrous flash floods. The study catchment is called Sleddalen that is located in Møre og Romsdal county in western Norway (62.07°N to 62.11°N and 6.39°E to 6.48°E). It has a complex mountainous topography and has an average slope of 48%. The catchment is mainly covered by open land, forests, bare rock and scarce vegetation as shown in Figure 2.1.

Input data used in this study are Digital Terrain Model (DTM), observed discharge, temperature, precipitation, land cover and land use data. DTM with a resolution of 0.5 meter by 0.5 meter was downloaded from the Norwegian mapping authority database (hoydedata.no) which is based on a topographic LiDAR scan of the area. The land use- land cover data were downloaded from Geonorge (www.geonorge.no), which is a Norwegian national website for maps and other geographical information in Norway. The discharge data with 15 minutes and temperature data with 1 hour resolution were taken from the Sleddalen measurement station (ID: 97.5.0) within the catchment which is available from the Norwegian Water Resources and Energy Directorate (NVE) database (sildre.nve.no). Spatially distributed precipitation data for the study area were extracted from the RadPro dataset available from the Norwegian meteorological department (threadds.no). RadPro is a merged product of gridded point observations and radar data with 1 km × 1 km spatial and 1 hour temporal resolution (Engeland et al. 2018).

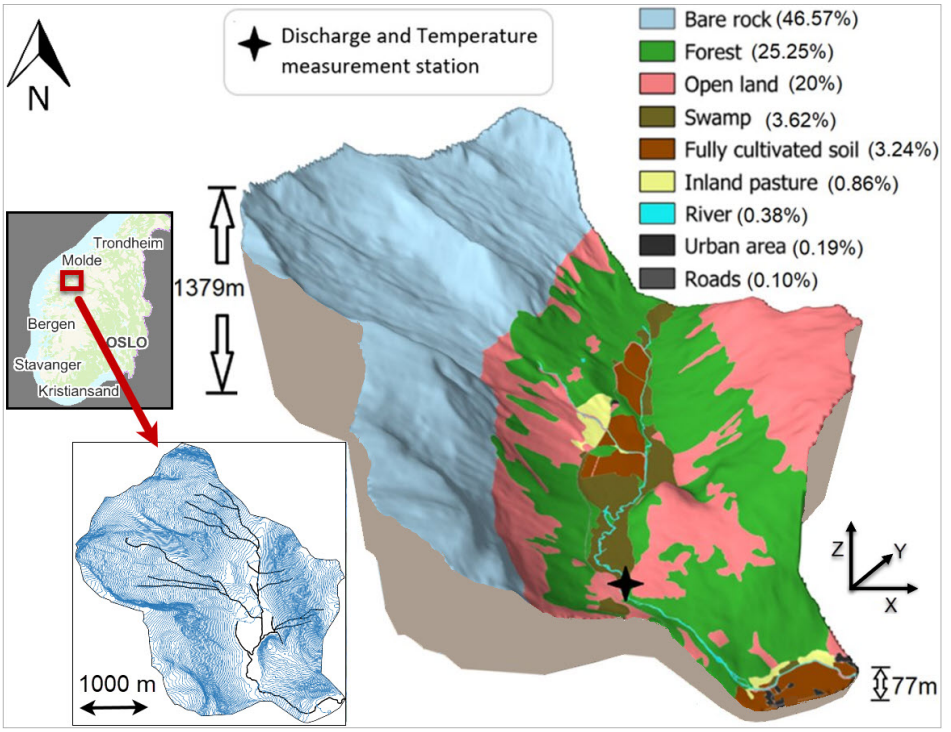

Figure 2.1: *Study area showing steepness, land cover-land use information, maximum and minimum elevations and the location of measurement stations in the catchment. Small figure in bottom left shows the DTM with contour lines at 10m vertical distance and the digitized river network from the Norwegian Water Administration database.*

2.2 Methodology and Models used

TELEMAC-2D hydrodynamic mode was used in this thesis because it has the option to include a hydrological module. In addition, it is an open source modelling tool; the source code could be accessed and modified by users. The source code of the model was modified to implement spatially distributed rainfall as input over the entire catchment (rain-on-grid technique). The example of the spatially distributed input rainfall used in this research work is shown in Figure 2.2. The initial moisture conditions in the catchment and the baseflow in the river are important parameters to simulate a peak flow event, which could not be simulated in TELEMAC-2D. Hence, the HBV hydrological model (Bergström and Forsman 1973) was used to set the base flow in the river to simulate the peak flows in TELEMAC-2D.

The hydrological module in TELEMAC-2D uses the SCS-CN (Curve-Number) infiltration method (USDA-SCS 2004). Spatially distributed CN and Manning's

roughness values were used, keeping all other parameters constant, such as mesh resolution and initial moisture conditions in the catchment, after performing a sensitivity analysis on these parameters. No soil and initial moisture data was available for the catchment, which is important to calculate the CN values. Additionally, as most part of the catchment comprises forest, open land, bare rock and sparse vegetation, spatially distributed CN values were manually calibrated solely for these land covers. For the other land cover types, CN values were calibrated once and then these values were used for all flood events.

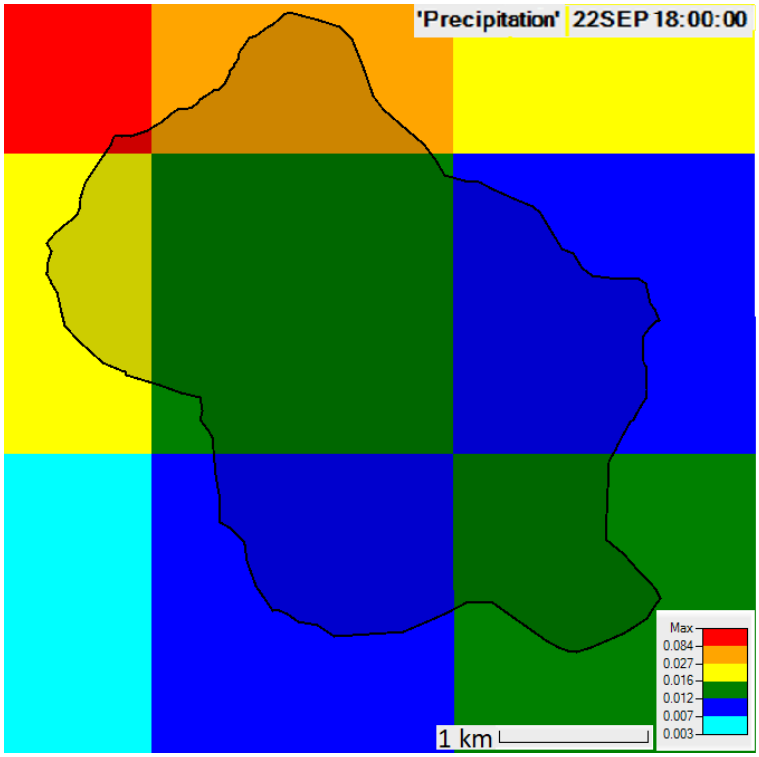

Figure 2.2: *An example of 1 km x 1 km spatially distributed precipitation used as input in the HDRR models.*

All peak flow events chosen in Paper 1 were triggered by pure rainfall events because TELEMAC-2D does not have a snow routine to account for the contribution of snowmelt to flash floods. However, in regions with snow-covered mountains, snowmelt plays a significant role in contributing to flash floods. Therefore, it was also essential to analyse the contribution of snowmelt in the hydrological modelling process. Hence, in Paper 2 and Paper 3, HBV was used to preprocess the raw precipitation data by separating snowfall from rainfall and by calculating the

snowmelt. The sum of rain and snowmelt, which eventually contributes to a flood, was implemented in the HDRR models as input precipitation. This work flow used in Paper 2 and Paper 3 is shown in Figure 2.3.

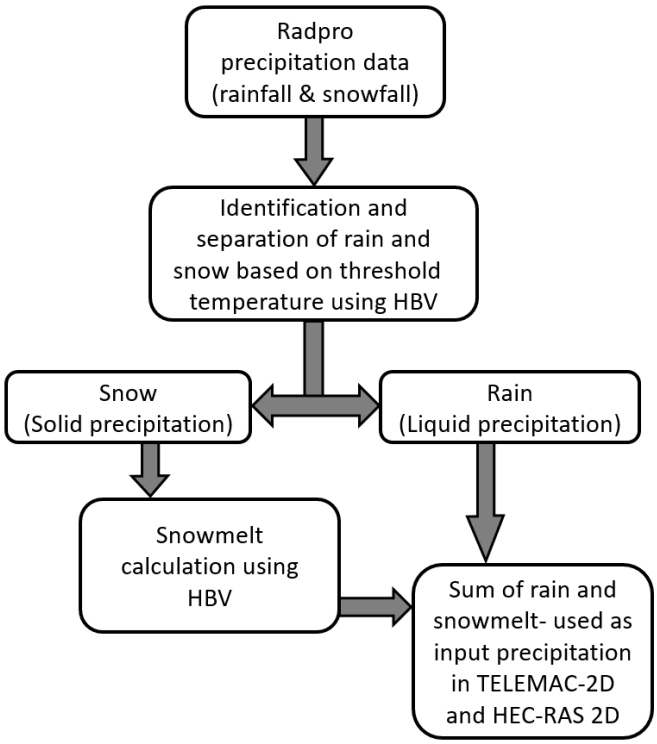

Figure 2.3: *Work flow used in Paper 2 and Paper 3.*

Same model-setup of TELEMAC-2D was used in Paper 2 as in Paper 1 but, given that the CN value serves as a calibration parameter in this research work, its values vary for each event and differ from the calibrated values for flood events in Paper 1. In Paper 2, long-duration multi-storm flood events were also simulated along with short-duration single-storm flood events.

In Paper 3, the HEC-RAS 2D hydrodynamic model with the CN and Green-Ampt Redistribution (GAR) infiltration methods was tested. In this paper, performances of TELEMAC-2D and HEC-RAS 2D was compared for their RoG technique for long- and short-duration flash flood events. The model setup used for TELEMAC-2D in Paper 3 was similar to the previous papers, except that even finer mesh with 3 meter by 3 meter resolution was introduced in the steeper sections of the river close to the catchment outlet to have same mesh resolution as in HEC-RAS

2D. The calibrated CN and roughness values used in the models, for various flood events, are mentioned in the corresponding research articles. All these models and methods are described in detail in the following sections.

2.2.1 TELEMAC-2D

TELEMAC-2D is a hydrodynamic model that calculates the water depth and velocity components in two dimensions of horizontal space. It solves Saint-Venant equations to calculate the hydraulic characteristics using a computational mesh of triangular elements (Figure 2.4). For the present work, the mesh size varies from a minimum triangle edge length of 5 meters around the river network to a maximum edge length of 100 meters in the rest of the catchment. In Paper 3, even finer mesh with 3 meters edge length was introduced in the steep section of the river from the measurement station shown in Figure 2.1 to the catchment outlet.

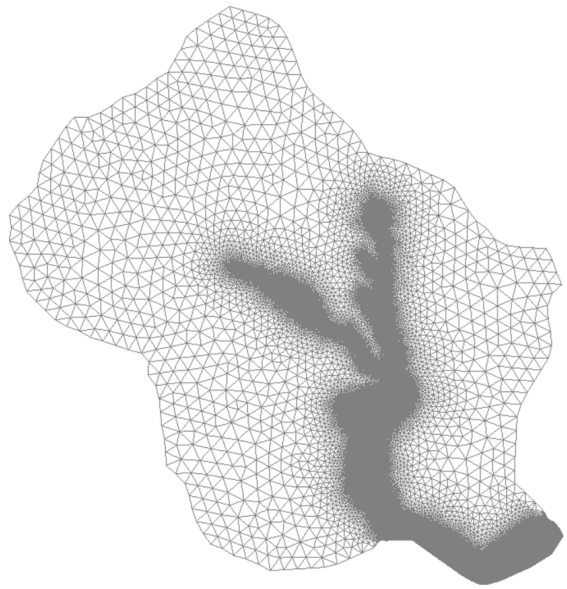

Figure 2.4: *TELEMAC-2D mesh having triangular elements with 3m x 3m resolution in the downstream part of the river, 5m x 5m in and around rest of the river and 100m x 100m in rest of the catchment (approximately 104600 cells).*

TELEMAC-2D provides the option to integrate a hydrological module using the SCS-CN method (Section 2.2.5) featuring the RoG technique as described by Broich et al. (2019) and Ligier (2016). Consequently, TELEMAC-2D has the ability to simulate the integrated flow of both overland and river systems, making it suitable for modelling flash floods. The model has an option to choose either the

finite-volume or finite-element method, and for this research, version v8p2 of the model is used with the finite-volume method.

Main input files necessary for TELEMAC-2D simulations are boundary condition file, precipitation file, simulation/ steering file (*.CAS), and the geometry file containing mesh information and catchment characteristics such as roughness and CN values. TELEMAC-2D uses the geometry and precipitation files in SELAFIN (*.slf) format. Geometry and boundary condition files were prepared using Bluekenue (Barton 2019) software. Python and R were used to convert the netCDF format precipitation file to SELAFIN format. PostTelemac plugin in QGIS was used for result visualization and to generate water depth and velocity maps.

2.2.2 HEC-RAS 2D

Developed by the U.S. Army Corps of Engineers, HEC-RAS includes 1D steady flow, 1D and 2D unsteady flow, sediment transport, water temperature, and water quality analysis (Brunner 2021). HEC-RAS 2D is a freely available software but not open-source, which implies that users are unable to check and modify its source code. Versions 6.3.1 and 6.4.1 of HEC-RAS 2D was used in this research work. This model uses a computational mesh comprising square-shaped elements (Figure 2.5) and solves the full momentum shallow water equations among other options. Small figure in the left in Figure 2.5 shows a typical mesh containing square shaped elements with finer grid cells in and around the river. The bigger figure on the right shows the actual mesh, with various breaklines, used in this research work.

Necessary input files for HEC-RAS 2D simulations are mostly the same as those required for TELEMAC-2D, with the exception of the simulation file exclusive to TELEMAC-2D. This distinction arises because HEC-RAS 2D incorporates a user interface, allowing the simulations to be executed directly from the main window without the need for a simulation file. The format of the input files is also different for both models. The precipitation file, in netCDF format, was used directly in HEC-RAS 2D. Spatially distributed Manning's roughness and CN values were used. RAS-Mapper was used to prepare input files such as geometry, roughness, and infiltration files, as well as to perform post-processing and visualization tasks, including the water depth and velocity maps. Furthermore, for the multi-storm flood event, the GAR infiltration method (Section 2.2.6) was tested.

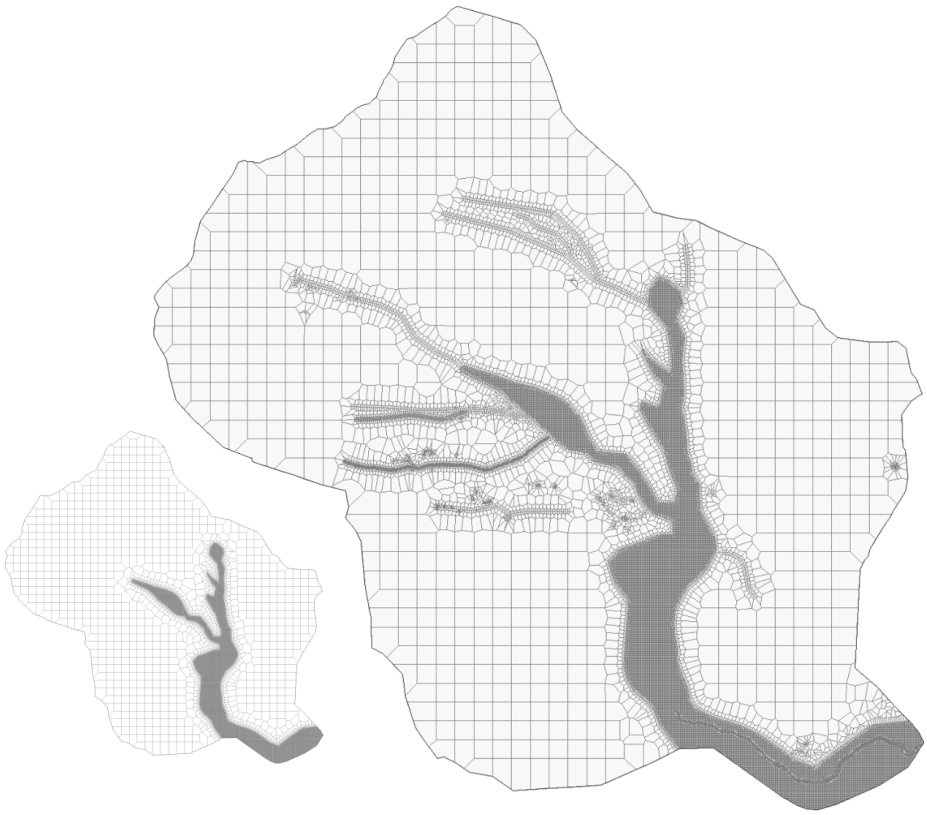

Figure 2.5: *HEC-RAS 2D mesh having square elements with 5m x 5m in and around the river and 100m x 100m in rest of the catchment. The big figure in right shows additional 3m x 3m resolution in the downstream part of the river along with various other breaklines (approximately 56100 cells in total).*

2.2.3 Shallow water equations used in the HDRR models

Shallow water equations are a set of partial differential equations governing the behavior of shallow water waves and flows. These equations are derived by depth-integrating the Navier-Stokes equations under the assumption of shallow water, where the horizontal length scales are much greater than the vertical length scales. Mass conservation and momentum conservation equations solved by the HDRR models are given as follows:

Mass conservation / Continuity equation

$$\frac{\partial h}{\partial t} + \mathbf{V} \cdot \nabla(h) + h\nabla \cdot (\mathbf{V}) = S_h \tag{2.1}$$

where

$$\mathbf{V} \cdot \nabla(h) + h\nabla \cdot (\mathbf{V}) = u\frac{\partial h}{\partial x} + v\frac{\partial h}{\partial y} + h\left(\frac{\partial u}{\partial x} + \frac{\partial v}{\partial y}\right) \tag{2.2}$$

This equation ensures that the rate of change of water depth with time, combined with the divergence of the mass flux, is balanced by any sources or sinks of mass within the flow domain.

Momentum equations

In vector form:

$$\frac{\partial V}{\partial t} + \mathbf{V} \cdot \nabla(V) = -g\nabla Z + \frac{1}{h}\nabla \cdot (hv_t\nabla V) + S \tag{2.3}$$

- Momentum equation along x:

$$\frac{\partial u}{\partial t} + \mathbf{V} \cdot \nabla(u) = -g\frac{\partial Z}{\partial x} + \frac{1}{h}\nabla \cdot (hv_t\nabla u) + S_x \tag{2.4}$$

- Momentum equation along y:

$$\frac{\partial v}{\partial t} + \mathbf{V} \cdot \nabla(v) = -g\frac{\partial Z}{\partial y} + \frac{1}{h}\nabla \cdot (hv_t\nabla v) + S_y \tag{2.5}$$

The above equations are given in Cartesian coordinates, where

h (m) = water depth;
V and u, v (m/s) = Velocity and velocity components in the x, y direction respectively;
g (m/s^2) = gravity acceleration;
v_t (m^2/s) = momentum coefficient;
Z (m) = free surface elevation;
t (s) = time;
x, y (m) = horizontal space coordinates;
S_h (m/s) = source or sink of fluid;
S (m/s^2) = source terms representing the wind, Coriolis force, bottom friction, a source or a sink of momentum within the domain;
and h, u, and v are the unknowns.

2.2.4 HBV

Hydrologiska Byråns Vattenbalansavdelning (HBV) is a hydrological model developed by Swedish Meteorological and Hydrological Institute (SMHI). It is a

semi-distributed conceptual model that divides a catchment into zones based on the catchment properties. HBV model (Bergström and Forsman 1973) was used to set the river base flow in the TELEMAC-2D simulations. The antecedent moisture conditions of the catchment and initial base flow in the river are highly significant for accurately simulating peak flow in TELEMAC-2D. But the RoG implementation in TELEMAC-2D cannot realistically simulate these factors, hence HBV was used for this purpose.

In a catchment with varying altitudes, precipitation can occur as rain or snow simultaneously at different elevations within the same time step. However, snowfall does not contribute to runoff until it melts. The HBV model has a dedicated snow routine that determines the precipitation type and calculates snowmelt based on the available precipitation and temperature data. Therefore, in Paper 2 and Paper 3, this model was used to calculate the rain and snowmelt from raw precipitation data. The summation of which was further used as input precipitation for the RoG modelling in TELEMAC-2D and HEC-RAS 2D Hydrodynamic Rainfall-Runoff (HDRR) Models.

Within the HBV model, the catchment was divided into ten elevation zones of equal size (Figure 2.6). For each zone, the model calculates the air temperature, precipitation amount and precipitation type. It does so by analyzing the temperature and precipitation gradients, and the threshold temperature for snowfall (T_x) (Killingtveit and Sælthun 1995). The model also tracks the accumulation of snow in each elevation zone and computes the subsequent snowmelt (Equation 2.6) based on whether the temperature in a particular zone is higher or lower than the threshold temperature for snowmelt (T_s) (Figure 2.6 d,e). Snowmelt intensity is computed based on the degree day factor (C_x) and the air temperature (T_a) above the snowmelt threshold using the following equation:

$$M = C_x(T_a - T_s) \tag{2.6}$$

In this equation, M is the snowmelt in mm/h, C_x is the degree day factor in mm/h°C, T_a is air temperature and T_s is the threshold temperature for snowmelt, both in °C.

The observed temperature and precipitation are adjusted to each elevation zone according to the lapse rate for temperature (dry or wet adiabatic) and precipitation (Figure 2.6e). Threshold temperature for snowfall (T_x) and the degree day factor were calibrated for each event. Lapse rates, threshold temperatures, and the degree- day factor were also calibrated to fit the simulated discharge from the snowmelt events to the observed discharge, and to fit the simulated snow storage to the actual snow storage which is depleted by the end of each summer. The snow routine additionally considers the accumulation of liquid water within the snow,

thereby accounting for the delayed release of rain and snowmelt water from the snowpack (Bruland 2021).

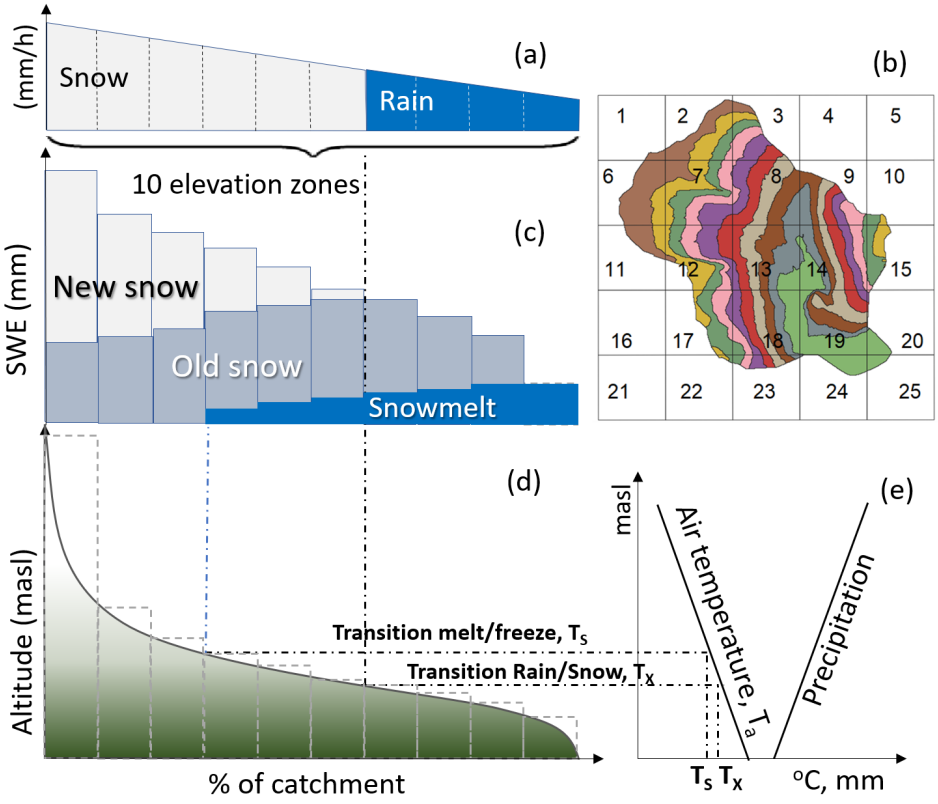

Figure 2.6: *Snow routine in the HBV model with (a) hourly precipitation input in the form of rain and snow defined by (e) the temperature and precipitation gradients, threshold values and intensities from (b) 1 km^2 grid cells with the Rad-Pro precipitation (also showing the 10 elevation zones with different colors), (c) resulting accumulated new and old snow and snowmelt, (d) Hypsographic curve of the catchment with the ten elevation zones.*

2.2.5 The Curve Number method

The RoG module in the HDRR models uses the SCS-Curve Number (CN) infiltration method (USDA-SCS 2004) among other infiltration methods for the hydrological calculations. The CN method was used in TELEMAC-2D for the hydrologic module in all the three research articles included in this thesis and also in HEC-RAS 2D in the Paper 3. CN method calculates the excess depth as surface runoff using the following equation:

$$Q = \frac{(P - \lambda S)^2}{(P + S - \lambda S)} \; when \; P \geq I_a \; and \; \lambda = \frac{I_a}{S}, \qquad Q = 0, \; when \; P < I_a \tag{2.7}$$

Where Q (mm) is the direct runoff depth, P (mm) is the event rainfall depth, I_a (mm) is initial abstraction or event rainfall required for the initiation of runoff, S (mm) is the potential maximum retention and λ is the initial abstraction ratio. The default value of initial abstraction ratio (λ = 0.2) was used in this study.

Curve number (CN) is a dimensionless parameter derived empirically which is associated with land use, land cover, hydrological conditions, hydrological soil group, and antecedent soil moisture condition within the catchment. The CN is related to the above equation in the following way:

$$CN = \frac{25400}{(254 + S)} \tag{2.8}$$

Antecedent Moisture Conditions (AMC) are classified into three categories based on soil moisture levels in the catchment: dry (I), normal (II), and wet (III). CN value for normal AMC can be converted to the CN for dry and wet AMCs. One of the most popular equation set for this conversion is given by Chow et al. (1988):

$$CN(I) = \frac{4.2 \; CN(II)}{10 - 0.058 \; CN(II)} \tag{2.9}$$

$$CN(III) = \frac{23 \; CN(II)}{10 + 0.13 \; CN(II)} \tag{2.10}$$

However, for the Sleddalen catchment, due to the absence of available information regarding the soil's moisture level before the events, the CN values were not adjusted for different AMCs. We kept the CN value as a calibration parameter keeping the AMC constant corresponding to normal condition. Nonetheless, the TELEMAC-2D has an option for steep slope correction to accommodate the mountainous nature of the catchment, as per the following equation introduced by Huang et al. (2006):

$$CN(II)_\alpha = CN(II) \; \frac{(322.79 + 15.63\alpha)}{(\alpha + 323.52)} \tag{2.11}$$

Where $CN(II)$ is the curve number corresponding to the normal antecedent moisture condition (AMC II), α is the terrain slope in m/m and varies from 0.14 m/m to 1.4 m/m. The $CN(II)$ values can be raised by up to 6% for α =1.4 (Ligier 2016).

2.2.6 Green-Ampt and Green-Ampt Redistribution infiltration methods

Unlike the CN method, Green-Ampt (GA) method is a physically based model. The rate of infiltration in this approach varies over time, taking into account soil properties such as initial and residual moisture content, hydraulic conductivity, porosity, suction head, and soil texture (pore size distribution) (Ogden and Saghafian 1997). The CN method assumes an initial abstraction before the initiation of surface runoff, on the other hand, the GA method assumes that runoff begins only when the rainfall rate exceeds the infiltration rate. GA approach assumes a clear boundary between the wet and dry soil, with the moisture potential changing along the wetting front in the dry soil according to its water content (Green and Ampt 1911). The GA equations, offering a simplified understanding of the infiltration process, are widely recognized as a suitable method for calculating the vertical water flow in the soil.

The GA approach is well-suited for replicating single peak flow events in which the impact of evapotranspiration and unsaturated gravity-driven flow is negligible. However, when modelling long-duration flood events resulting from multiple precipitation storms, it becomes crucial to account for the soil moisture redistribution. In such cases, the Green-Ampt Redistribution (GAR) method is used to simulate soil moisture recovery during periods of rainfall hiatus. For these events, it may be necessary to consider two wetting fronts. The following sections show the equations for the GA and GAR methods.

Equations for the basic GA method:

The basic GA method relies on four parameters: saturated hydraulic conductivity (K_S), suction head (ψ), initial moisture content (θ_i), and saturated moisture content (θ_s). However, the GAR method considers two parameters in addition: the residual moisture content (θ_r) and the pore size distribution index (λ).

- Potential infiltration rate:

$$f(t) = K_s(1 + \frac{\psi\theta_d}{F}) \tag{2.12}$$

- Actual infiltration rate:

$$\textbf{Actual infiltration} = \textbf{Minimum of} \quad \textbf{[f(t),} \quad \textbf{Precipitation rate]} \tag{2.13}$$

- Cumulative infiltration depth is then computed as:

$$F(t) = Kt + \psi\ \theta_d\ ln(1 + \frac{F(t)}{\psi\theta_d}) \tag{2.14}$$

Where θ_d is the moisture deficit given as $(\theta_s - \theta_i)$ and t is time.

Equations for the GAR method:

Onset of a rainfall hiatus period occurs when the saturated hydraulic conductivity (K_S) exceeds the rainfall intensity. Within this interval, the soil moisture content initiates a decline, and the corresponding change in the moisture content (θ_0) for the redistribution process is computed using the following formula (Smith et al. 1993):

$$\frac{d\theta_0}{dt} = \frac{1}{Z_0}(f - E_{v,0} - [K_0 + \frac{K_s G(\theta_i, \theta_0)}{Z_0}]) \tag{2.15}$$

Where Z_0 is the depth to the wetting front given as $F_0/(\theta_0 - \theta_i)$, $E_{v,0}$ is the evapotranspiration rate, K_i, K_S and K_0 are the unsaturated hydraulic conductivity corresponding to the initial moisture content θ_i, saturated moisture content θ_S and a moisture contents of θ_0 respectively. $G(\theta_i, \theta_0)$ is the integral of capillary drive through the saturated front which is computed (Ogden and Saghafian 1997) as follows:

$$G(\theta_i, \theta_0) = \psi \ \frac{\theta_0^{3+\frac{1}{\lambda}} - \theta_i^{3+\frac{1}{\lambda}}}{1 - \theta_i^{3+\frac{1}{\lambda}}} \tag{2.16}$$

Chapter 3

Summary of the papers

The main goal of this doctoral work was to develop and test methodologies for modelling flash floods in small and steep snow-covered mountainous catchments to estimate peak flows, flood hydrograph and catchment response during extreme events. One of the objectives of this research was to calculate extreme flood hydrographs and their consequences such as water depth and velocities at any location and in any arbitrary water course to identify potential flood damage spots in the catchment. In other words, the objective was to analyze flash floods in such a way that it is possible to extract hydrological and hydraulic characteristics anywhere within a catchment. To achieve this, the first goal was to choose or create such a model which can simulate hydrology and hydraulics in a single simulation using spatially varied precipitation.

In order to find out a suitable model, several hydrological models were reviewed, such as HBV, SHyFT (Statkraft Hydrologic Forecasting Toolbox) (Burkhart et al. 2021), MIKE SHE (Systeme Hydrologique European) (Refshaard and Storm 1995), HEC-HMS (hydrologic engineering center hydrologic modelling system) (Chu and Steinman 2009), SWAT (Soil and Water Assessment Tool) (Arnold et al. 1998) etc. In the end, the TELEMAC-2D hydrodynamic model was chosen for this study because it has the option to include a hydrologic module, making TELEMAC-2D a hydrodynamic rainfall-runoff (HDRR) model, which can model both hydrology and hydraulics in a single simulation. In addition, TELEMAC-2D is an open source modelling tool, meaning that the source code can be accessed and modified by the users.

In Paper 1, source code of the TELEMAC-2D model was modified to implement spatially distributed rainfall as an input over the entire catchment (rain-on-grid).

This Paper aimed to analyse the fully integrated hydrologic- hydrodynamic modelling approach and rain-on-grid technique in TELEMAC-2D. The model was tested for single-storm floods induced by rainfall events. Results showed that the calibrated models can satisfactorily reproduce peak flows and produce relevant information on hydraulic characteristics. Furthermore, the results indicated that this technique has the advantages of both hydrologic and hydraulic models. The peak flow events analysed in Paper 1 had no contribution of snowmelt in the flood. But the flash floods caused by heavy rainfall with snowmelt contribution due to sudden rise in temperature have become common in the changing climate. Hence, it was also important to analyse the flash floods occurring due to such Rain-on-Snow (RoS) events.

Therefore, in Paper 2, we investigated the effect and importance of including snowmelt for distributed runoff generation. Since, TELEMAC-2D doesn't have a snow-routine, the HBV hydrological model, was used to preprocess the raw precipitation data to calculate the rain and snowmelt which actually contribute to floods. The sum of rain and snow-melt was then used as input precipitation for simulations in TELEMAC-2D. The integrated model worked particularly good for short- duration single peak events, but it struggled to reproduce a flood event with sustained flow induced from a multi-storm precipitation event. The results indicated a need for time-varying CN values for flood events with multiple peaks or testing another infiltration method for hydrological part of the HDRR model .

Hence, in Paper 3, we tested another hydrodynamic model, HEC-RAS 2D to overcome the limitations observed in TELEMAC-2D because HEC-RAS 2D has an option of implementing rain-on-grid technique using other infiltration methods. The results showed that both the models successfully replicated the peak flow for single storm-events. However, neither the CN method in TELEMAC-2D nor the GAR or CN method in HEC-RAS 2D could satisfactorily reproduce the long-duration floods with sustained flow between the flow peaks. This study found out that it was not the CN method that was the problem identified in Paper 2, but it was the fact that the infiltrated water in these HDRR models is lost permanently out of the domain which should be contributing as the sustained flow during a flood event.

The following sections of this chapter provide a summary and main findings from each of the three research articles included in this thesis. Figure 3.1 shows an outline of all the papers contributing to the purpose of this thesis.

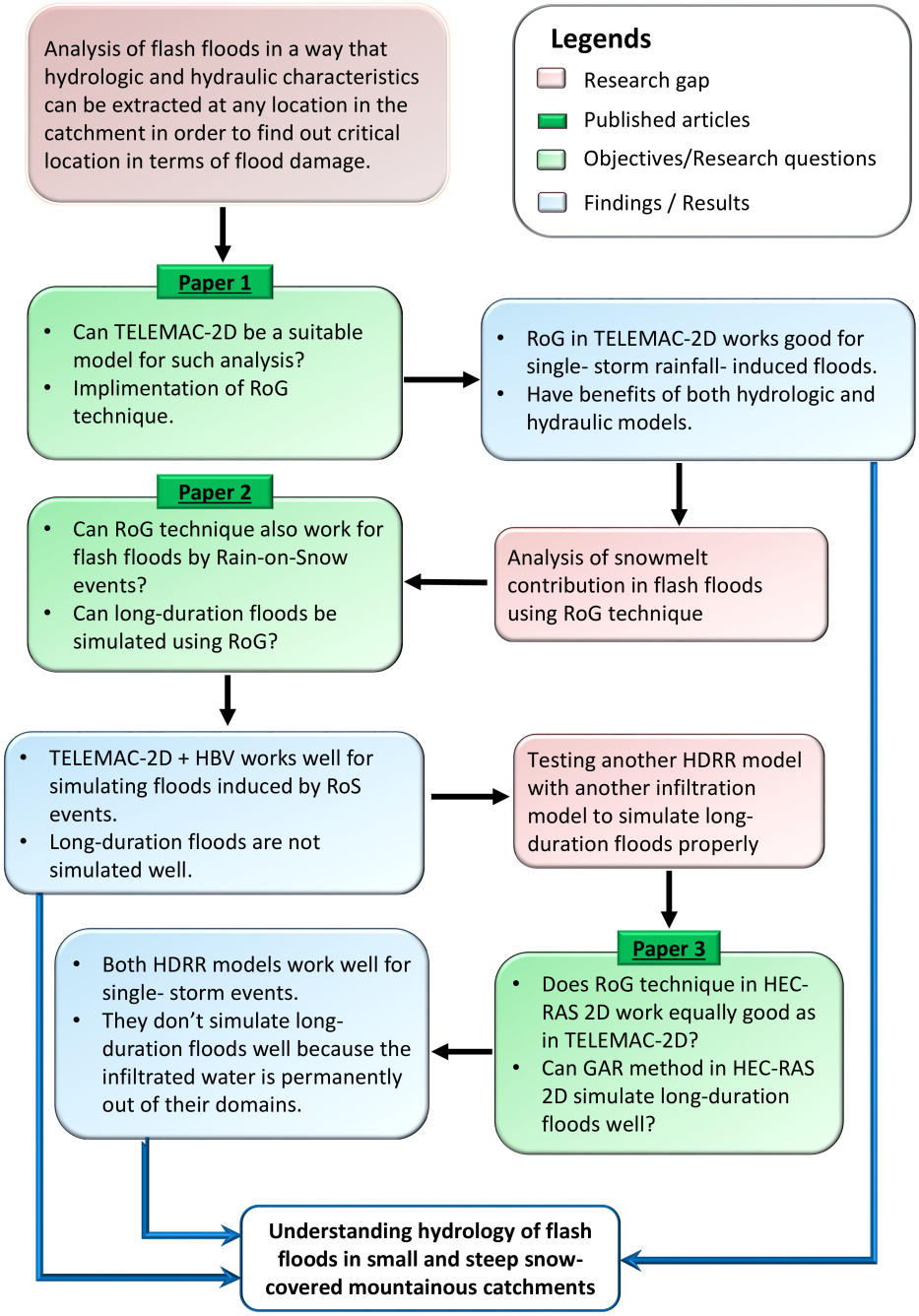

Figure 3.1: *Flowchart presenting the studies conducted as parts of this doctoral work that address several literature gaps and contribution in the field of flash flood hydrology of small and steep snow-covered mountainous catchments.*

3.1 Paper 1: Simulation of flash flood peaks in a small and steep catchment using rain-on-grid technique

This research article aimed to develop and analyse the methodology for a fully integrated hydrologic- hydrodynamic model using spatially distributed precipitation. TELEMAC-2D has an optional hydrologic module therefore, it was chosen in this study for its Rain-on-Grid technique. The resulting model was analysed for single-storm flood events using CN infiltration method available in TELEMAC-2D.

In this article, seven peak flow events, between years 2018 and 2021, caused by rainfall were chosen depicting a range of scenarios in which the accuracy of precipitation and runoff data was considered satisfactory. These events were selected based on the availability of high-quality precipitation and runoff data, covering a diverse range of situations. The results showed that the fully integrated HDRR models can satisfactorily reproduce peak flows (Figure 3.2) and produce relevant information about hydraulic characteristics such as water velocities and inundation. Moreover, the findings suggest that this approach offers the benefits of both hydrological and hydraulic models.

The model was also tested for using a single averaged CN value for the entire catchment and the findings indicate that it can produce equally satisfactory results as those obtained by the use of spatially distributed CN values, in case there is no soil data available for a catchment. A 200-year design flood was also simulated to illustrate the potential damages in the catchment in terms of the velocity and water depth. Figure 3.3 shows the depth, velocity, and product of the water as a result of the design flood in the catchment region with the highest potential for damage and consequences.

Moreover, a sensitivity analysis was done for the CN values, roughness, mesh resolution and different antecedent moisture conditions in the catchment. The results showed that the runoff volume is highly sensitive to the CN values and AMCs. The results also indicated that coarser mesh size, drier catchment (dry (AMC I, Low CN value) , and higher roughness values lead to lower runoff volumes and conversely.

The peak flow events analysed in Paper 1 had no contribution of snow-melt to the floods. But the flash floods caused by rain-on-snow events have become common in the changing climate. Hence, it was also important to analyse the flash floods triggered by RoS events, which was done in the next phase of the research, described in the subsequent sections.

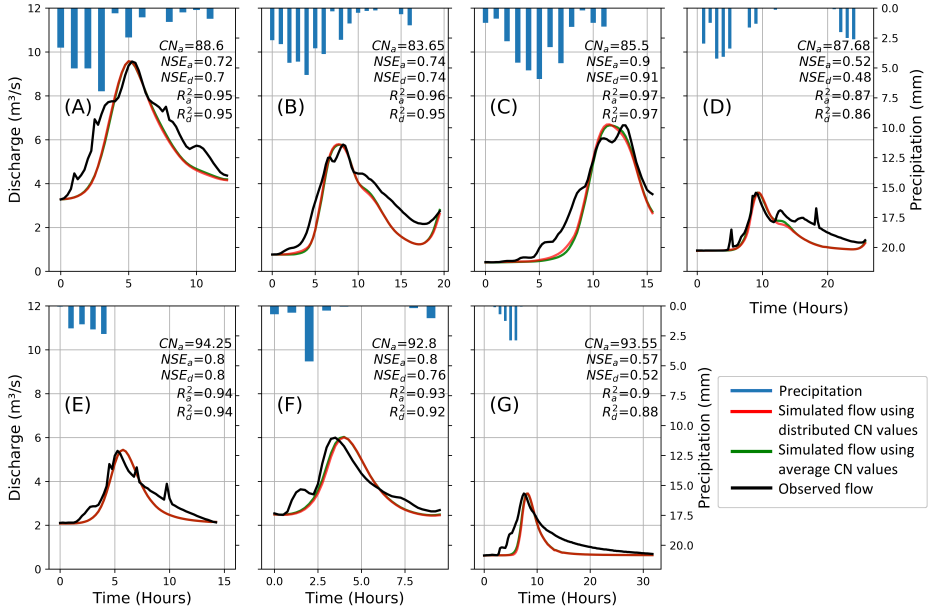

Figure 3.2: *Peak flows from RoG simulations in TELEMAC-2D using distributed CN values (red) and using a single averaged CN value (CN_a) (green) compared to observed flow (black), and correlation and Nash Suthcliff model efficiency in case of distributed CN values (R^2_d, NSE_d) and average CN values (R^2_a, NSE_a) corresponding to the seven events selected for the current study.*

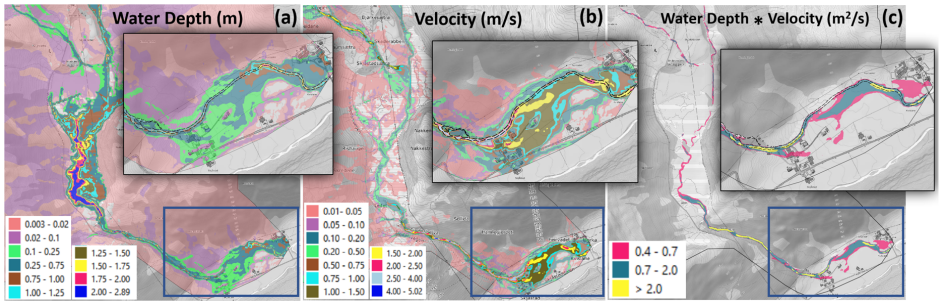

Figure 3.3: *Water depth (a) deeper than 0.1m and Velocities (b) higher than 0.25m/s, and the product of depth and velocity (c) higher than critical levels for pedestrians ($0.4m^2/s$), vehicles ($0.7m^2/s$) and buildings ($2m^2/s$) for the design storm with 200-yr return period.*

3.2 Paper 2: Modelling flash floods driven by RoS events using rain-on-grid technique in the hydrodynamic model TELEMAC-2D

Flash floods caused by heavy rainfall and snowmelt due to sudden temperature rise have become more common during autumn and winter in Norway and other countries with snow-covered mountains (Pall et al. 2019). It is therefore crucial to investigate these events. In Paper 2, the effects and importance of including snowmelt for distributed runoff generation was investigated. Since, TELEMAC-2D does not have a snow-routine, HBV hydrological model was used for calculating snowfall, rainfall and snowmelt from the raw precipitation data. The sum of rain and snowmelt was then used as input precipitation for simulations in TELEMAC-2D (workflow in Figure 2.3). HBV calibration results for the period 2018 to 2021 gave NSE (Nash and Sutcliffe 1970) value of 0.70. Results in Figure 3.4 show that the integrated model worked particularly well for single-storm events.

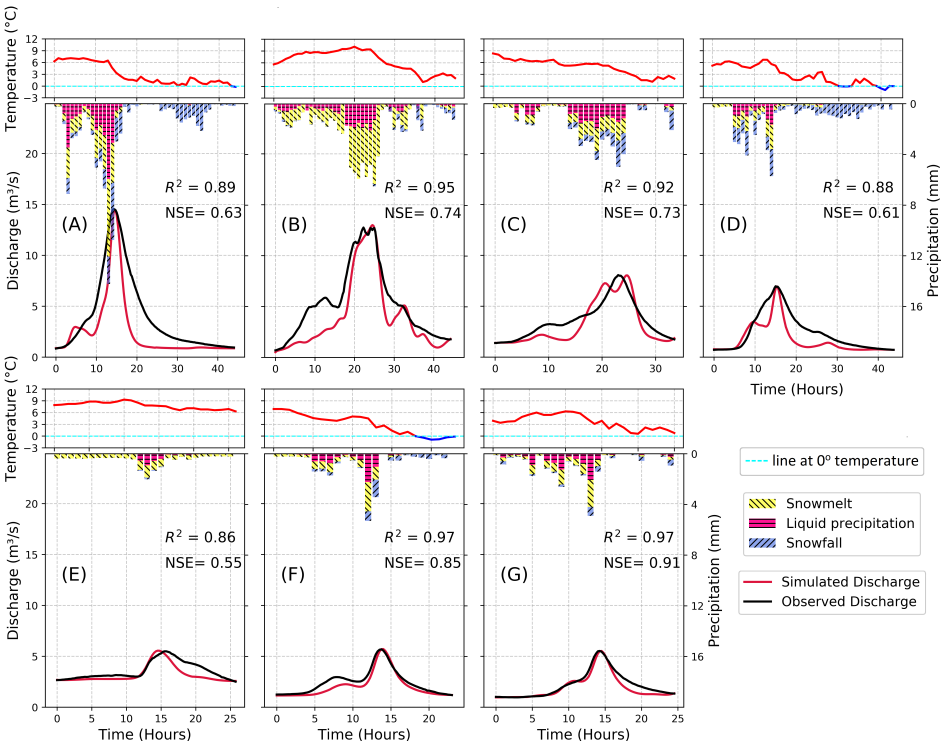

Figure 3.4: *Observed and simulated discharge, liquid precipitation (rain) and snowmelt, temperature (upper) corresponding to the events. The figure also shows solid precipitation (snow) that does not contribute to the runoff.*

However, the model could not reproduce all peaks of a flood event with sustained flow induced by a multi-storm precipitation event. It was tried to calibrate the model for such scenarios (Figure 3.5). Initially, the event was simulated with an average CN value of 41 for the catchment, which successfully captured the first peak but overestimated the second peak because the CN value of 41 was apparently too high as the catchment reached saturation after the first peak flow. To address this issue, another simulation was performed for the event with a lower CN value to reproduce the second peak, using the output from the first simulation as the initial condition.

The same event was also simulated in the hydrologic model, HBV without the integration with any hydraulic model. The hydrologic model alone performed better in reproducing the flood peaks and the sustained flow event. However, unlike TELEMAC-2D with the RoG technique, the HBV model did not provide any crucial information such as water levels, velocities, and inundated areas along the watercourses in the catchment. TELEMAC-2D might struggled to reproduce such events because it lacks water storage and soil routines which are available in HBV. As a consequence, the infiltrated water does not contribute back to the river as subsurface flow in the later stages of the flood. For the same reason, a steeper recession limb was also observed compared to actual discharge in all the cases.

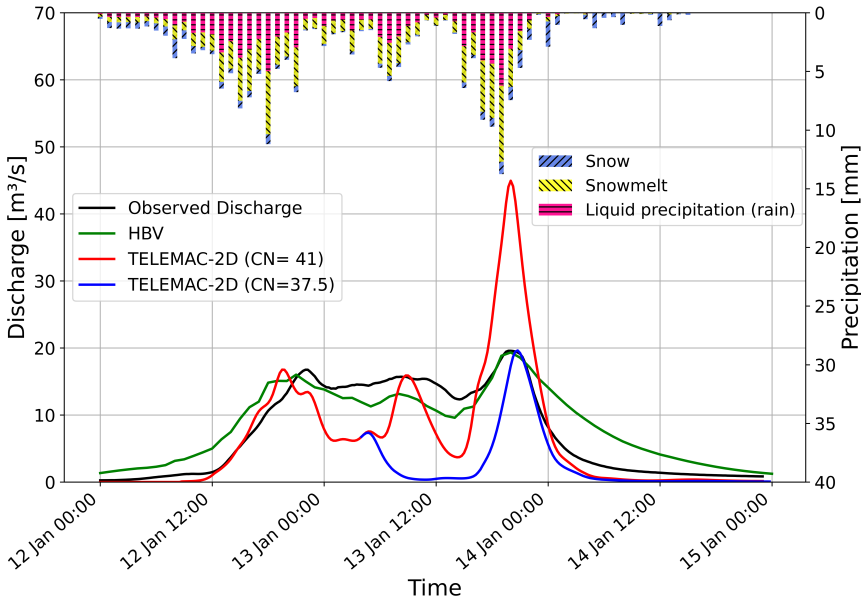

Figure 3.5: *Single simulation in TELEMAC-2D for entire event with CN= 41 (red), another TELEMAC-2D simulation with CN= 37.5 (blue) to calibrate the second peak, and the result from calibrated HBV alone (R^2= 0.87) (green).*

These findings indicate a requirement for varying CN values over time for flood events with multiple peaks, or implementation of an alternative infiltration approach which changes with time into the hydrological component of the HDRR model. Therefore, in the next phase of the research, another HDRR model was tested with other infiltration method as described in the following sections.

3.3 Paper 3: Comparison of two hydrodynamic models for their rain-on-grid technique to simulate flash floods in steep catchment

In Paper 3, another HDRR model, HEC-RAS 2D was tested which has an option of implementing a rain-on-grid technique using various infiltration methods. For this Paper, we selected Green-Ampt Redistribution infiltration method because of its capacity to vary infiltration capacity over time. Moreover, HEC-RAS 2D was compared with TELEMAC-2D for its rain-on-grid technique as well as for the calibration process, mesh elements and results such as the inundated areas, water depths and velocity of water during a flood.

Results showed that both models successfully replicated the peak flow for short-duration single storm events (Figure 3.6). However, to achieve the similar runoff volume in HEC-RAS 2D, it required lower Manning's roughness and higher CN values compared to TELEMAC-2D. The calibrated CN and roughness values used in both the models for these events in are shown in Table 3.1.

Final results for the inundation area and water depth from both the models were similar. However, HEC-RAS 2D computed higher velocities in the steeper sections of the river as compared to TELEMAC-2D. Results shown in Figure 3.7 indicate that the differences between the calculated velocity by the two models is proportional to the slope of the river. The steeper the slope, the higher the difference between velocities calculated by the two models.

GAR infiltration method in HEC-RAS 2D was also tested for simulating longer-duration flood events generated by multi-storm precipitation events. The results in Figure 3.8 show that neither the CN method in TELEMAC-2D nor the GAR and CN method in HEC-RAS 2D satisfactorily reproduced the sustained flow between the flood peaks. A sensitivity analysis of the GAR parameters was performed to understand the results for the long-duration multi-peak flow floods. The analysis was done on a small model with only two cells. The results showed that the runoff volume is not very sensitive to the two parameters which affect the second peak of the flood. Furthermore, the results of the sensitivity analysis were as expected and according to the theory, which are shown in detail in Paper 3. So, the real

reason behind the models not being able to reproduce sustained flow between the flow peaks and the recession limb of the hydrograph is that the infiltrated water is permanently lost from the model. When this infiltrated water returns as surface flow, it contributes to the recession part of floods, and it is also responsible for the sustained flow between the flow peaks, which is lost from the HDRR models.

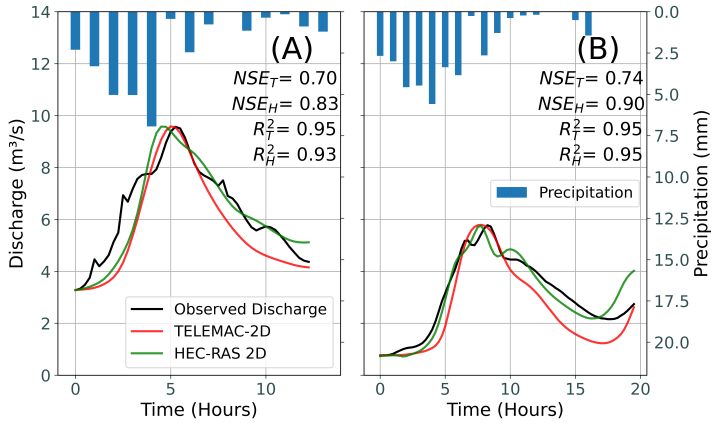

Figure 3.6: *Precipitation (blue columns on top), observed discharge (black) and results from TELEMAC-2D (red) and HEC-RAS 2D (green) simulations.*

Table 3.1: *Calibrated CN and Manning's roughness values used for various land covers in both the models. (*T2D = TELEMAC-2D, HR2D = HEC-RAS 2D)*

Land-cover	CN (T2D*)		CN (HR2D*)		Roughness (T2D*)	Roughness (HR2D*)
	Event A	Event B	Event A	Event B		
Bare rock and scarce vegetation	89	85	99	98	0.02	0.1
Forest	88	80	95	96	0.2	0.2
Open land	80	75	94	95.5	0.05	0.15
Marsh	90	90	95	92	0.2	0.2
Fully cultivated soil	90	90	94	90	0.04	0.04
Inland pasture	89	89	95	89	0.259	0.259
River	100	100	100	100	0.04	0.055
Urban Area	89	89	95	96	0.1	0.1
Roads	91	91	99	91	0.02	0.02

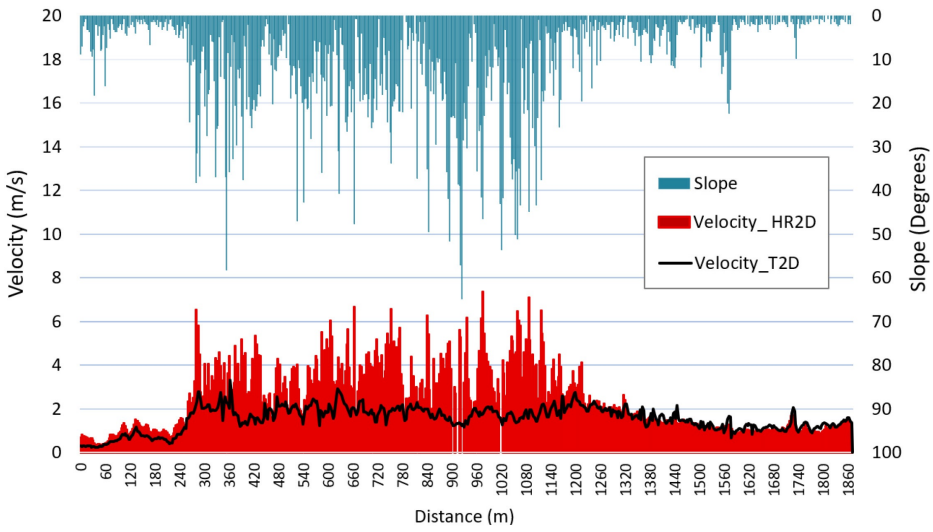

Figure 3.7: *Slope (blue) and velocity distribution along the centerline of the steep river stretch from the measurement station to outlet of the catchment. In the legends, T2D = TELEMAC-2D and HR2D = HEC-RAS 2D.*

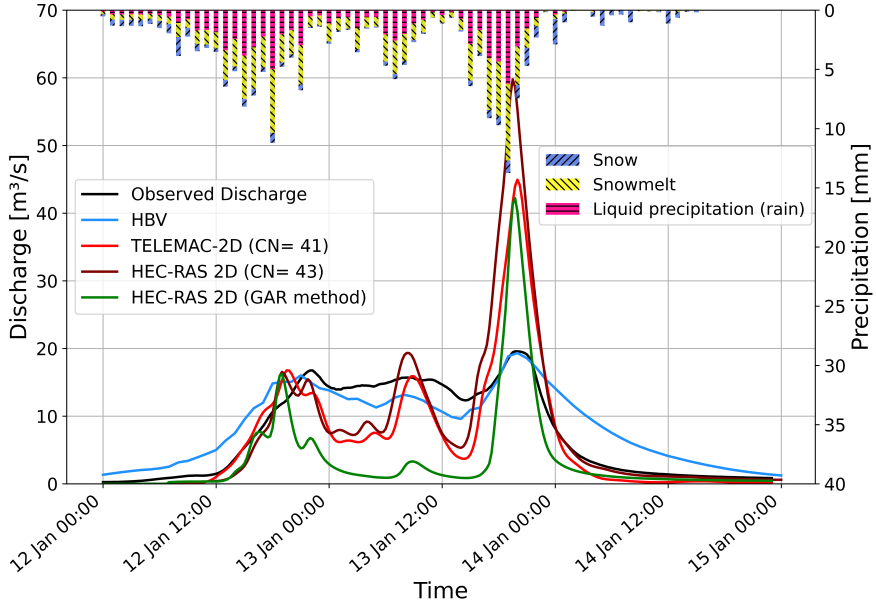

Figure 3.8: *Multi-storm flood event with two peaks induced by a RoS event. Observed discharge (black) and results from the hydrologic model HBV (blue) and hydrodynamic rainfall-runoff models TELEMAC-2D (red) and HEC-RAS 2D from CN (maroon) and GAR method (green).*

Chapter 4

Discussion

4.1 Rain-on-Grid technique in HDRR models

There have been disastrous flash floods in small watercourses in Norway in the past (Roald 2019). These flash floods were often induced by extreme rainfall events or the combined effect of extreme rainfall and snowmelt in steep snow-covered catchments (Pall et al. 2019; Hansen et al. 2014). Therefore, this thesis has focused on understanding and simulating the flash flood hydrology of such catchments. The results of this thesis work show that the integrated model using RoG technique satisfactorily reproduces single peak flows, the inflow sources and tributaries. The main finding from this research work is that a fully integrated hydrologic-hydraulic model with the RoG technique can be a solution to properly model single-storm flash floods in snow-covered steep catchments. These flash floods can be caused by either only extreme rainfall or an RoS event that has a mix of rain and snowmelt.

The RoG technique has the benefits of both hydrologic and hydrodynamic models. It satisfactorily reproduces the peak flow as well as the consequences of the flow in the river and in the catchment, such as flooded areas and critical water velocity. Additionally, it simulates the residual flow along the river, which is usually not simulated and difficult to estimate in the traditional way of 2D hydraulic modelling. A conventional hydrologic model typically produces a hydrograph at the catchment outlet, offering no insights into hydraulic attributes such as river routing, water velocities, and depths. Conversely, a hydraulic model provides detailed information on these hydraulic characteristics, but relies on data from a hydrologic model for boundary conditions. RoG implementation within hydraulic models integrate hydrologic and hydraulic modeling to effectively route runoff throughout the entire catchment. Consequently, rather than merely defining boundary condi-

tions to introduce inflow into the river system, RoG models facilitate the simulation of discharge and hydraulics across any tributary, including their contributions to the main river's inflow.

Moreover, this approach provides valuable information on critical locations within the river system where water velocities, depths, and sediment loads can have significant consequences. However, it is important to note that RoG approach in HDRR models, on its own, lacks representation of key hydrological processes such as snowmelt, soil, and groundwater storage. As a result, it relies heavily on accurate initial soil conditions and input data for snowmelt. But the HBV-integrated approach with HDRR models used in this study shows satisfactory results for the snowmelt events too.

The implementation of the RoG technique on a catchment scale shows the development of source areas and how the potential flood waves evolve through small streams in upstream areas and in the main water course in the downstream. In addition, this methodology enables users to extract the runoff hydrograph and hydraulic characteristics at any point within the catchment at any time-step. This functionality makes it an appropriate tool for evaluating erosion, sedimentation, and associated challenges during a flood event, as highlighted by Ali et al. (2017). Moreover, it allows the examination of the combined impact of water depth and velocities (Shand et al. 2011; Kreibich et al. 2009), as addressed in the Norwegian national regulation act (Direktoratet for byggkvalitet 2017). The fully integrated HDRR models have a reduced simulation run-time as compared to the traditional method of manual coupling of the two types of models. However, it can be the opposite if this technique is used for larger areas (Hariri et al. 2022; Rangari et al. 2019) because of exceptionally large number of grid cells.

The following sections delve deeply into several additional findings from this study concerning the model-setup, the impact of differing mesh resolution, roughness values, and CN values. We discuss findings regarding the use of the ROG technique in HDRR models for both short and long duration floods, a comparison between the two HDRR models, the uncertainties that are associated with the use of this approach, and the concept of equifinality. We also discuss how the results obtained support and contribute to the WoWW project.

4.1.1 Mesh resolution

Calibration results of the HDRR models from the papers in this thesis show that the size of mesh grid cell is an important factor in determining the amount of runoff, similar to what was discovered in a study by Clark et al. (2008). The finer the mesh resolution, the higher the runoff volume. However, using a finer mesh leading

to more cells makes the simulations computationally more expensive (Caviedes-Voullième et al. 2012). When the flow is generated by a precipitation event, water moves downstream by solving shallow water equations in a hydrodynamic model. Water depths in the flat and large cells of the model (100 m × 100 m) can be too shallow before it joins a water stream. This means that the Manning's friction coefficient, which is often too large for these shallow water depths, can trap water in the roughnesses and affect the actual water-flow propagation time. Additionally, using a coarse grid might not accurately represent the true geometry of the catchment, which can also cause more water to stay in the model (David and Schmalz 2021) and result in a lower peak flow compared to a simulations with a finer mesh.

4.1.2 Roughness

The roughness coefficients used in the HDRR models were adjusted based on the initial values from Chow (1988) for various land uses in the catchment to get a better fit of the peak flows, as done in various other studies (Garrote et al. 2016; Shen et al. 2017). Results from sensitivity analysis showed that increasing the roughness values to improve peak flow timing may sometimes lead to excessively high friction values, particularly for events with shallow water depths (Hall 2015). This situation can result in a considerable amount of water being trapped within the domain, and even increased CN values (decreased infiltration) may not compensate for this. This was experienced in HEC-RAS 2D while calibrating single-storm events in Paper 3. Therefore, the grid cell size in catchment was decreased to get a higher runoff volume and calibrate the peak flow.

4.1.3 CN Method

The calibration results from Paper 1 show that as the flood size decreases, higher CN values is needed, which is contrary to what was expected (Hjelmfelt 1991). This can be explained by the fact that a higher CN value reduces the simulated infiltration. This effect compensates for the lack of subsurface water transfer to the river, as the infiltrated water is lost from the HDRR models. In case of high discharges, this compensation is less important because a smaller part of the discharge comes from infiltrated water. This also affects the simulation of the recession limb and the total volume of water in the floods.

Average and spatially distributed CN values

Initially, in Paper 1, single CN value (CN_{avg}) was used for the entire catchment due to the lack of soil data. However, the tabulated CN values in National Engineering Handbook (Section-4) (USDA-SCS 2004) have been shown to be inadequate to get the correct runoff volume in many cases (Mishra and Singh 2006). Therefore, the CN_{avg} values were calibrated in this study. The HDRR models were also calib-

rated for distributed CN values based on land-cover data, which could be done in a reasonable time because of the small catchment size. However, for large catchments, this approach would not be possible due to the high computational time. The result from Paper 1 showed that the model can give equally good results in both the cases i.e; by using single CN_{avg} value for the entire catchment and by using distributed CN values.

Antecedent Moisture Condition (AMC)

The conventional formula by Chow et al. (1988) and Hjelmfelt (1991) encounters an issue that the CN value gets a sudden jump when converting from one AMC level to another which is not the case in real life. Also, it is not physically realistic to have only three fixed moisture conditions in a catchment, but CN method is not a physically based method, instead it is an empirical method. Several recommendations have been made in the past regarding the selection of AMC based on antecedent cumulative rainfall (Hope and Schulze 1982; Schulze 1982), but some later studies (Mishra and Singh 2006) have shown that the existing criteria of calculating AMC from the cumulative rainfall of the previous 5 days is unrealistic.

Similar was the case in the current research work where the sensitivity test showed that the runoff volume was significantly influenced by the CN and AMC, but there was no apparent relationship between the CN and the cumulative rainfall of the previous days, base flow or flow peak. Hence, a constant AMC II was used in TELEMAC-2D and the model was calibrated for CN instead. HEC-RAS 2D does not have an option to choose AMCs, so only CN values (distributed based on land use -land cover) were calibrated similar to that in TELEMAC-2D. Moreover, since each event had varying antecedent rainfall events with different characteristics, intensity, duration, and distribution, it was necessary to calibrate the CN values individually for each event selected for this study.

4.1.4 Comparison of the two HDRR models

For the single- storm short-duration rainfall-induced flood events, CN method was used in both the HDRR models. When the same roughness and CN values were used in both the models, a lower runoff volume and peak flow were calculated in HEC-RAS 2D. One potential explanation for the disparity in results for identical CN and Manning's roughness values could be the steep slope correction implemented in TELEMAC-2D. The steep correction increases the CN value based on the slope observed at the specific location which means lower infiltration and higher runoff volume. To obtain an equally good runoff volume in HEC-RAS 2D, the mesh- resolution (David and Schmalz 2021) and CN values were increased, and to get correct peak timing, the roughness values were increased compared to

TELEMAC-2D.

In HEC-RAS 2D, when the mesh resolution was too coarse, a significant amount of water was trapped in the grid cells (Hall 2015). This was also observed by David and Schmalz (2021) in their HEC-RAS 2D RoG study, which concluded that the coarser the mesh resolution, the higher the volume retention in the catchment. Large grid cells don't catch the terrain details well. Water in a grid cell can only flow out through the edges, and with a fine grid, there are more flow paths for water to move out. But with a large cell, the edges of the cells may end up slightly higher than the actual terrain within the cell trapping water inside. This trapped water resulted into lower runoff volume and smaller flow peak in HEC-RAS 2D. This problem was solved by introducing a finer mesh and breaklines in the steep sections of the catchment.

Inundation area and water depth results obtained in Paper 3 from both the HDRR models were almost similar, but HEC-RAS 2D tended to produce higher velocities in the steep sections of the river. The reason behind this could be pushing the application of HEC-RAS beyond its recommended limits in this study, particularly considering that the river slope exceeds 20-degree threshold, recommended in the HEC-RAS 2D user manual (Brunner 2020).

Both the HDRR models also showed a slightly steeper rising limb than the observed hydrograph. It was also observed in a study by (Vu et al. 2015), where the best agreement for inundation area between the simulated and observed was for the peak flow, not for the pre- and post- peak flow time. Pilotti et al. (2020) also observed a slightly steeper rising limb and early peak of the hydrograph for their 2D hydraulic dam-break analysis using HEC-RAS 2D and TELEMAC-2D, which aligns with the findings of this study. However, they noted a gentler recession limb compared to the observed data.

In most of the simulated cases, the recession limb of the hydrograph, was underestimated by both the models, which was also observed in some previous studies (Hall 2015; Costabile et al. 2021; Ali 2024). Possible reasons for this could be infiltrated water is permanently lost from the model and cannot resurface and contribute to the hydrograph in later stages of flood. The second reason could be the large mesh size (100m) used in the catchment, where small streams and channel would connect and drain into the main river, but are not captured and represented in the large grid cells (Hall 2015).

4.1.5 Long-duration multi-storm flood events

TELEMAC-2D model with CN infiltration method could not produce satisfactory results for long-duration multi-peak flood events in Paper 2. Therefore, an-

other HDRR model, HEC-RAS 2D with the CN and GAR infiltration methods was tested in Paper 3 as an alternative approach to simulate such events. But the results showed that none of the models could correctly simulate all the peaks and the sustained flow between the peaks in a long-duration flood event.

In theory, the GAR method should be able to address the limitations of the CN method, as it is designed to recover the infiltration capacity during dry periods. On the other hand, the steep catchment used in this study has shallow soils that contain a return flow component, which is not taken into account in TELEMAC-2D nor in HEC-RAS 2D. Since, these hydraulic models permanently loose the infiltrated water and do not simulate the subsurface return flow, the infiltrated water cannot contribute to the runoff on a later stage as sustained flow between two flow peaks of the hydrograph. This is also one of the reason to have a underestimated falling limb of the flow hydrograph (Hall 2015).

In reality, infiltrated water in shallow soils contributes significantly to runoff (Scanlon et al. 2000). Therefore, introducing a delay mechanism that can allow the infiltrated water to resurface and contribute to runoff between two precipitation events can address this issue. This is precisely what the soil routine of the HBV model does, where a retention delay follows the release of water from the soil routine to the runoff to mimic the dynamics of subsurface water. In HBV model, the subsurface water, stored in the soil routine, is available for future time-steps, ensuring a continued runoff generation throughout the entire event (Bergström 1975). In contrast, the infiltrated water is lost in both the HDRR models and can not contribute to the runoff as delayed flow which limits their ability to correctly reproduce long-duration flood events.

4.1.6 Uncertainties

A famous quote by eminent statistician George E. P. Box "Essentially, all models are wrong, but some are useful." encapsulates the inherent uncertainty present in models, emphasizing that while no model can fully capture the complexity of reality, some models can still provide valuable insights and utility despite their imperfections. The results obtained in this research work also associated with various sources of uncertainty. The most pertinent and extensively researched sources of uncertainty in hydrologic-hydraulic modelling include multiple aspects (Teng et al. 2017). Some examples are: the selection of model structures, as highlighted by Apel et al. (2009), as well as the determination of model parameters such as roughness (Beven and Binley 1992; Pappenberger et al. 2005), model inputs such as precipitation, land-cover data, soil type and soil-depth data, terrain, bathymetry and boundary conditions etc. (Abily et al. 2016).

For analysing the snowmelt contribution in this research, the snow routine in HBV was used to pre-process the input precipitation for the two HDRR models. The good fit between the observed and simulated runoff in HBV model confirms the reliability of the calculated snowmelt as input to the RoG- HDRR models. However, in complex mountainous regions like western Norway, it is challenging to obtain the correct spatial and temporal distribution of precipitation from gauge stations, radar dataset, or high-resolution interpolated data sets, as the complex terrain strongly influences this pattern (Li et al. 2020) leading to uncertainties in model results. Furthermore, the spatial differences in land-cover, soil type, and soil depth significantly influence the catchment's runoff behavior, impacting infiltration, soil moisture levels, the timing of peak discharge (referred to as lag time), and potentially resulting in multiple peaks in the hydrograph.

Moreover, there are uncertainties related to the large grid cells which have limitations capturing the terrain correctly, initial soil moisture, CN values and GAR parameter because no soil data was available for the study area. Furthermore, constant Manning's roughness with respect to time was used in this study, but usually the roughness changes with change in water depth and steepness (Hinsberger et al. 2022). Therefore, there is uncertainty associated with the model results due to various factors.

4.1.7 Equifinality

During model calibrations, it was observed that various combinations of Manning's friction coefficient and CN values provided acceptable results. This concept is known as equifinality (Beven 2012). Higher initial soil moisture levels, which should produce higher runoff, can be compensated by increasing infiltration (reducing CN values) to get a better fit. This might explain why lower CN values were needed for higher observed runoff during calibration. Similarly, roughness affects water retention in the catchment, and excessive roughness can be balanced with unrealistic CN values. Equifinality can be reduced by using a more physically correct hydrological module that includes soil moisture variability and subsurface flow in hydrodynamic models. A Monte Carlo optimization that includes all parameters might provide a more accurate model, but it can take unrealistically high computational time due to the long hydrodynamic simulations and large variety of parameters in case of GAR infiltration method.

4.2 Contribution to the WoWW project

An effective visualization tool for hazard management is necessary because of the risk posed by flash floods on communities and infrastructure. The methodology employed in this thesis serves as a crucial tool for visualizing the runoff process

and its implications in terms of water depth and velocities. Results generated from the HDRR models provide a foundation for understanding flash floods and are fundamental to comprehensive visualization. Utilizing a distributed model, as implemented in this research, streamlines the visualization process, aligning with the primary focus of the WoWW project on visualization techniques. Although no further efforts were made towards visualization in this study, it lays down the fundamental groundwork for future visualization endeavors and further research within the WoWW project.

Despite the potential of serious gamification in flood hazard management, progress in interactivity remains sluggish due to prolonged simulation times associated with hydrodynamic models. Future research should focus on enhancing interactivity in visualization and reducing simulation run times to facilitate quick analysis of altered scenarios, such as the impact of a damaged infrastructure or bridge in downstream or increased precipitation. The findings from this PhD work provide valuable insights into the visualization of flash floods. Integration of these findings into other work packages of the project can contribute to the creation of comprehensive visualization tools for hazard management.

4.3 General comments

Despite the above mentioned limitations, the methodology used in this research holds potential in simulating the hydrology of a steep catchment and determines the propagation and volume of water throughout the catchment, which is crucial for assessing the damages caused by flash floods. There have been done many studies using the RoG technique (Hariri et al. 2022; Costabile et al. 2022; Zeiger and Hubbart 2021; Hinsberger et al. 2022), but this type of study has not been done before on catchment- scale level in a steep catchment with an average slope of 26 degrees. The HDRR models with RoG technique used in this study provide realistic inflow to any point along the watercourse and is more reliable in identifying critical locations with high potential for local or downstream damages, compared to the traditional hydrological and 2D hydraulic models. This approach satisfies the requirements of the national regulation act, as well as the studies by Kreibich et al. (2009) and Shand et al. (2011) by addressing the combined effects of water depth and velocities. This approach also provides useful information on water velocities, depths, and discharges along watercourses, tributaries, and flooded areas at any given time, making it a useful tool for assessing shear stresses, erosion, sedimentation, and related challenges.

Chapter 5

Conclusions and Recommendations

5.1 Conclusion

This PhD thesis focused on exploring and modelling the hydrology of flash floods in small, steep, snow-covered mountainous catchments. The main goal was to simulate flash floods in a manner that computes both hydrological and hydraulic features at any spot within a catchment in a single simulation. This comprehensive approach aimed to facilitate the identification of critical locations prone to flash flood damage, thereby aiding in the selection of optimal operational methods for mitigation and preparedness.

The results of this work show that the RoG technique is an effective tool to achieve this objective. Single-storm flash flood peaks within small and steep catchments were satisfactorily replicated, along with a comprehensive representation of the flash flood's consequences throughout the entire catchment, in terms of water depths and velocities. The results show that if calibrated for particular event, the HDRR models, such as TELEMAC-2D and HEC-RAS 2D with RoG, can be an efficient tool for estimating realistic design floods and corresponding water depths and velocities along the tributaries, watercourses and in the entire catchment.

Since many flash floods in Norwegian catchments with small watercourses are induced by RoS events, this research identified and simulated the contribution of snowmelt in flash floods by integrating the snow routine from the hydrological model HBV and the RoG technique in the HDRR models. The results indicated that the approach used in this study satisfactorily reproduces single storm floods,

the inflow sources and tributaries throughout the catchment. The results provide crucial information for flood protection at any point along the entire river system in a catchment.

Such a combination can also be used to combine the snowmelt and rain with the hydraulic simulations in rain-on-grid models as demonstrated in Paper 2. In addition, implementing soil routine and snow storage in HDRR models can give a valuable contribution to flash flood mitigation and contingency work because such a combination gives both the hydrology and the hydraulics in the river and the catchment in a continuous operational simulation model.

Both models successfully replicated peak flow for single storm flood events. However, the RoG technique in both the HDRR models was unable to reproduce all peaks in a multi-peak flood event with sustained flow between the peaks, regardless of the choice of CN values and GAR parameters. It was observed that fully integrated hydrodynamic rainfall-runoff modelling with the RoG tool is only suitable for flash floods in small rivers, not for large river floods with long duration events, where a significant amount of water infiltrates. Analysis of plots from this research work suggests that such models are effective in simulating single-storm flood events lasting 10-15 hours or events where infiltrated water percolates into deep groundwater flow without subsurface return flow.

For longer duration single-storm floods, the recession phase of the hydrograph is not accurately simulated, and similarly, for multi-storm events, the tool fails to capture flow dynamics between multiple storms. Although sensitivity analysis of the GAR parameters in multi-storm events yielded expected results, none of the HDRR models with CN or GAR infiltration methods could simulate this accurately. This limitation is primarily due to the absence of a soil routine module capable of accounting for delayed subsurface water contribution to the resulting flow hydrographs. Future work should focus on incorporating a subsurface water routine into HDRR models. Nonetheless, the results from the HDRRM comparison study in Paper 3 can be used by engineers and researchers to select appropriate models among the available hydrodynamic rainfall-runoff models, specifically those tailored for steep catchments and river systems using the rain-on-grid technique.

The findings of this PhD work offer significant implications for flood risk management, infrastructure planning, and risk and vulnerability analysis for flash floods. The research serves as a valuable resource for contingency planners and crisis managers by facilitating the identification of critical areas for people, buildings, and infrastructure during floods. Furthermore, it offers an enhanced tool for regional planners and infrastructure owners to conduct more thorough risk and vulnerab-

ility analyses. Decision-makers can leverage these insights to formulate optimal socioeconomic solutions for adapting to climate change scenarios. With an expected increase in flash floods due to short-duration, high-intensity precipitation events, the models and methodology used in this work hold direct relevance in future climate change impact assessments.

5.2 Recommendations for future work

In this doctoral study, a fully integrated hydrologic-hydraulic model using Rain-on-Grid technique was tested in TELEMAC-2D and HEC-RAS 2D, using distributed precipitation as input. The main aim was to simulate the hydrology of flash floods and their hydraulic consequences. Although the study successfully achieved its objectives, recommendations for future work are outlined as follows:

- A significant drawback associated with using the RoG technique in the HDRR models is the permanent loss of infiltrated water, which ideally should remain within the model as the subsurface flow and contribute to the overall flow. This limitation can be overcome by incorporating a subsurface model in conjunction with the existing infiltration model in the HDRR models. This approach ensures that the infiltrated water is retained and effectively contributes to the hydrodynamic processes.

- In this study, a separate hydrologic model, HBV, was used to calculate the rainfall and snowmelt from the raw precipitation data, which partially deviates from the objective of utilizing a fully integrated hydrologic-hydraulic model. Incorporating a snow routine within the RoG- HDRR models could reduce the overall processing time and avoid the necessity of a separate hydrologic model for its snow module and its calibration.

- It is recommended to compare the inundation maps obtained in this study with observed inundation maps to further validate and verify the calculated flooded area. Further research could also focus on collecting observed inundation data and validating models to improve the predictive capabilities of flood inundation models in similar catchments.

- Further investigation is needed to understand the factors affecting CN values and their suitability for specific storms. This can involve analyzing the influence of base flow and precipitation on antecedent moisture conditions to improve model accuracy. Additionally, future research could investigate an infiltration setup applicable to all flood events in a catchment and identify a single parameter set specific to that catchment for forecasting purposes.

- Manning's roughness used in this study does not vary with water-depth. Therefore, additional investigation is needed to determine the suitability of the Manning's equation and roughness values for the extremely shallow water depths in HDRRM simulations.
- Hydrodynamic simulations tend to be highly time-consuming. Hence, it is imperative to consider implementing automatic calibration for these models to enhance time efficiency and to make the process less cumbersome. Additionally, an alternative approach could involve optimizing the hydrodynamic models to be compatible with GPUs or high-power computers, thereby significantly reducing simulation run-time.

Paper 1

Simulation of flash flood peaks in a small and steep catchment using rain-on-grid technique

Nitesh Godara, Oddbjørn Bruland, Knut Alfredsen

Published: Journal of Flood Risk Management (24 April 2023).

Received: 29 December 2021 | Revised: 9 September 2022 | Accepted: 10 December 2022

DOI: 10.1111/jfr3.12898

ORIGINAL ARTICLE

CIWEM Chartered Institution of Water and Environmental Management | Journal of Flood Risk Management | WILEY

Simulation of flash flood peaks in a small and steep catchment using rain-on-grid technique

Nitesh Godara | **Oddbjørn Bruland** | **Knut Alfredsen**

Department of Civil and Environmental Engineering, Norwegian University of Science and Technology, 7491 Trondheim, Norway

Correspondence
Nitesh Godara, Department of Civil and Environmental Engineering, Norwegian University of Science and Technology, 7491 Trondheim, Norway.
Email: nitesh.godara@ntnu.no

Abstract

The frequency of extreme events is increasing as the consequences of climate change. In steep terrains, flash floods with high-flow velocities induce erosion and sedimentation with potentially disastrous changes of flood path. Hence, the analysis of flash floods in steep terrains in terms of inundation area and flow-velocity to identify critical points becomes more important. The output of a flood simulation with a traditional hydrologic model provides the flood hydrograph which must be combined with a hydraulic model for downstream consequences. In small and steep catchments, the inflow contribution from every section of the water course can be important to determine where critical conditions may arise. In this study, rain-on-grid technique in the hydraulic model Telemac-2D is used to simulate flash-flood peaks with spatially distributed precipitation as input in a small and steep catchment in western Norway. Seven events were simulated and sensitivity tests on parameters were conducted. A 200-year design flood was simulated to show the potential consequences in the catchment. The results show that calibrated models can satisfactorily reproduce peak flows and produce relevant information about water velocities and inundation which decision makers can use for mitigation measures. The paper explores the benefits and limitations through a description of model construction, calibration, and test of sensitivities.

KEYWORDS

hydrological modelling, rainfall-runoff modeling, TELEMAC-2D, hydraulic modelling, climate change adaption

1 | INTRODUCTION

The frequency and severity of extreme events are increasing as the consequences of climate change (Costache et al., 2022; Seneviratne et al., 2021). According to the World Meteorological Organization (WMO, 2021), floods are the third largest hazard in terms of human losses (58,700 deaths) and second largest in terms of economic losses (US$115 billion). Among all the flooding types, flash floods are one of the most disastrous natural hazards causing significant loss of life and economy throughout the world and Europe (Adnan et al., 2019; Gaume et al., 2009; Hu et al., 2018; Merz et al., 2021; Saharia et al., 2017; Trigo et al., 2016; Zhai et al., 2021). Hence, the analysis of flash floods is crucial to predict and prevent their consequences. Such studies are also necessary

for the development of decision support tools for efficient flood mitigation works and for planning infrastructure against flash flood damages, the design of hydraulic structures (Kayan et al., 2021) and watershed management. Flash floods are usually triggered by heavy rainfall events in a short period or/and contribution from sudden snow melt because of high temperature or/and rainfall on the snow (Zhai et al., 2021). The catchment response time is even shorter in small and steep mountainous catchments (Bruland, 2020) as compared to the larger and flatter catchments. Small catchments are frequently affected by flash floods (Bryndal et al., 2017) specially when the slope is also high (Costache et al., 2021). The high precipitation intensity in such catchments leads to extreme peak flows and high flow velocities (Jia et al., 2018) sometimes causing landslides due to high shear stresses (Moraru et al., 2021). Flash foods can lead to erosion and sedimentation which can cause the river channels to change its path (Roald, 2019). Hence, the current study focuses on the flash flood analysis in small and steep catchments.

The impact is enhanced by human activities such as concretizing of the natural soil decreasing its water retention capacity, settlement in flood plains changing land cover and land use (Boithias et al., 2017). Damages due to flash floods are not only dependent on the rainfall intensity and duration, catchment and water course properties also play a significant role (Merz et al., 2010). Water velocities, erosion, and sedimentation can cause severe problems which need to be addressed in areal and infrastructure planning (Kreibich et al., 2009). Shand et al. (2011) focuses on the safety of people and vehicles in a floodplain. Their study shows that the product of water velocities and water depth should be between 0.4 and 0.7 m^2/s to keep pedestrians and vehicles safe, respectively. Smith (1994) presents a relation between critical velocity and depth for building failure. The Norwegian Building Acts and Regulations (DiBK, 2017) includes a paragraph saying that if the product of water velocities and water depth exceeds 2 m^2/s, the risk level is higher compared to other areas. Hence, it is important to analyze both the response of the catchment and the river to understand floods and their consequences and how to implement this in societal planning.

Most of the hydraulic models need to have a hydrograph from a hydrologic model as a boundary condition to assess flood damages. Whereas most of the traditional hydrologic models only give the hydrographs as an output commonly at the outlet of the catchment, but do not present the consequences of those peaks such as the velocity, water depths, and shear stresses along the water course. If hydrologic and hydraulic models can be integrated in an efficient way, it can be the solution to assess catchment response and hydraulic impacts and thereby the consequences of floods. Many studies have loosely coupled the models, also called the offline coupling (Felder et al., 2017; Nguyen et al., 2016), in which the output from the hydrologic model is used as the input to the hydrodynamic model and set as a boundary condition before the hydrodynamic model runs. Therefore, the timely delivery of output from the hydrological model is required to get the hydraulic models running and getting the results in time. Moreover, the offline coupling requires the separate calibration of two models which makes it even more time-consuming (Li et al., 2021). Also, there is the issue of where in the catchment this input boundary condition should be set in the hydraulic model. Sometimes due to many tributaries, more than one boundary condition is required. In addition to this, there is always some residual flow along the river from the catchment or the water from small tributaries which is difficult to estimate and add in the hydraulic model calculations.

To overcome these challenges and to remove the hassle of offline-coupling of the two kinds of model, the direct rainfall method (DRM), also referred as the rain-on-grid (RoG) technique, is used. This technique allows the user to apply the input rainfall directly on the grid cells of a 2D hydraulic model (David & Schmalz, 2020; Hall, 2015). Hall (2015) used RoG on a portion of a 185 km^2 big flat catchment with a grid size of 20 m, and for the rest of the catchment, a traditional hydrological model was used to reduce the total computational time. The study mentions some limitations of using the RoG method, such as shallow flows in the catchment and the Manning's roughness parameters being outside the range of the model for these shallow flows, a strong need for high quality DTM, grid size affecting the flood extent and its magnitude, the flow paths and delayed hydrograph response due to the artificially trapped water in the grids and the high computational time. Zeiger and Hubbart (2021) combined the hydraulic model HEC-RAS (Brunner, 2016) to simulate RoG 2D hydrodynamics at a catchment scale with the SWAT model (Arnold et al., 1998) to get effective rainfall. The results showed that the HEC-RAS model is able to produce realistic simulations of stage hydrograph response when calibrated for each event and highlights the necessity for time-varying friction coefficients to account for the antecedent moisture conditions (AMCs). David and Schmalz (2020) compared the traditional method of coupling hydrological and hydrodynamic models with the RoG approach for flood assessments in a 38 km^2 catchment. They concluded that the traditional approach produced a better hydrograph, but the RoG approach gave more detailed information in many aspects, such as the origin of the

overland flow, its path, and the floodplain. The study also showed that the RoG approach has much lower computational time than the traditional approach of offline coupling of two separate hydrological and hydraulic models. RoG technique has also been applied for analyzing the use of urban streets and pathways as floodways to route the flood water during extreme events (Skrede et al., 2020). One of the limitations of this technique is that it may not be feasible for a very large catchment because of the high computational time of the hydrodynamic simulations.

HEC-RAS has been presented with various RoG implementations (David & Schmalz, 2021; Krvavica & Rubinić, 2020; Rangari et al., 2019; Zeiger & Hubbart, 2021). In addition, there are several other studies presenting models using RoG such as Flood-Area (Tyrna et al., 2018), Infoworks ICM v.5.5 (Pina et al., 2016), GUAD-2D (Cea & Rodriguez, 2016), P-DWave (Leandro et al., 2016), FloodMap (Yu & Coulthard, 2015), Sipson/UIM (Chen et al., 2010), CCHE2D (Jia et al., 2018), MIKE Flood (Hall, 2015), TUFLOW/SOBEK (Clark et al., 2008), TELEMAC-2D (Ligier, 2016). In these studies, RoG has been applied in a variety of catchments such as urban and rural catchments of various sizes, spatial resolutions, and the number of cells in the mesh for different purposes. The studies have shown that RoG technique is able to simulate the hydrology of the catchment to determine the total volume of water as well as the propagation of that water simulating the hydraulic features of the river system which are important in the assessment of the flash flood damages. Also, they show that this technique has lower computational time as compared to the traditional offline coupling of the two separate hydrological and hydraulic models. There have been many studies using integrated hydrologic-hydraulic modeling in medium and large sized catchments (Coulthard et al., 2013; Hankin et al., 2019; Li et al., 2021; Saksena et al., 2019) and in urban areas (Skrede et al., 2020; Zhu et al., 2016). However, presently there is a lack of studies using RoG approach for simulating flash flood peaks in small and steep mountainous catchments, as well as studies testing the limitation of the method and the hydraulic modeling in steep terrain and for operational purposes. There is a clear need for a better understanding of such floods in such topographies, their behavior and how to simulate them to predict their consequence. This is important for better climate adaptation to mitigate future events like those seen in Utvik in Norway in 2017 (Bruland, 2020) and in Kvam, Norway in 2012 and 2013 (Aalstad et al., 2014) and in Ahr, Germany in 2021 (Fekete & Sandholz, 2021).

The objectives of this study are (1) to apply RoG technique in small and steep catchments for reproducing high peak flows and analyze the response of such catchments, and (2) to test and evaluate if the open-source hydrodynamic model TELEMAC-2D can be efficiently used for this purpose and to predict the following water velocities and inundated areas. We show the suitability of this model for fully integrated hydrologic-hydraulic modeling in small mountainous catchments. It has the advantages of both types of models and reduced simulation time as compared to traditionally offline coupled models. The TELEMAC-2D model is used to compute the flood hydrograph and see the corresponding hydraulic effects and a traditional rainfall-runoff model is used to set the baseflow for the TELEMAC-2D simulations.

2 | MATERIALS AND METHODS

2.1 | Study area and input data

There have been many flash flood events in small and steep catchments of Norway in recent years but most of them are ungauged. The catchment chosen for this study has a potential for extreme flash flood events and is one of the few steep, small and gauged catchments in Norway. The Sleddalen catchment located in Møre og Romsdal county in western Norway (Figure 1). The catchment has an elevation drop of 1379 to 77 m over a catchment length of 4.7 km with a mean slope of 26°. The area of the catchment is 10.5 km^2. The land-cover in the catchment is described in Table 1. Summer and winter precipitation in the catchment is 879 and 1734 mm respectively. The digital elevation model (DEM) for the catchment was downloaded from the Norwegian mapping authority database (www.hoydedata.no) which is based on a topographic LiDAR scan of the area with 10 m × 10 m resolution. Due to non-availability of any nearby precipitation measurement station, precipitation data was extracted from RadPro, a spatially distributed precipitation dataset with 1 km × 1 km resolution based on a merged product of precipitation radar data and gridded precipitation point observations (Engeland et al., 2018). The observed discharge data was downloaded from the database of Norwegian Water Resources and Energy Directorate (www.nve.no) from the station Sleddalen (Station ID: 97.5.0).

2.2 | Models used

Telemac-2D is originally a 2D hydrodynamic model solving shallow water equations. Later versions of

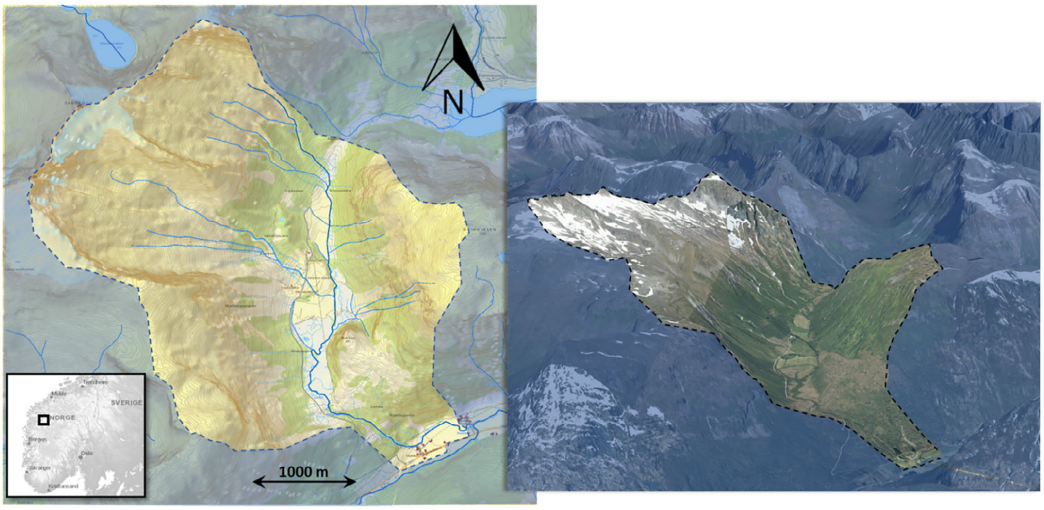

FIGURE 1 Map of study area (left) and aerial photo indicating steepness of the catchment (right).

TABLE 1 Land cover-land use distribution in the catchment.

Description	Area (km^2)	Area (%)
Bare rock and scarce vegetation	4.89	46.57
Forest	2.63	25.05
Open land	2.10	20.00
Swamp	0.38	3.62
Fully cultivated soil	0.34	3.24
Inland pasture	0.09	0.86
River water	0.04	0.38
Urban area	0.02	0.19
Roads	0.01	0.10

TELEMAC-2D (v8p2) have an option to include a hydrological module with RoG technique (Broich et al., 2019; Ligier, 2016). Thus, TELEMAC-2D can simulate the combined overland and river flow for flash floods. Because of the hydraulic part of the model, it is possible to get the hydrograph at any point at any time in the catchment which is useful in determining where and when the situation will be critical along the water courses during extreme events. The model enables to not only evaluate the runoff from each part of the catchment to the river, but also the velocities and shear stress causing erosion or sedimentation combined with the water depths at any part of the river and the catchment. This gives important hydraulic information to evaluate the cause and consequences of flood events such as those reported by Aalstad et al. (2014), Bruland (2020), and Fekete and Sandholz (2021).

The RoG module uses the SCS-CN curve method for runoff calculation (Equation 1). This method is also known as the Natural Resources Conservation Service (NRCS) CN Method developed by USA's Soil Conservation Services (USDA-SCS, 2004). The CN method was developed to estimate the excess precipitation/direct runoff using the storm rainfall depth. Hydrological processes such as infiltration, groundwater recharge, and recession are not considered in the RoG module in TELEMAC-2D. Thus, the model cannot handle the soil and ground water storage and the runoff can be used best only to simulate the peaks of single storms. The relation between surface runoff and infiltrated or "lost" water depends on a dimensionless parameter, the curve number, which is calculated from the hydrologic soil group, land use and AMC in the catchment (USDA-SCS, 2004).

$$Q = \frac{(P-\lambda S)^2}{(P+S-\lambda S)} \text{ when } P \geq I_a \text{ and } \lambda = \frac{I_a}{S}, \quad Q = 0, \text{ when } P < I_a \tag{1}$$

where Q is the direct runoff depth, P is the event rainfall depth, I_a is initial abstraction or event rainfall required for the initiation of runoff, λ is the initial abstraction ratio and S is a site storage index defined as the maximum possible difference between P and Q. The rainfall-runoff modeling with SCS-CN method in TELEMAC-2D has been previously used with point rainfall (Ata, 2017; Kelly et al., 2018; Ligier, 2016) and spatially distributed rainfall (Broich et al., 2019) with some enhancement in the model

code. In this study, spatially rainfall is implemented as input directly over the grid cells in the entire catchment. The main input data used for the simulation in TELEMAC-2D are DEM, rainfall, bottom friction, and CN value. Spatially distributed friction coefficients and CN values are used for the current study (Table 2). They were calibrated for each event. More than 90% of the catchment is mainly covered by forest, open land, bare rock, and scarce vegetation. Hence, the CN value for only these land covers were calibrated (Table 3, grayed cells) and other were kept constant when the distributed curve numbers were used for the simulations. Since the calibration of TELEMAC-2D is manual and computationally expensive, we also simulated the same events using a single CN value for the entire catchment to see if it can give satisfactory results. Averaged values of CN were also used because the required soil data were not available to calculate the distributed CN values in the catchment, which is the case in many other similar catchments. The land cover data for the catchment was downloaded from the database of Norwegian Mapping Authority (www.kartverket.no). The input files were prepared using Bluekenue software (Barton, 2019). Blukenue (3.3.4) and QGIS (3.16) were used for the post processing of the simulation result files and generating the velocity and water depth graphs.

The default value of initial abstraction ratio ($\lambda = 0.2$) was used inside the model. The mean and maximum slopes in the catchment are 0.5 and 5.2 m/m. Since the catchment is very steep, it was important to consider the effect of steep slope. Hence, the correction for steep slope was applied in TELEMAC-2D as per Equation 2 (Huang et al., 2006). Inside the model, the CN value is adjusted for the steep slope using the formula introduced by Huang et al. (2006):

$$\mathrm{CN(II)}_{\alpha} = \mathrm{CN(II)}\frac{(322.79 + 15.63\alpha)}{(\alpha + 323.52)}, \quad (2)$$

where CN(II) is the CN value for normal antecedent moisture condition (AMC II), α is the terrain slope in m/m and varies from 0.14 to 1.4 m/m. The CN(II) values can be raised by up to 6% for $\alpha = 1.4$ (Ligier, 2016). As TELEMAC-2D does not return the abstracted water to the system, the model is used only to simulate single storm events in this study. For operational use in forecasting and planning, it is necessary to combine the RoG simulation in TELEMAC-2D with another model to get realistic hydrological conditions in the catchment prior to flood events. For this purpose, the rainfall-runoff model HBV (Bergström & Forsman, 1973) was used for the design storm simulation. The HBV model was calibrated to the observed discharge for Sleddalen river using the precipitation data from the gridded timeseries RadPro.

TABLE 2 Manning's roughness coefficients for various areal types in the catchment.

Areal type	Manning's roughness coefficient	Sources
Urban area	0.1	Chow (1959)
Roads	0.02	Garrote et al. (2016)
Fully cultivated soil	0.04	Chow (1959)
Inland pasture	0.259	Van der Sande et al. (2003)
Forest	0.2	Van der Sande et al. (2003)
Open land	0.05	O'Brien and Garcia (2009)
Swamp	0.2	Mtamba et al. (2015)
River water	0.04	Chow (1959)
Bare rock and scarce vegetation	0.02	Garrote et al. (2016)

3 | RESULTS

A total of seven events from the year 2018 to 2021 representing a variety of situations where the quality of precipitation data and runoff data was considered good, were selected for this study (Figure 2). These were used to calibrate the TELEMAC-2D model for different rainfall patterns, base flows and peak flows. The mesh size used for each simulation was 5 m × 5 m for the river up to 100 m × 100 m for the rest of the catchment. Spatially distributed Manning's roughness coefficients and CN values as well as one averaged CN value were used in the catchment. The base flow for each case was set up based on the observed flow. The initialization and evolution of the simulated flood depends on antecedent condition, baseflow, mesh size and roughness, and the CN value. Due to the long computational time, an optimization based on all these parameters was not possible.

3.1 | Hydrodynamic rainfall-runoff modeling in TELEMAC-2D

In the steering file of the TELEMAC-2D simulation, AMC was set to 2 (normal conditions) only. Hence, the CN values were not converted for the different antecedent conditions. Since the 2D hydraulic models were not originally developed for the hydrology of the catchment

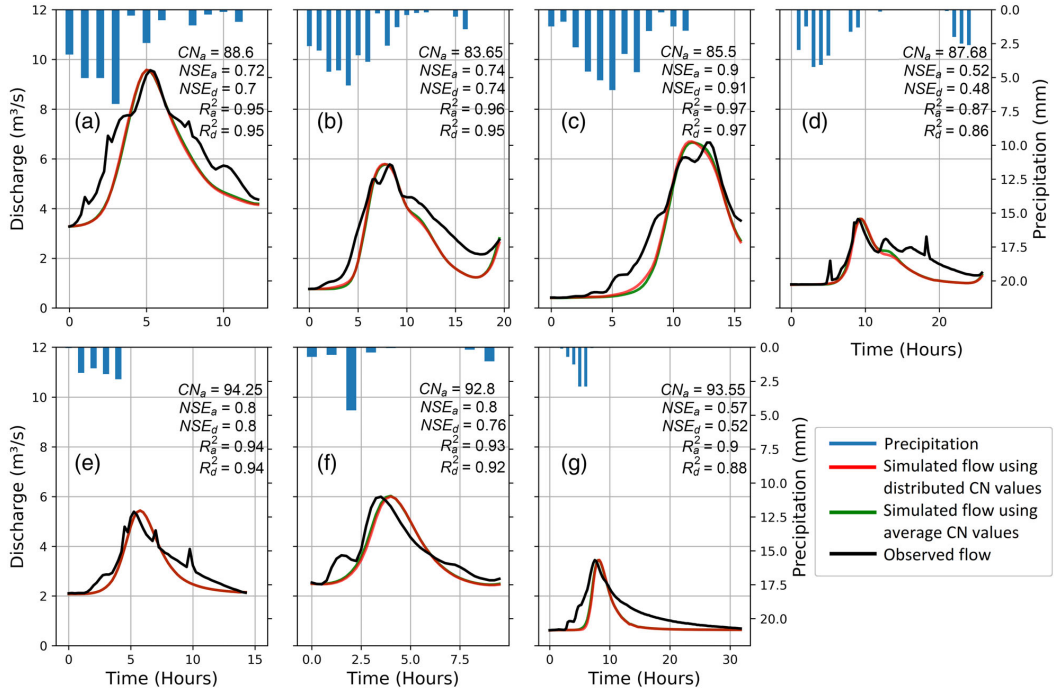

FIGURE 2 Peak flows from rain-on grid simulations in TELEMAC-2D using distributed CN values (red) and using a single averaged CN value (CN_a) (green) compared to observed flow (black), and correlation and Nash Suthcliff model efficiency in case of distributed CN values (R^2_d, NSE_d) and average CN values (R^2_a, NSE_a) corresponding to the seven events selected for the current study.

TABLE 3 Calibrated CN values for each event in Figure 2.

Description	Area (%)	Event 2A	2B	2C	2D	2E	2F	2G
Bare rock and scarce vegetation	46.57	91	87	90	90	97	96	95
Forest	25.05	86	78	74	83	93	92	89
Open land	20.00	83	78	79	81	93	90	88
Swamp	3.62	90	90	90	90	90	90	90
Fully cultivated soil	3.24	90	90	90	90	90	90	90
Inland pasture	0.86	89	89	89	89	89	89	89
River water	0.38	100	100	100	100	100	100	100
Urban area	0.19	89	89	89	89	89	89	89
Roads	0.10	91	91	91	91	91	91	91

and very shallow water depths, some parameters can be more sensitive as compared to the case when the model is used only for the hydraulics of the river which is the original field of application of such models (David & Schmalz, 2021). Hence, it is important to check the effect of the model parameters before using the model. In this study, effects of the following parameters were analyzed from the simulation results: (a) CN value, (b) AMCs in the catchment, (c) mesh resolution, and (d) roughness coefficients.

3.2 | Sensitivity analysis

3.2.1 | Curve number

The sensitivity of various values of CN values from 30 to 100 were tested keeping the values of all the other parameters constant. The values lower than 30 had a negligible effect on the runoff volume, hence was not used to test the sensitivity. The results showed that the runoff volume (Figure 3a) is very sensitive to the CN value.

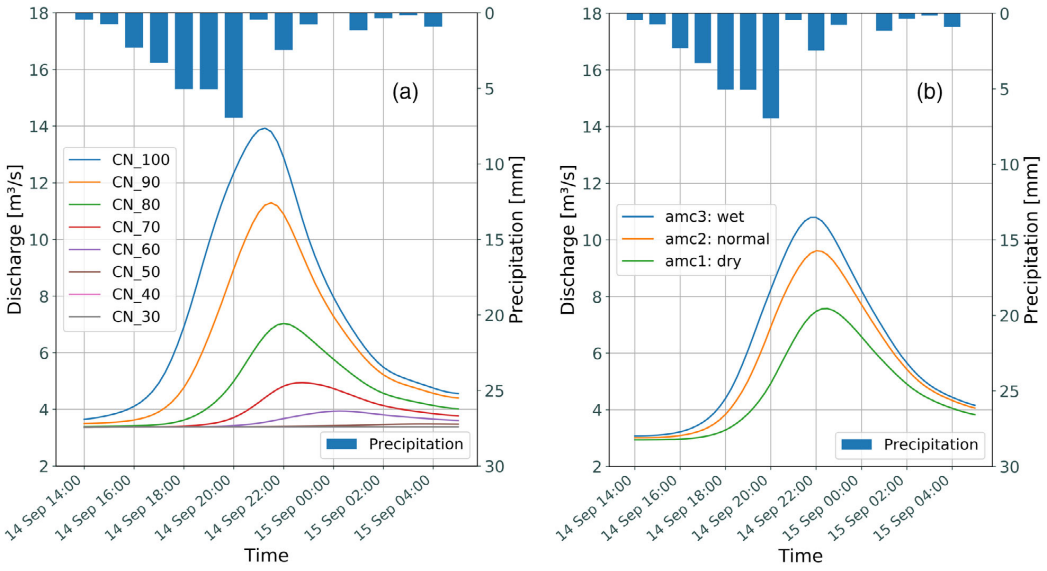

FIGURE 3 Simulated peak flows for the same event where only CN values are varied (a) and where only the antecedent moisture conditions are varied (b).

3.2.2 | Antecedent moisture condition

There is a significant difference in the runoff volume for the three classes of the AMCs (Figure 3b). The formula used for converting CN values for normal AMC to CN values for wet and dry AMC conditions was used as per described by Chow et al. (1988) and Hjelmfelt (1991).

3.2.3 | Roughness

Roughness of the terrain influences the water retained in the catchment and thus it has an influence on the output flood hydrograph. To test the sensitivity to the roughness, the model was tested for different roughness values based on the land use types in the catchment from the literature. The results showed that when the roughness was higher, more water remained in the domain hence less water goes out through the measurement cross-section leading to the reduced the peak of the hydrograph in the hydrograph and vice-versa.

3.2.4 | Mesh resolution

To make the simulations faster, a coarser mesh was used in the hill slopes than in the river. Various mesh sizes for the river and the rest of the catchment were evaluated to check its sensitivity (Table 4). The results showed that the mesh size was an influential parameter for runoff volume. The coarser the mesh resolution, the lower the runoff volume.

TABLE 4 Applied mesh sizes along the river and for the catchment.

Scenario	Mesh size in river	Mesh size in the rest of the catchment
1	3 m × 3 m	5 m × 5 m
2	5 m × 5 m	100 m × 100 m
3	5 m × 5 m	500 m × 500 m
4	10 m × 10 m	500 m × 500 m

Note: Scenario 2 (marked green) is used in the study.

3.3 | Hydrologic modeling in HBV for calculating base flow in TELEMAC-2D simulations

The HBV model was established for Sleddalen catchment and calibrated and run on hourly resolution with the gridded RadPro precipitation data and temperature data from Sleddalen station. The precipitation in each grid cell within the catchment was averaged to the catchment altitudes. The calibration was done for the period with available Radpro data for Sleddalen, September 2018 to

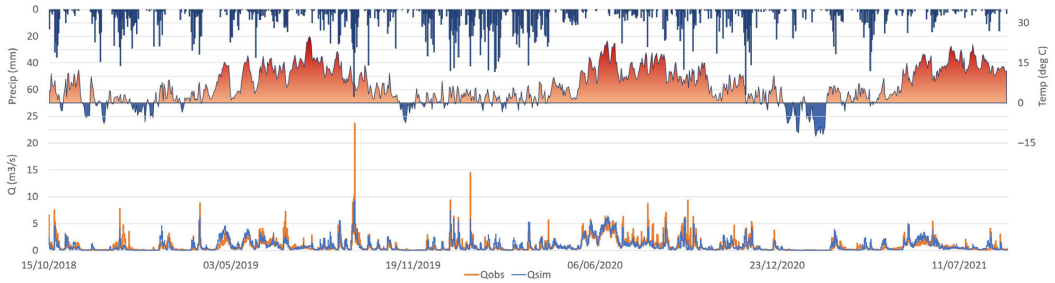

FIGURE 4 Precipitation and temperature input data to the HBV model (upper) and the resulting simulated runoff compared to observed for Sleddalen catchment (lower).

September 2021. The calibration gave a Nash-Suthcliff—R^2 of 0.70. For the validation period from 2013 to 2018, Radpro data was not available and precipitation input was taken from the Met Office's observations at Kroken, Stryn in Norway about 20 km south-southeast of Sleddalen. R^2 for the validation period was 0.51 which is satisfactory considering the less representative precipitation data. As Figure 4 shows the model reproduced the base flow quite well but under-predicted the peak flows, this was the case both in the calibration and the validation period. The inability to catch the peaks is most likely due to higher precipitation intensities in reality than what RadPro and observations shows. Considering the strong topographical variation in the region and the poor density of precipitation observations, a R^2 of 0.7 and even of 0.5 was satisfactory and since the purpose of the HBV model in this study is to get a relevant base flow to initialize TELEMAC-2D, the calibrated model is considered suitable for the purpose.

3.4 | Design storm

The HBV model was also used to find the most critical combination of design storms with different durations and 200 year return period and the preceding conditions to evaluate the dimensioning 200-year flood design flood according to the national regulations (DiBK, 2017). A 200-year design precipitation was constructed for durations from 1 to 24 h using the intensity-duration-frequency curves downloaded from the database of Norwegian Center for Climate Services (NCCS) (klimaservicesenter.no). Six design precipitation cases (60, 120, 180, 360, 720, and 1440 min duration) with total volumes between 20 mm for 1 h and 147 mm for 24 h, were run superimposed over observed data for the period from 2018 to 2021 and a 200-year flood event in this period was found to be between 20 and 25 m^3/s with the HBV model when snow was not present. A duration of

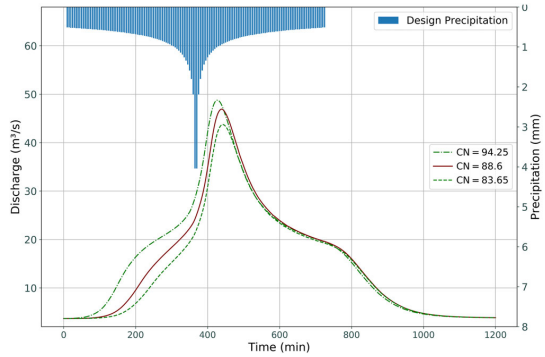

FIGURE 5 200-year design storm runoff from a 12-h design precipitation with a high (94.25), the best fit (88.6), and a low (83.65) curve number (CN) from the calibration to selected events.

between 12 and 24 h gave the highest discharges. The effect of snowmelt was included by using max observed daily average temperature for the simulated day combined with a design precipitation. This combination gave the highest peak flow up to 29 m^3/s. As it is likely that snowmelt can saturate the soils prior to an extreme rain event but not necessarily contribute significantly to the flood, the base flow from the HBV model and AMC prior to this event were used to initialize the design flood simulation in TELEMAC-2D.

The design storm was simulated in TELEMAC-2D using the highest (CN = 94.25), the lowest (CN = 83.65) and the CN value that gave the best fit for the highest observed discharge in the calibration (CN = 88.6) (Figure 5). The resulting hourly maximum discharges ranged from 42 m^3/s for the lowest CN to 46 m^3/s for the highest CN for 12-h duration and from 37 to 39 m^3/s for a 24-h duration. In both the cases, there is a significant difference in the discharge prior to the peak. Higher infiltration at lower CN decreases the discharges in the early stage of the event with between 7 and 10 m^3/s. Figure 6

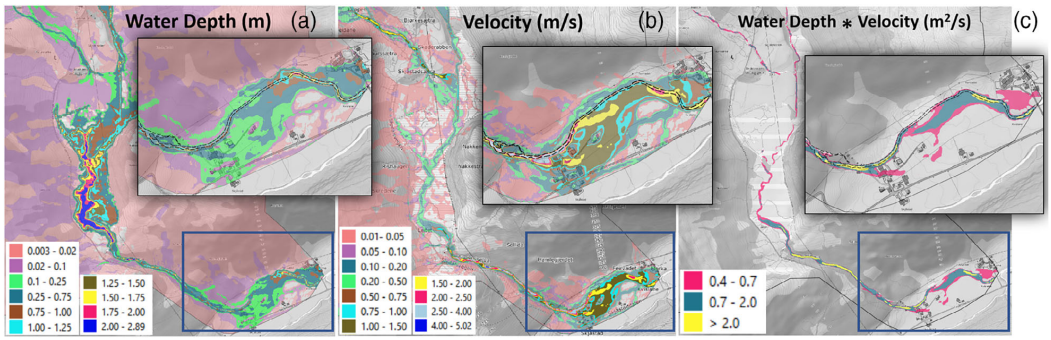

FIGURE 6 Water depth (a) deeper than 0.1 m and velocities (b) higher than 0.25 m/s, and the product of depth and velocity (c) higher than critical levels for pedestrians (0.4 m^2/s), vehicles (0.7 m^2/s), and buildings (2 m^2/s) for the design storm with 200-year return period.

shows the velocity, water depth and the product of depth and velocity in the region of the catchment with the highest damage and consequence potential for the 200-year design storm based on CN = 88.6. The highest velocity is 2.54 m/s, the deepest area is 1.77 m deep and the depth-velocity product is up to 11.32 m^2/s.

4 | DISCUSSION

In this study, we used TELEMAC-2D to simulate flood discharges in a small and steep catchment in Norway. The model was calibrated on seven observed floods and were found to give good results. The results show how the model provides both the peak flood and information relevant for estimation of its consequences in and along the river like flooded areas and critical water velocity. The hydrodynamic model also simulates the residual flow along the river which is usually difficult to estimate in the traditional way of offline coupling of the two separate hydrologic and hydrodynamic models. The current study shows the development of source areas and facilitates the user to extract the runoff hydrograph at any point in the catchment at any time-step unlike the traditional hydrologic model or hydrodynamic model with one source input.

4.1 | Curve number

The calibration results indicate that the CN increases with decreasing flood size in contradiction to what could be expected (Hjelmfelt, 1991). This can be explained by an increasing CN reducing the simulated infiltration and compensating for the lack of subsurface discharge of infiltrated water to the river. At higher discharges, this compensation is less important as in reality a relatively smaller portion of the discharge originates from infiltrated water. This also influences the simulation of the recession limb (e.g., Figure 2d,h) and the duration and total volume of water in the floods. In turn, this can lead to underestimation of consequences caused by longer duration and higher volumes such as increased erosion and sedimentation volumes, more severe inundation and potential shifts of river course. As the purpose in this study is to investigate and demonstrate the use of RoG to extract important hydraulic properties of floods in a water course related to the peak discharges, the simulation of the recession is considered less important.

The CN method is a widely used method mainly because of its simplicity and because it is based on one parameter. There have been developed many tables in National Engineering Handbook (Section-4) (NEH-4) (USDA-SCS, 2004) for determining CN value for various hydrologic soil groups, land use land covers, and AMCs. Due to limited knowledge about soil covers in the catchment, only one value of CN for the entire catchment was used at first to capture the flow peaks, and because the tabulated CN values have been shown to be inadequate to get the correct runoff volume in many cases (Mishra & Singh, 2006), CN values were calibrated in this study. Nevertheless, there are a wide range of soil covers in the catchment ranging from deep soils to mountainous areas with non or very shallow soil covers, and a more realistic runoff from the catchment is likely if a good relation between these soil covers, CN value and antecedent soil moisture conditions were found and applied. Since this is a small catchment, we were able to calibrate the model using distributed CN values in a reasonable time. This would not be possible in a large catchment because of high computational time.

Another problem with the traditional formula by Chow et al. (1988) and Hjelmfelt (1991) is that there is a sudden jump in the CN while converting it from one

AMC level to another. Mishra and Singh (2006) showed that the exiting criteria of calculating AMC from the cumulative rainfall of the previous 5 days is unrealistic. Some studies have suggested the previous 15 days (Hope & Schulze, 1982) and previous 30 days (Schulze, 1982) of antecedent cumulative rainfall for humid areas and previous 5 days cumulative rainfall in case of arid areas. There was a need for individual calibration for each event because each event had different antecedent rainfall events with different intensities, duration, and distribution. Hence, the CN was calibrated for each event in this study, as also done by Zeiger and Hubbart (2021) in their study. The test of sensitivity shows that the CN and AMC are very critical factors influencing the runoff volume but there was no clear relationship found between the CN and the cumulative rainfall of previous 5-day, base flow or the flow peak in the current study. To investigate this significantly more simulations for more events should be done, but due to the long simulation time this was not conducted in this study. However, in further investigation, the factors which affect the CN value and how to choose a CN value for a particular storm including the impact of base flow and precipitation on the AMC should be studied.

4.2 | Design storm

A 200-year flood was simulated to demonstrate a practical use of the coupling between a continuous hydrological model and RoG in TELEMAC-2D. As AMC and initial base flow are highly important for the simulated peak flow in TELEMAC-2D and since this cannot be simulated realistically by the RoG implementation in TELEMAC-2D, it is necessary to combine TELEMAC-2D with a calibrated hydrological model that provides realistic initial conditions for operational use and to estimate design flood properties. For this purpose, the HBV model was used. The duration giving the highest peak flow was found to be between 12 and 24 h and with total precipitation volumes of 107 and 147 mm respectively.

The HBV model gave an hourly peak discharge of 29 m^3/s while the TELEMAC-2D model with the same initial conditions gave a peak discharge up to 47 m^3/s. Compared to the observations, the HBV model underestimated the peak discharges while TELEMAC-2D simulated a value closer to the peak discharges. There is a difference of up to 10% between the peak flows simulated by the different CN. Even though this is within the uncertainty for flood peak calculations, the calibration indicates that a lower CN gives a better fit at higher flows and thus in these situations a lower CN is probably more realistic than the highest. The combination between the HBV-model and TELEMAC-2D increases the simulation efficiency and gives more reliable results. A closer coupling between these models would allow for continuous hydrological and hydraulic simulation that have the advantage of integrating antecedent ground and moisture conditions to the flood event (Tsegaw et al., 2020).

4.3 | Roughness

In the current study, distributed values of roughness are used in the catchment. Based on initial values from Chow (1959), the manning numbers can be adjusted to get a better fit of the peaks similar to several previous studies (Garrote et al., 2016; Kalyanapu et al., 2009; Mtamba et al., 2015; Shen et al., 2017; van der Sande et al., 2003). But by doing this, the friction values can possibly become too high for some of the events at shallow water depths (Hall, 2015). It can cause a significant portion of water to get trapped in the domain and even increased CN values will not compensate for this.

4.4 | Mesh resolution

The result of the analysis shows that the mesh resolution can also control the outflow volume. The coarser the mesh resolution, the lower the runoff volume. The use of finer mesh resolution made the simulations computationally more expensive. High performance multi-core super computers can decrease the time for computationally expensive hydrodynamic simulations, but TELEMAC-2D is not compatible for GPU yet, hence, it can only be run on one CPU. The benefit of using coarser mesh was that the computational time was decreased many-fold. But there are some limitations of using a coarser mesh. The flow generated from the rainfall migrates downstream by solving the shallow water equations in the hydrodynamic model. Here, the water depths are too shallow on the flat and large cells of 100 m $\times$ 100 m before this water joins a stream. The manning's friction coefficient is often too large for these shallow water depths that water at these depths get trapped in the roughness and thus affect the actual water-flow propagation time. Neither does a course grid represent the true geometry of the catchment, and this might also cause more water to stay in the domain showing lower peaks as compared to simulations where finer mesh is used. This needs to be considered while planning the model. The results show that the mesh resolution is one of the controlling factors for outflow volume. These results are in coherence with the results from the study by Clark et al. (2008) where it was

shown that the model results were very sensitive to the changes in grid-sizes.

4.5 | Equifinality

During the calibration process of the events, it was found that different combinations of the Manning's friction coefficient and CN gave equally acceptable results as well as the different combinations of the spatially distributed CN values. This phenomenon, called equifinality, is addressed by Beven (2012). High initial moisture conditions (high AMC) which hydrologically should give high discharge can be compensated with a high infiltration (low CN) reducing the runoff to get a good fit. This effect is probably the explanation for the calibration giving lower CN at higher observed runoff. Similarly, the roughness influences retention of water in the catchment and too high roughness can be compensated with unrealistically high CN. An improved and more physically correct hydrological module including soil moisture variability and subsurface outflow in TELEMAC-2D could possibly reduce the challenging equifinality in this case. Also, a Monte Carlo optimization including all the parameters could give a more physically correct model. Due to the long simulation time this was not achievable in this study.

Despite the limitations mentioned above, the procedure used in the paper still serves the purpose of simulating the hydrology of such a steep catchment to determine the volume of water as well as the propagation of that water simulating the hydraulic features of the river system which are important in the assessment of the flash flood damages. Similar study has not been done yet as per our knowledge in such a small and steep catchment having an average slope of 26°. RoG model like demonstrated here, gives realistic inflow to any point along the water course and will be a more realistic approach for identifying critical locations where a flood has high potential for creating local or downstream damages as compared to a traditional hydraulic or hydrological model alone. It also provides water velocities and depth along the water courses, in tributaries and in the inundated areas at any time in addition to the discharges. This feature makes it a suitable tool for assessing the erosion and sedimentation during a flood and related challenges (Moraru et al., 2021) and thus, the combined effect of water depth and velocities as addressed in the national regulation act (DiBK, 2017), by Kreibich et al. (2009) and by Shand et al. (2011).

The results can be used by planners and decision makers for optimizing mitigation measures and to get correct dimensioning criteria for infrastructure and areal planning. The results can also be helpful for contingency people to be better prepared beforehand the extreme events with better and more precise flood forecasting including the scenarios for local consequences and potential mitigation measures to reduce the damages during the event.

5 | CONCLUSION

This study focuses on an approach to reproduce the flash flood peaks in small and steep mountainous catchments together with representing the consequences of the flash flood in the entire catchment in terms of water depths and high velocities. This is important knowledge in areal and infrastructure planning processes, for optimizing mitigation measures and for adapting to the climate changes. TELEMAC-2D model is used in the current study as an integrated hydrologic-hydrodynamic toolbox. The rainfall was directly applied as input over the entire catchment which is called DRM or RoG technique. A total of seven events caused by rainfall of different characteristics were reproduced for the high flows during the summers of the years 2018 to 2021. The results show a good correlation between the observed and simulated flood peaks with correlation coefficient (R^2) ranging from 0.97 to 0.87. Combined with the HBV-model, it is shown that TELEMAC-2D can be an efficient tool for estimating realistic design floods and their corresponding water depths and velocities along the water course, in the tributaries and in the entire catchment. Such results will provide a tool for contingency planner and crisis management for identification of critical locations for people, buildings and infrastructure during a flood, a better tool for areal planners and infrastructure owners in their risk and vulnerability analysis and for decision makers to identify the optimal socio-economic solution in the societal adaptation to climate change scenarios.

DATA AVAILABILITY STATEMENT

The data that support the findings of this study are available from the corresponding author upon reasonable request.

ORCID

Nitesh Godara https://orcid.org/0000-0003-2906-3649

REFERENCES

Aalstad, G. H., Berg, H., & Helgaas, G. (2014). *The flood protection concept in Kvam, Norway. 1*, 2–3.

Adnan, M. S. G., Dewan, A., Zannat, K. E., & Abdullah, A. Y. M. (2019). The use of watershed geomorphic data in flash flood susceptibility zoning: A case study of the Karnaphuli and Sangu

river basins of Bangladesh. *Natural Hazards*, *99*(1), 425–448. https://doi.org/10.1007/s11069-019-03749-3

Arnold, J. G., Srinivasan, R., Muttiah, R. S., & Williams, J. R. (1998). Large area hydrologic modeling and assessment part I: Model development. *JAWRA Journal of the American Water Resources Association*, *34*(1), 73–89. https://doi.org/10.1111/J.1752-1688.1998.TB05961.X

Ata, R. (2017). *Telemac2d user manual. Version 7.2*.

Barton, A. J. (2019). Blue Kenue enhancements from 2014 to 2019. https://doi.org/10.5281/zenodo.3611511

Bergström, S., & Forsman, A. (1973). *Sveriges Meteorologiska och Hydrologiska Institut Development of a conceptual deterministic rainfall - runoff model*.

Beven, K. (2012). Rainfall-runoff modelling. In *Rainfall-runoff modelling*. Wiley. https://doi.org/10.1002/9781119951001

Boithias, L., Sauvage, S., Lenica, A., Roux, H., Abbaspour, K. C., Larnier, K., Dartus, D., & Sánchez-Pérez, J. M. (2017). Simulating flash floods at hourly time-step using the SWAT model. *Water (Switzerland)*, *9*(12), 1–25. https://doi.org/10.3390/w9120929

Broich, K., Pflugbeil, T., Disse, M., & Nguyen, H. (2019). Using TELEMAC-2D for hydrodynamic modeling of rainfall-runoff. *XXVIth Telemac & Mascaret User Club, October*.

Bruland, O. (2020). How extreme can unit discharge become in steep Norwegian catchments? *Hydrology Research*, *51*(2), 290–307. https://doi.org/10.2166/nh.2020.055

Brunner, G. W. (2016). *HEC-RAS river analysis system 2D modeling user's manual*.

Bryndal, T., Franczak, P., Kroczak, R., Cabaj, W., & Kołodziej, A. (2017). The impact of extreme rainfall and flash floods on the flood risk management process and geomorphological changes in small Carpathian catchments: A case study of the Kasiniczanka river (Outer Carpathians, Poland). *Natural Hazards*, *88*(1), 95–120. https://doi.org/10.1007/s11069-017-2858-7

Cea, M., & Rodriguez, M. (2016). Two-dimensional coupled distributed hydrologic–hydraulic model simulation on watershed. *Pure and Applied Geophysics*, *173*(3), 909–922. https://doi.org/10.1007/s00024-015-1196-5

Chen, A. S., Djordjević, S., Leandro, J., & Savić, D. A. (2010). An analysis of the combined consequences of pluvial and fluvial flooding. *Water Science and Technology*, *62*(7), 1491–1498. https://doi.org/10.2166/wst.2010.486

Chow, V. T. (1959). Open channel hydraulics. In *Open channel hydraulics*. Elsevier.

Chow, V. T., Maidment, D. R., & Mays, L. W. (1988). *Applied_Hydrology_Chow_1988.pdf*. (pp. 1–294). http://ponce.sdsu.edu/Applied_Hydrology_Chow_1988.pdf

Clark, K., Ball, J., & Babister, K. (2008). Can fixed grid 2 hydraulic models be used as hydrologic models? *Proceedings of Water Down Under*, *2008*, 2496–2507.

Costache, R., Barbulescu, A., & Pham, Q. (2021). Integrated framework for detecting the areas prone to flooding generated by flash-floods in small river catchments. *Water*, *13*(6), 758. https://doi.org/10.3390/w13060758

Costache, R., Tin, T. T., Arabameri, A., Crăciun, A., Costache, I., Islam, A. R. M. T., Sahana, M., & Pham, B. T. (2022). Stacking state-of-the-art ensemble for flash-flood potential assessment. *Geocarto International*, *1–27*, 13812–13838. https://doi.org/10.1080/10106049.2022.2082558

Coulthard, T. J., Neal, J. C., Bates, P. D., Ramirez, J., de Almeida, G. A. M., & Hancock, G. R. (2013). Integrating the LISFLOOD-FP 2D hydrodynamic model with the CAESAR model: Implications for modelling landscape evolution. *Earth Surface Processes and Landforms*, *38*(15), 1897–1906. https://doi.org/10.1002/esp.3478

David, A., & Schmalz, B. (2020). Flood hazard analysis in small catchments: Comparison of hydrological and hydrodynamic approaches by the use of direct rainfall. *Journal of Flood Risk Management*, *13*(4), 1–26. https://doi.org/10.1111/jfr3.12639

David, A., & Schmalz, B. (2021). A systematic analysis of the interaction between rain-on-grid-simulations and spatial resolution in 2d hydrodynamic modeling. *Water (Switzerland)*, *13*(17), 2346. https://doi.org/10.3390/w13172346

DiBK. (2017). *Veiledning om tekniske krav til byggverk* (TEK17, Issue July). https://dibk.no/regelverk/byggteknisk-forskrift-tek17

Engeland, K., Abdella, S. Y., Azad, R., Arrturi Elo, C., Lussana, C., Tadege Mengistu, Z., Nipen, T., & Randriamampianina, R. (2018). Use of precipitation radar for improving estimates and forecasts of precipitation estimates and streamflow. *20th EGU General Assembly, In EGU General Assembly Conference Abstracts*, 12207.

Fekete, A., & Sandholz, S. (2021). *Here comes the flood, but not failure? Lessons to learn after the heavy rain and pluvial floods in Germany 2021 science-based support to the Sendai framework for disaster risk reduction view project INCREASE: Inclusive and integrated multi-hazard risk man*. https://doi.org/10.3390/w13213016

Felder, G., Zischg, A., & Weingartner, R. (2017). The effect of coupling hydrologic and hydrodynamic models on probable maximum flood estimation. *Journal of Hydrology*, *550*, 157–165. https://doi.org/10.1016/j.jhydrol.2017.04.052

Garrote, J., Alvarenga, F. M., & Díez-Herrero, A. (2016). Quantification of flash flood economic risk using ultra-detailed stage–damage functions and 2-D hydraulic models. *Journal of Hydrology*, *541*, 611–625. https://doi.org/10.1016/j.jhydrol.2016.02.006

Gaume, E., Bain, V., Bernardara, P., Newinger, O., Barbuc, M., Bateman, A., Blaškovičová, L., Blöschl, G., Borga, M., Dumitrescu, A., Daliakopoulos, I., Garcia, J., Irimescu, A., Kohnova, S., Koutroulis, A., Marchi, L., Matreata, S., Medina, V., Preciso, E., … Viglione, A. (2009). A compilation of data on European flash floods. *Journal of Hydrology*, *367*(1–2), 70–78. https://doi.org/10.1016/j.jhydrol.2008.12.028

Hall, J. (2015). Direct rainfall flood modelling: The good, the bad and the ugly. *Australian Journal of Water Resources*, *19*(1), 74–85. https://doi.org/10.7158/13241583.2015.11465458

Hankin, B., Metcalfe, P., Beven, K., & Chappell, N. A. (2019). Integration of hillslope hydrology and 2D hydraulic modelling for natural flood management. *Hydrology Research*, *50*(6), 1535–1548. https://doi.org/10.2166/nh.2019.150

Hjelmfelt, A. T. (1991). Investigation of curve number procedure. *Journal of Hydraulic Engineering*, *117*(6), 725–737. https://doi.org/10.1061/(ASCE)0733-9429(1991)117:6(725)

Hope, A. S., & Schulze, R. E. (1982). Improved estimates of storm-flow volumes using the SCS curve number method. In V. P. Singh (Ed.), *Rainfall-runoff relationships* (pp. 419–431). Water Resources Publications.

Hu, P., Zhang, Q., Shi, P., Chen, B., & Fang, J. (2018). Flood-induced mortality across the globe: Spatiotemporal pattern and

influencing factors. *Science of the Total Environment*, *643*, 171–182. https://doi.org/10.1016/j.scitotenv.2018.06.197

Huang, M., Gallichand, J., Wang, Z., & Goulet, M. (2006). A modification to the soil conservation service curve number method for steep slopes in the Loess Plateau of China. *Hydrological Processes*, *20*(3), 579–589. https://doi.org/10.1002/hyp.5925

Jia, Y., Shirmeen, T., Locke, M. A., Lizotte, R. E., Jr., & Douglas Shields, F., Jr. (2018). Simulation of surface runoff and channel flows using a 2D numerical model. In *Soil erosion - rainfall erosivity and risk assessment*. IntechOpen. https://doi.org/10.5772/intechopen.80214

Kalyanapu, A. J., Burian, S. J., & McPherson, T. N. (2009). Effect of land use-based surface roughness on hydrologic model output. *Journal of Spatial Hydrology*, *9*, 2. https://scholarsarchive.byu.edu/josh/vol9/iss2/2

Kayan, G., Riazi, A., Erten, E., & Türker, U. (2021). Peak unit discharge estimation based on ungauged watershed parameters. *Environmental Earth Sciences*, *80*(1), 1–10. https://doi.org/10.1007/s12665-020-09317-4

Kelly, D. M., Ata, R., & Li, Y. (2018). Modification of TELEMAC 2D for storm surge use. *The XXVth TELEMACMASCARET User Conference*, 4–10. https://hdl.handle.net/20.500.11970/105193

Kreibich, H., Piroth, K., Seifert, I., Maiwald, H., Kunert, U., Schwarz, J., Merz, B., & Thieken, A. H. (2009). Is flow velocity a significant parameter in flood damage modelling? *Natural Hazards and Earth System Science*, *9*(5), 1679–1692. https://doi.org/10.5194/nhess-9-1679-2009

Krvavica, N., & Rubinić, J. (2020). Evaluation of design storms and critical rainfall durations for flood prediction in partially urbanized catchments. *Water (Switzerland)*, *12*(7), 2044. https://doi.org/10.3390/w12072044

Leandro, J., Schumann, A., & Pfister, A. (2016). A step towards considering the spatial heterogeneity of urban key features in urban hydrology flood modelling. *Journal of Hydrology*, *535*, 356–365. https://doi.org/10.1016/j.jhydrol.2016.01.060

Li, Z., Chen, M., Gao, S., Luo, X., Gourley, J. J., Kirstetter, P., Yang, T., Kolar, R., McGovern, A., Wen, Y., Rao, B., Yami, T., & Hong, Y. (2021). CREST-iMAP v1.0: A fully coupled hydrologic-hydraulic modeling framework dedicated to flood inundation mapping and prediction. *Environmental Modelling and Software*, *141*(April), 105051. https://doi.org/10.1016/j.envsoft.2021.105051

Ligier, P. (2016). *Implementation of a rainfall-runoff model in TELEMAC-2D*. https://hdl.handle.net/20.500.11970/104541

Merz, B., Blöschl, G., Vorogushyn, S., Dottori, F., Aerts, J. C. J. H., Bates, P., Bertola, M., Kemter, M., Kreibich, H., Lall, U., & Macdonald, E. (2021). Causes, impacts and patterns of disastrous river floods. *Nature Reviews Earth & Environment*, *2*(9), 592–609. https://doi.org/10.1038/s43017-021-00195-3

Merz, B., Kreibich, H., Schwarze, R., & Thieken, A. (2010). Review article "assessment of economic flood damage.". *Natural Hazards and Earth System Science*, *10*(8), 1697–1724. https://doi.org/10.5194/nhess-10-1697-2010

Mishra, S. K., & Singh, V. P. (2006). A relook at NEH-4 curve number data and antecedent moisture condition criteria. *Hydrological Processes*, *20*(13), 2755–2768. https://doi.org/10.1002/hyp.6066

Moraru, A., Pavlíček, M., Bruland, O., & Rüther, N. (2021). The story of a Steep River: Causes and effects of the flash flood on 24 July 2017 in Western Norway. *Water*, *13*(12), 1688. https://doi.org/10.3390/W13121688

Mtamba, J., van der Velde, R., Ndomba, P., Zoltán, V., & Mtalo, F. (2015). Use of Radarsat-2 and Landsat TM images for spatial parameterization of Manning's roughness coefficient in hydraulic modeling. *Remote Sensing*, *7*(1), 836–864. https://doi.org/10.3390/rs70100836

Nguyen, P., Thorstensen, A., Sorooshian, S., Hsu, K., AghaKouchak, A., Sanders, B., Koren, V., Cui, Z., & Smith, M. (2016). A high resolution coupled hydrologic–hydraulic model (HiResFlood-UCI) for flash flood modeling. *Journal of Hydrology*, *541*, 401–420. https://doi.org/10.1016/j.jhydrol.2015.10.047

O'Brien, J. S., & Garcia, R. (2009). FLO-2D Reference manual. www.flo-2d.com, 595.

Pina, R. D., Ochoa-Rodriguez, S., Simões, N. E., Mijic, A., Marques, A. S., & Maksimović, Č. (2016). Semi- vs. fully-distributed urban stormwater models: Model set up and comparison with two real case studies. *Water (Switzerland)*, *8*(2), 58. https://doi.org/10.3390/w8020058

Rangari, V. A., Umamahesh, N. V., & Bhatt, C. M. (2019). Assessment of inundation risk in urban floods using HEC RAS 2D. *Modeling Earth Systems and Environment*, *5*(4), 1839–1851. https://doi.org/10.1007/s40808-019-00641-8

Roald, L. A. (2019). *Floods in Norway*. https://publikasjoner.nve.no/rapport/2021/rapport2021_01.pdf

Saharia, M., Kirstetter, P.-E., Vergara, H., Gourley, J. J., Hong, Y., & Giroud, M. (2017). Mapping flash flood severity in the United States. *Journal of Hydrometeorology*, *18*(2), 397–411. https://doi.org/10.1175/JHM-D-16-0082.1

Saksena, S., Merwade, V., & Singhofen, P. J. (2019). Flood inundation modeling and mapping by integrating surface and subsurface hydrology with river hydrodynamics. *Journal of Hydrology*, *575*, 1155–1177. https://doi.org/10.1016/j.jhydrol.2019.06.024

Schulze, R. E. (1982). The use of soil moisture budgeting to improve stormflow estimates by the SCS curve number method. In *University of Natal, Department of Agricultural Engineering, Report 15, Pietermaritzburg*.

Seneviratne, S. I., Zhang, X., Adnan, M., Badi, W., Dereczynski, C., Di Luca, A., Ghosh, S., Iskandar, I., Kossin, J., Lewis, S., Otto, F., Pinto, I., Satoh, M., Vicente-Serrano, S. M., Wehner, M., & Zhou, B. (2021). *IPCC - climate change 2021: The physical science basis - chapter 11: Weather and climate extreme events in a changing climate* (p. 1610). Cambridge University Press. https://doi.org/10.1017/9781009157896.013

Shand, T., Smith, G., Cox, R., & Blacka, M. (2011). Development of Appropriate Criteria for the Safety and Stability of Persons and Vehicles in Floods. *Proceedings of the 34th World Congress of the International Association for Hydro- Environment Research and Engineering: 33rd Hydrology and Water Resources Symposium and 10th Conference on Hydraulics in Water Engineering, Brisbane, Australia, 26 June–1 J...*, 9.

Shen, Y., Goodall, J. L., & Chase, S. B. (2017). Method for rapidly assessing the overtopping risk of bridges due to flooding over a large geographic region. *JAWRA Journal of the American Water Resources Association*, *53*(6), 1437–1452. https://doi.org/10.1111/1752-1688.12583

Skrede, T. I., Muthanna, T. M., & Alfredesen, K. (2020). Applicability of urban streets as temporary open floodways. *Hydrology Research*, *51*(4), 621–634. https://doi.org/10.2166/NH.2020.067

Smith, D. I. (1994). Flood damage estimation-a review of urban stage-damage curves and loss functions. *Water SA*, *20*(3), 231–238. https://hdl.handle.net/10520/AJA03784738_1124

Trigo, R. M., Ramos, C., Pereira, S. S., Ramos, A. M., Zêzere, J. L., & Liberato, M. L. R. (2016). The deadliest storm of the 20th century striking Portugal: Flood impacts and atmospheric circulation. *Journal of Hydrology*, *541*, 597–610. https://doi.org/10.1016/j.jhydrol.2015.10.036

Tsegaw, A. T., Thomas Skaugen, K. A., & Muthanna, T. M. (2020). A dynamic river network method for the prediction of fl oods using a parsimonious rainfall-runoff model Aynalem Tassachew Tsegaw, Thomas Skaugen, Knut Alfredsen. *Hydrology Research*, *51*, 146–168. https://doi.org/10.2166/nh.2019.003

Tyrna, B., Assmann, A., Fritsch, K., & Johann, G. (2018). Large-scale high-resolution pluvial flood hazard mapping using the raster-based hydrodynamic two-dimensional model FloodArEaHPC. *Journal of Flood Risk Management*, *11*, S1024–S1037. https://doi.org/10.1111/jfr3.12287

USDA-SCS. (2004). Part 630 Hydrology National Engineering Handbook Chapter 10 estimation of direct runoff from storm rainfall. In *National Engineering Handbook*. USDA-NRCS (United States Department of Agriculture-Natural Resources Conservation Service).

van der Sande, C. J., de Jong, S. M., & de Roo, A. P. J. (2003). A segmentation and classification approach of IKONOS-2 imagery for land cover mapping to assist flood risk and flood damage assessment. *International Journal of Applied Earth Observation and Geoinformation*, *4*(3), 217–229. https://doi.org/10.1016/S0303-2434(03)00003-5

WMO. (2021). Water-related hazards dominate disasters in the past 50 years. https://public.wmo.int/en/media/press-release/water-related-hazards-dominate-disasters-past-50-years

Yu, D., & Coulthard, T. J. (2015). Evaluating the importance of catchment hydrological parameters for urban surface water flood modelling using a simple hydro-inundation model. *Journal of Hydrology*, *524*, 385–400. https://doi.org/10.1016/j.jhydrol.2015.02.040

Zeiger, S. J., & Hubbart, J. A. (2021). Measuring and modeling event-based environmental flows: An assessment of HEC-RAS 2D rain-on-grid simulations. *Journal of Environmental Management*, *285*(February), 112125. https://doi.org/10.1016/j.jenvman.2021.112125

Zhai, X., Zhang, Y., Zhang, Y., Guo, L., & Liu, R. (2021). Simulating flash flood hydrographs and behavior metrics across China: Implications for flash flood management. *Science of the Total Environment*, *763*(142), 977. https://doi.org/10.1016/j.scitotenv.2020.142977

Zhu, Z., Oberg, N., Morales, V. M., Quijano, J. C., Landry, B. J., & Garcia, M. H. (2016). Integrated urban hydrologic and hydraulic modelling in Chicago, Illinois. *Environmental Modelling & Software*, *77*, 63–70. https://doi.org/10.1016/j.envsoft.2015.11.014

How to cite this article: Godara, N., Bruland, O., & Alfredsen, K. (2023). Simulation of flash flood peaks in a small and steep catchment using rain-on-grid technique. *Journal of Flood Risk Management*, e12898. https://doi.org/10.1111/jfr3.12898

Paper 2

Modelling flash floods driven by rain-on-snow events using rain-on-grid technique in the hydrodynamic model TELEMAC-2D

Nitesh Godara, Oddbjørn Bruland, Knut Alfredsen

Published: Water (13 November 2023).

water

MDPI

Article

Modelling Flash Floods Driven by Rain-on-Snow Events Using Rain-on-Grid Technique in the Hydrodynamic Model TELEMAC-2D

Nitesh Godara *, Oddbjørn Bruland and Knut Alfredsen

Department of Civil and Environmental Engineering, Norwegian University of Science and Technology, 7491 Trondheim, Norway; oddbjorn.bruland@ntnu.no (O.B.); knut.alfredsen@ntnu.no (K.A.)
* Correspondence: nitesh.godara@ntnu.no

Abstract: Due to the changing climate, flash floods have been increasing recently and are expected to further increase in the future. Flash floods caused by heavy rainfall with snowmelt contribution due to sudden rises in temperature or rain-on-snow events have become common in autumn and winter in Norway. These events have caused widespread damage, closure of roads and bridges, and landslides, leading to evacuations in the affected areas. Hence, it is important to analyze such events. In this study, the rain-on-grid technique in the TELEMAC-2D hydrodynamic model was used for runoff modelling and routing using input of snowmelt, and precipitation partitioned on snow and rain was calculated via the hydrological model HBV. The results show the importance of including snowmelt for distributed runoff generation and how the rain-on-grid technique enables extracting flow hydrographs anywhere in the catchment. It is also possible to extract the flow velocities and water depth at each time step, revealing the critical locations in the catchment in terms of flooding and shear stresses. The rain-on-grid model works particularly well for single peak events, but the results indicate the need for a time-varying curve number for multiple peak flood events or the implementation of another infiltration model.

Keywords: hydrology; extreme events; small and steep catchments; snowmelt; hydraulic modelling

Citation: Godara, N.; Bruland, O.; Alfredsen, K. Modelling Flash Floods Driven by Rain-on-Snow Events Using Rain-on-Grid Technique in the Hydrodynamic Model TELEMAC-2D. *Water* **2023**, *15*, 3945. https://doi.org/10.3390/w15223945

Academic Editor: Paolo Mignosa

Received: 30 September 2023
Revised: 5 November 2023
Accepted: 9 November 2023
Published: 13 November 2023

1. Introduction

Flood events, which generally happen within a time of less than 6 h [1], are categorized as flash floods. Due to warming climates, flash floods have become more frequent and severe over the last few years, and following the climate scenarios, this trend is expected to increase in the future [2–4]. Flash floods lead to river erosion [5] because of high stream power and shear stresses and the deposition of sediments [6] in downstream reach. The unusually heavy rainfall and flash flood events can also lead to debris flow [7], debris slides, and landslide events in the wet season. Moreover, snowmelt at higher altitudes infiltrating the ground can lead to landslides, especially along small and steep rivers [8]. Both the hindcast and forecast of the occurrence and consequences of such flood events are challenging and become more difficult in complex topography with complex temporal and spatial characteristics of precipitation. Rain-on-snow events lead to an additional effect, including snowmelt, resulting from an energy balance, which is a challenge to model in itself.

Rain-on-snow (RoS) events are complex processes on and within a snowpack because of the combined effect of rainfall and snowmelt on snow-covered ground [9]. At higher latitudes and altitudes, snow cover and RoS events can be expected throughout the year [10]. Such events have caused several widespread floods in central and northeastern Europe [11,12], Germany [13], and Switzerland [12]. The importance of snow cover in the winter season and its melting for flash floods in Europe is also documented by Uhlemann et al. [14] and Gvoždíková and Müller [15]. Furthermore, there have been cases of

floods triggered by just RoS events in many other countries such as in several regions of the USA [16–18] and Canada [19]. These examples show how disastrous the increasing temperatures and combined rain and snowmelt floods can be [20]. There is a potential for even higher temperatures, more intense snowmelt and an increase in RoS events in coming years [21], and this development is more pronounced at higher latitudes [22,23], leading to more frequent and severe floods, snow avalanches [24,25], and landslides [26,27]. Hence, it is important to analyze these combined rain and snowmelt-induced flash floods.

Usually, large RoS floods occur at the end of the winter season when the rivers already have high flows prior to snowmelt or in the early winter season caused by alternating snowfalls, heat spells, snowmelt, and rainfall events [28]. In the latter conditions, even moderate rainfall events on a relatively thin but evenly distributed snow layer can cause large flash floods. Sui and Koehler (2001) investigated the characteristics of the runoff generated via such events in various catchments in forest regions of Southern Germany. Their study concludes that the extreme peak flow values were higher in the winter season because of the snowmelt contributions, even though the average and extreme daily rainfalls in the winter were less than the rainfalls in summer. The spatial and seasonal variability of RoS events is also altitude dependent. A study by Surfleet and Tullos [29] indicated a decreasing frequency of high-flow RoS in low and middle altitudes while increasing frequency at higher altitudes due to increasing temperatures in the future. According to Blöschl et al. [30], RoS events produce larger floods than expected, but when, how, and why these events produce exceptional runoffs is still one of the main unsolved problems in hydrology.

Snowmelt is a slow runoff-generating process, and a snow cover can dampen the effect of rainfall; thus, RoS flood events can be expected to have a different propagation of flash floods than the flash floods occurring due to torrential rain alone [24]. Li et al. [31] quantified the runoff contribution of RoS into extreme floods using the VIC hydrologic model for simulating a snow water equivalent (SWE) and calculated the runoff over the entire catchment. In their study, the catchment was divided into five elevation bands and 12 vegetation tiles. To the best of our knowledge, there are no investigations on the combined effect of hydrology and hydraulics on the causes and consequences of flash flood events resulting from rainfall with significant contribution of snowmelt, particularly in steep catchments.

A traditional hydrologic model typically generates a hydrograph at the outlet of the catchment, and it gives no information about the hydraulic characteristics such as river routing, water velocities and water depths. In contrast, a hydraulic model provides information on these hydraulic characteristics but relies on input from a hydrologic model for boundary conditions. Rain-on-grid (RoG) implementations in hydraulic models [32,33] combine hydrologic and hydraulic modelling to route the runoff through the entire catchment. Thus, rather than defining boundary conditions to add inflow to the river system as in a traditional hydraulic model, RoG models enable the simulation of the discharge and hydraulics in any tributary in addition to their inflow contribution to the main river. Furthermore, this property of RoG models adds valuable information to the analysis of critical locations in the river system where water velocities, depth, and sediment load can cause serious consequences. However, this technique lacks hydrological processes like snowmelt, soil, and groundwater storage, and thus, it is dependent on correct initial conditions and snowmelt input. Therefore, the snowmelt contribution to the flash floods needs to be estimated and added to the rainfall before using a rain-on-grid hydrodynamic model.

Many Norwegian counties have suffered considerable damage to the infrastructure such as roads and houses from flash floods in small and steep water courses [34]. Hence, the study area chosen for this research work is a small and steep catchment, which has the potential for disastrous flash floods. In this study, we consider catchments smaller than 50 km^2 with rivers steeper than 2–3% as small and steep catchments. The objective of the current study is to model high peak flows caused by RoS events, where substantial snowmelt plays a significant role in flood generation. Therefore, we combine the output

from the snow routine in a hydrologic model with a rain-on-grid implementation in an HDRRM module of a hydrodynamic model. The primary goal of this integration is to facilitate an in-depth analysis of the outcomes of flash flood events triggered by RoS events and subsequently utilize the findings to identify critical locations within the catchment concerning flooding and the extent of damage following a flash flood event. To achieve this, we have incorporated the snow routine from the hydrologic model HBV [35] and integrated it with the rain-on-grid HDRRM module from the TELEMAC-2D model (v8p2) [36].

2. Materials and Methods

2.1. Study Area and Input Data

A small and steep catchment, Sleddalen, in Møre og Romsdal county in western Norway, was selected for this study (Figure 1). The catchment is 10.5 km^2, with altitudes ranging from 77 to 1379 masl and an average slope of 0.5 m/m. Half of the catchment is covered by bare rock and scarce vegetation, while the other half is mainly covered by forest and open land. The catchment has snow-covered mountains for most of the year except for a few weeks in late summer. Digital terrain model (DTM) with a spatial resolution of 0.5 m × 0.5 m was downloaded from the Norwegian mapping authority database (hoydedata.no).

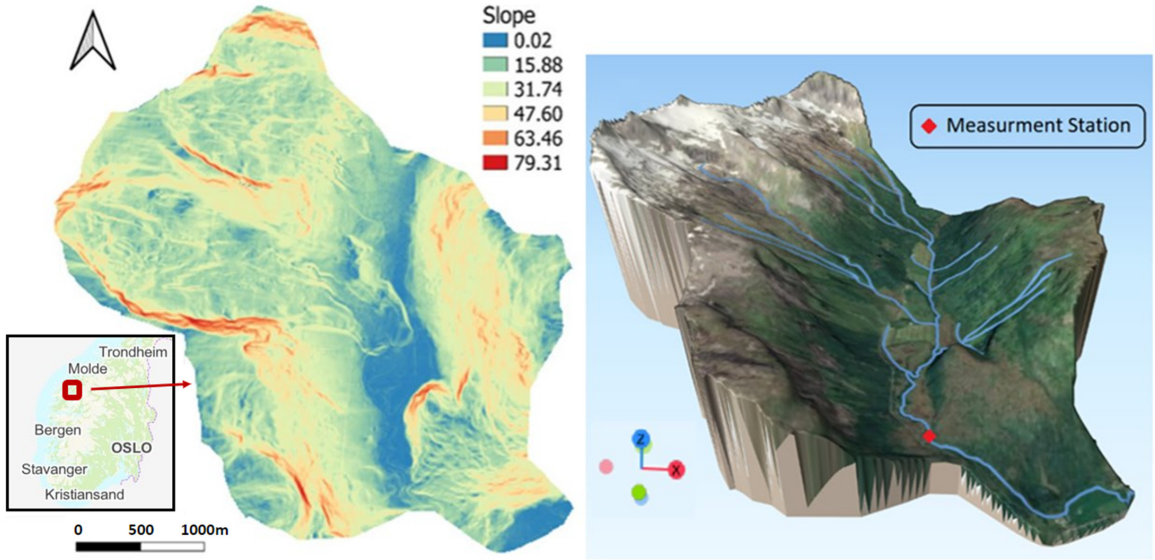

Figure 1. Location of the study area in Norway along with the catchment slope in degrees (**left**) and a picture showing the steepness, vegetation cover and the discharge and temperature measurement stations in the area (**right**).

Seven peak flow events (A to G in Figure 2) from 2018 to 2022, all caused by rainfall with RoS events, were selected for the current study. Distributed precipitation data with 1 km × 1 km spatial and 1 hour temporal resolution was extracted for the catchment from the RadPro dataset from the Norwegian meteorological departments (https://www.met.no/en/projects/radpro, last accessed on 20 October 2023). RadPro is a merged product of gridded point observations and radar precipitation data [37]. Measured discharge data with 15 min temporal resolution and air temperature data with hourly resolution were downloaded for the Sleddalen measurement station (ID: 97.5.0) from Norwegian Water Resources and Energy Directorate (NVE) database available at 'sildre.nve.no' (Figure 2).

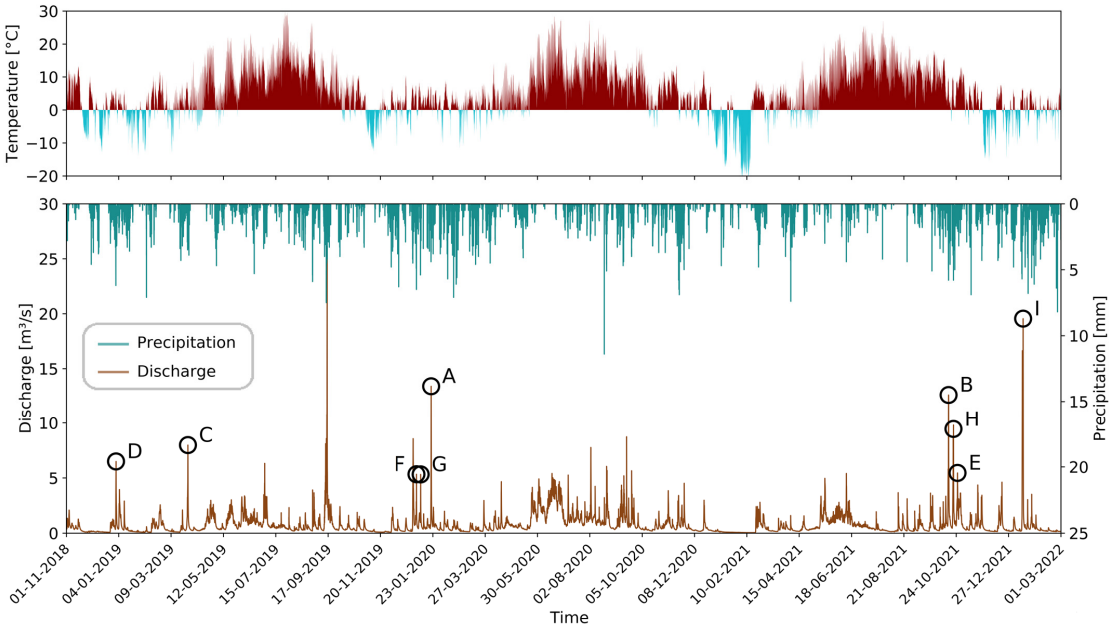

Figure 2. Time series with hourly temporal resolution from November 2018 to March 2022 showing observed discharge, precipitation, temperature, the seven single peak events (A to G), and two longer flood events with multiple peaks (H and I) selected for this study.

2.2. Methods and the Combination of Snow Routine with Integrated Hydrologic–Hydraulic Model

In a catchment with high altitude ranges, precipitation can occur both as rain and snow in the same timestep at different altitudes, but the snowfall does not contribute to runoff before the snow melts. The Radpro precipitation dataset does not distinguish between rain and snow. Therefore, we used HBV snow routine [35] to compute the snowmelt. The snow routine (Figure 3) calculates precipitation type and the snowmelt based on the precipitation and temperature dataset. The HBV model divides the catchment into ten equally sized elevation zones and calculates air temperature and amount and type of precipitation in each zone depending on the temperature gradients, precipitation gradients, and the threshold temperature (T_x) for snowfall [38]. The model keeps track of the accumulated snow storage in each of the elevation zones and calculates snowmelt (Equation (1)) when the temperature at the respective elevation bands is higher than the threshold for snowmelt (T_s). The snowmelt is calculated with an intensity depending on the degree day factor (C_x) and air temperature (T_a) above a snowmelt threshold temperature.

$$M = C_x(T_a - T_s) \quad (1)$$

where M is the snowmelt given in mm/h, C_x is the degree day factor in mm/h °C, T_a is the air temperature in °C, and T_s is the threshold temperature for snowmelt in °C. Parameters T_x and C_x are calibrated for each event. The observed temperature and precipitation are adjusted to each elevation zone according to the lapse rate for temperature (dry or wet adiabatic) and precipitation (Figure 3e). Snowfall occurs at temperatures below a snowfall threshold temperature (Figure 3a,e). Lapse rates, threshold temperatures, and the degree-day factor are calibrated to fit discharge from simulated snowmelt events to observed and simulated snow storage to actual snow storage (exhausted at the end of summer). The snow routine also accounts for accumulation of liquid water in the snow and, thus, the delayed rain and snowmelt–water output from the snowpack [39].

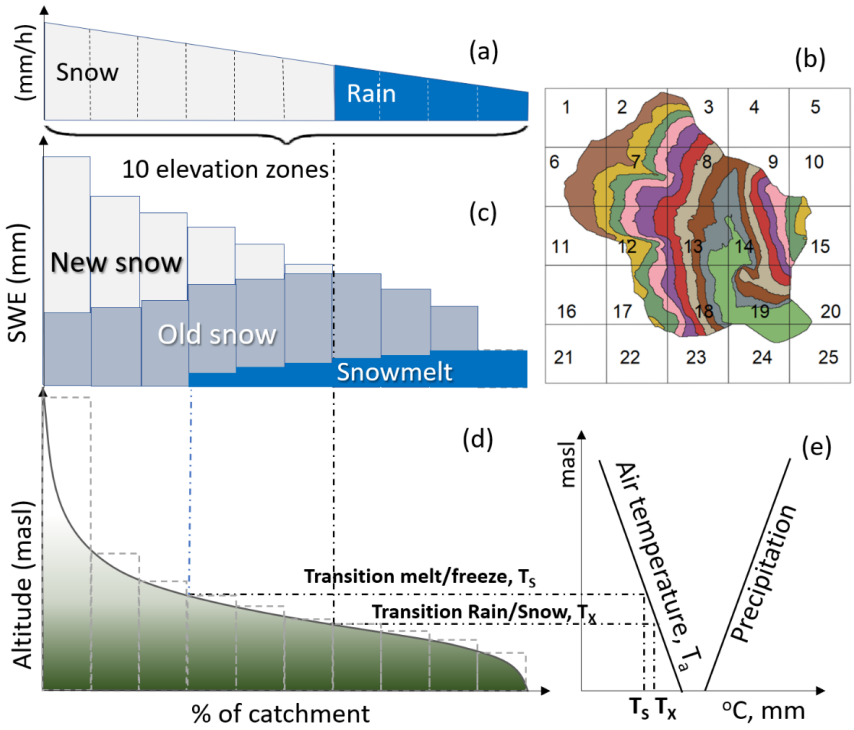

Figure 3. Snow routine in the HBV model with (**a**) hourly precipitation input in the form of rain and snow defined by (**e**) the temperature and precipitation gradients, threshold values and intensities from (**b**) the RadPro grid cells (also showing the elevation zones), (**c**) resulting accumulated new and old snow and snowmelt, (**d**) Hypsographic curve of the catchment with the ten elevation zones.

The model was run on hourly resolution with precipitation calculated to the elevation zone from the 1 km × 1 km spatially distributed RadPro precipitation data (Figure 3b) and locally observed temperature data from the Sleddalen station. The HBV model was calibrated for a three-year period (2018–2021) to evaluate the overall performance, but since the purpose of this study was to evaluate the effect of snow melt in a RoG model, a calibration was also performed for each of the specific events used in this case to obtain the snowmelt as precise as possible. Better calibration of the snow routine in HBV ensures the correct precipitation input to the HDRRM. The snowmelt values and the liquid precipitation for each timestep and elevation zone were extracted from the HBV snow routine and averaged into each grid cell in the HDRRM module of TELEMAC-2D model [36]. The flow chart for this methodology is shown below in Figure 4.

TELEMAC-2D is used as an integrated hydrological–hydraulic model (aka HDRRM) in this study. It is originally a hydrodynamic model that focuses on two-dimensional depth-averaged free surface water flows and relies on the Saint Venant equation. This software (v8p2) is designed to simulate free-surface dynamics within a two-dimensional horizontal spatial framework. At each node or point within the computational grid, T2D computes parameters such as water depth and two velocity components. A finite element mesh is incorporated to enhance the precision in representing details like rivers, embankments, and roads. Additionally, there is a parallel version available, enabling the model to operate efficiently on multi-processor computers. The model's calculation sub-routines are scripted in Fortran-90 and Python. Users have the flexibility to customize the code to suit their specific needs. The source code of T2D model is customized in this study to use spatially distributed precipitation as input from a previous study [40]. The main

inputs required are DTM, roughness values, and boundary conditions such as water flow or water surface elevation. The code in T2D model simultaneously solves the following hydrodynamic equations:

(a) Continuity equation:

$$\frac{\partial h}{\partial t} + u \cdot \nabla(h) + h div(u) = S_h$$

(b) Momentum equation along x:

$$\frac{\partial u}{\partial t} + u \cdot \nabla(u) = -g \frac{\partial Z}{\partial x} + S_x + \frac{1}{h} div(h\, v_t \nabla u)$$

(c) Momentum equation along y:

$$\frac{\partial v}{\partial t} + u \cdot \nabla(v) = -g \frac{\partial Z}{\partial y} + S_y + \frac{1}{h} div(h\, v_t \nabla v)$$

where the equations are given here in Cartesian coordinates;

h (m) = water depth;
u, v (m/s) = velocity components;
g (m/s^2) = gravity acceleration;
v_t (m^2/s) = momentum coefficient;
Z (m) = free surface elevation;
t (s) = time;
x, y (m) = horizontal space coordinates;
S_h (m/s) = source or sink of fluid;
h, u, and v are the unknowns.

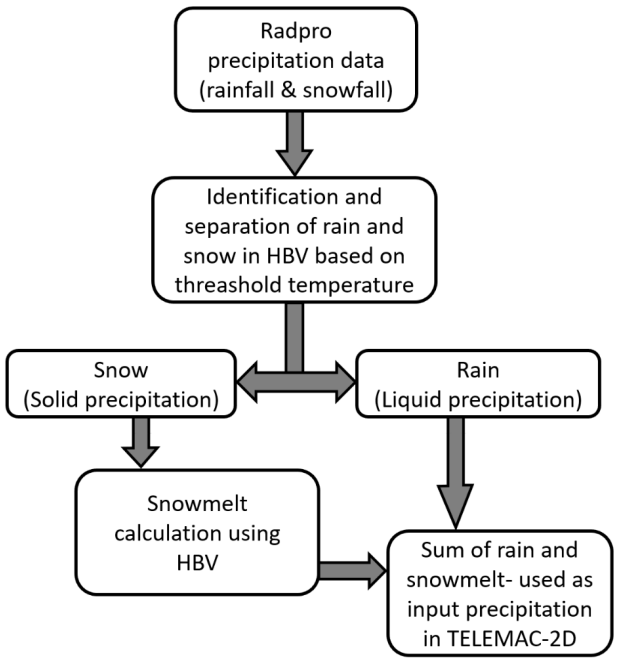

Figure 4. Flow chart for the methodology used.

The model also has a supplement to include a spatially distributed rainfall-runoff module making it a hydrodynamic rainfall–runoff model (HDRRM) [41]. The curve number (CN) method is used for infiltration modelling in TELEMAC-2D. This method was developed by the USDA Natural Resources Conservation Services (NRCS) in 1950s [42] for predicting direct runoff. CN is a dimensionless empirical parameter based on the land use, soil cover, and antecedent moisture and hydrological conditions in the catchment. The following equation is used to calculate the direct runoff depth:

$$Q = \frac{(P - \lambda S)^2}{(P + S - \lambda S)} when\ P \geq I_a\ and\ \lambda = \frac{I_a}{S}, \quad Q = 0,\ when\ P < I_a \tag{2}$$

where Q is the direct runoff depth in mm, P is the event precipitation depth in mm, λ is the initial abstraction ratio in percentage, S in mm is the potential maximum retention, and I_a in mm is initial abstraction used as 20% of the potential maximum retention in the current study.

Based on findings from a previous study by Godara et al. [40] using TELEMAC-2D on the same catchment, parameters such as the antecedent moisture conditions (AMC), roughness, and mesh size were kept constant, and the model was calibrated only for CN values. The calibration results from that study showed that courser the mesh size, drier the catchment, and higher the roughness, the lower the runoff volume and vice versa. Since the CN value is a calibration parameter here, these values change for each event and are, therefore, different from the calibrated values for another set of events in the previous study by Godara et al. [40]. As most of the catchment is covered by forests, open land, bare rock, and scarce vegetation, spatially distributed CN values were calibrated manually only for these land covers (marked green in Table 1) whereas same CN values are used for the other land-covers (marked yellow in Table 1) for the seven peak flow events (events A to G in Figure 2).

Table 1. Calibrated CN values corresponding to the seven events A to G (in Figure 2) along with their date and time of occurrence.

Description	Area (%)	Event A [20 January 2020 (10:00)-44 hours]	Event B [13 October 2021 (16:00)-45 hours]	Event C [28 March 2019 (17:00)-33 hours]	Event D [31 December 2018 (04:00)-44 hours]	Event E [24 January 2020 (23:00)-25 hours]	Event F [2 January 2020 (12.00)-23 hours]	Event G [7 January 2020 (14:00)-24 hours]
Bare rock and scarce vegetation	46.57	50	84	64	72	80	72	74
Forest	25.05	45	73	61	68	74	68	71
Open land	20.00	43	70	59	65	72	65	69
Swamp	3.62				90			
Fully cultivated soil	3.24				90			
Inland pasture	0.86				89			
River water	0.38				100			
Urban Area	0.19				89			
Roads	0.10				91			

Manning's roughness values were calculated based on land use data from the Geonorge map catalogue, which were calibrated in a previous study for the same catchment [40] and used directly in this study.

AMC can be classified into three categories based on soil moisture levels: dry (I), normal (II), and wet (III). As there was no information available on the moisture level of the soil prior to the events, and since the CN values were not adjusted for the different moisture conditions in the catchment, we used AMC values corresponding to normal moisture conditions in this study. In addition, a correction of CN for the steep slope was applied for all these simulations. The base flow for each event was set based on the measured discharge. A 5 m by 5 m triangular mesh was used for the river and surrounding areas, while a 100 m by 100 m mesh was used for the rest of the catchment. The input file preparation such as

roughness, rainfall, mesh generation, CN values over the mesh, and the post-processing of TELEMAC-2D results were carried out using python, QGIS (3.16), and Blukenue (3.3.4) software [43].

3. Results

3.1. HBV

The overall calibration of the HBV model for the period September 2018 to September 2021 gave a Nash–Sutcliffe efficiency (NSE) of 0.70, whereas for the specific events (A to I) used in this study, the NSE values were 0.94, 0.94, 0.91, 0.71, 0.86, 0.93, 0.62, 0.95, and 0.96, respectively for HBV simulations.

3.2. TELEMAC-2D

The results from TELEMAC-2D simulations corresponding to the seven peak flow events (A to G) produced via combined liquid precipitation and snowmelt are shown in Figure 5. The solid precipitation (snow), which does not contribute to the runoff during the event, is also shown in the same figure. Nash–Sutcliffe efficiency (NSE) for these events ranged from 0.55 to 0.91, and Pearson correlation coefficient (R^2) values ranged from 0.86 to 0.97, as shown in Figure 5.

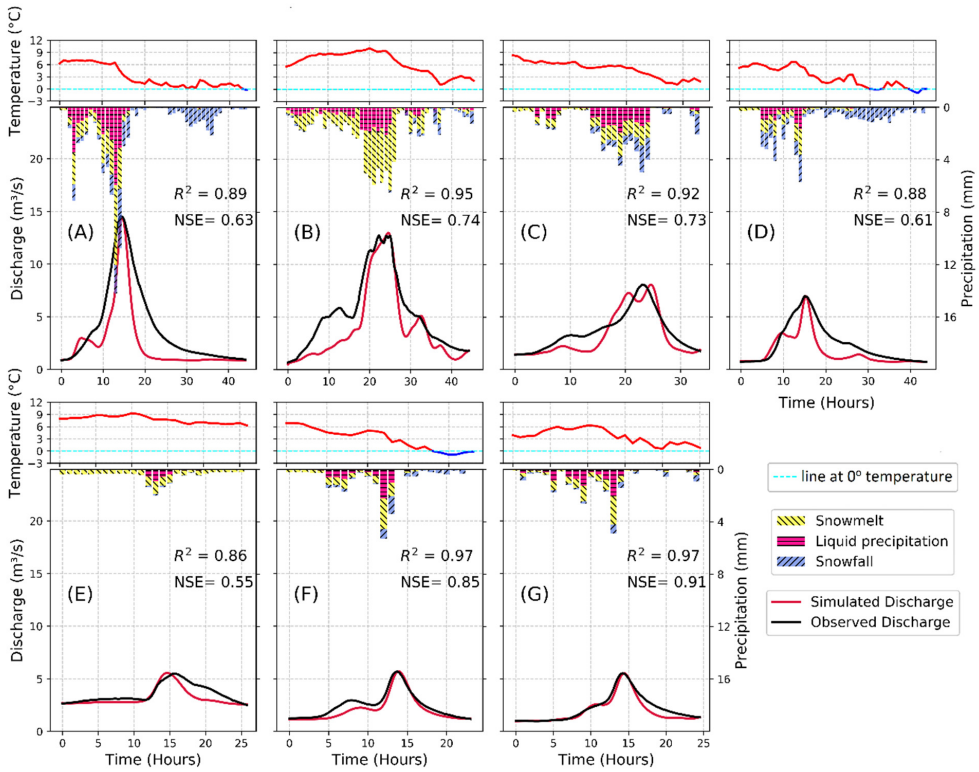

Figure 5. Simulated discharge from TELEMAC-2D, observed discharge, liquid (rain) and solid (snow) precipitation and snowmelt, temperature (upper) corresponding to the seven single peak events (**A**–**G**) selected for this study.

Figure 6a compares the results from a case-specific calibrated HBV model and TELEMAC-2D for the same event, as shown in Figure 5B. The HBV model accurately simulates the event with an NSE of 0.94, but TELEMAC-2D is not able to reproduce the first part of the flood as accurately with an NSE of 0.74. However, both models perform well in capturing

the magnitude and timing of the peak flow. For the events in Figure 6, the catchment was calibrated with a single averaged value of CN (CN_{avg}) to test if it gives equally satisfactory results if no soil data are available for catchment [40].

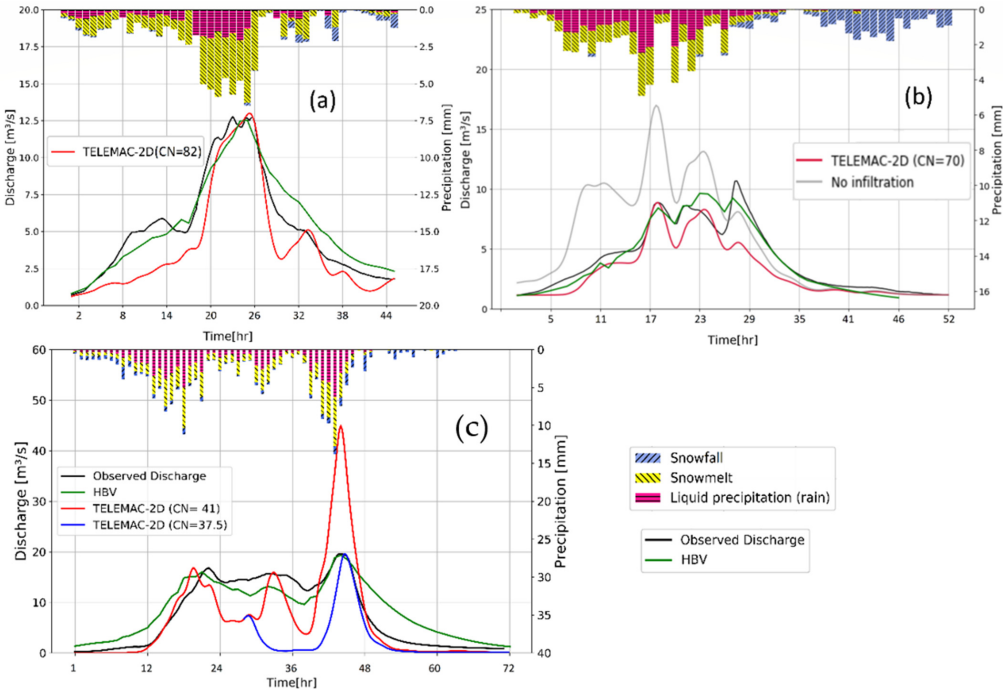

Figure 6. (**a**) Simulated discharge from TELEMAC-2D (red) and from HBV (green) calibrated for a single peak event B in Figure 2. (**b**) Simulated flow from TELEMAC-2D for CN = 70 (red) (R^2 = 0.93) and for CN = 100 (no infiltration) (grey) corresponding to the multi-peak event H in Figure 2. (**c**) Single simulation in TELEMAC-2D for entire event with CN = 41 (red), another TELEMAC-2D simulation with CN = 37.5 (blue) for 2nd peak, and the result from calibrated HBV only (R^2 = 0.87) (green) corresponding to the multi-peak event I in Figure 2.

In Figure 6c, the first simulation is run with a CN_{avg} of 41. It captured the first peak but overestimated the second peak since the CN 41 becomes too high as the catchment grows more saturated. So, to capture the second peak, another simulation was run with a lower CN value using the output from the first simulation as the initial condition (known as a hotstart file) keeping all the other parameters the same.

Figure 6b,c show that the HBV model can simulate rain-on-snow events with longer durations and multiple peaks (NSE > 0.95), while TELEMAC-2D is not able to capture the entire events. In Figure 6b, the hydrograph from TELEMAC with a CN value of 100 (grey) represents the flow without infiltration, while the hydrograph with a CN_{avg} of 70 satisfactorily reproduces the first peak but fails to capture the last. In Figure 6c, a CN_{avg} of 41 in TELEMAC-2D accurately simulates the first peak, but a higher average infiltration rate is needed to simulate the last peak (CN_{avg} = 37.5). However, it was not possible to accurately simulate the high sustained discharge throughout the event, regardless of the choice of curve number.

Figure 7 shows the maximum water depth and velocity results in the entire catchment for the event shown in Figure 5A with a peak discharge of 14.55 m^3/s from RoG HDRRM modelling. The figure also shows that the river network generated via the model is similar to the digitized river network from the Norwegian Water Administration database in

Figure 7a. Maximum water velocities are 3.21 m/s, which may cause erosion, leading to serious sedimentation problems in the lower regions where the water depths are up to 1.86 m. The figure shows also that even with a 100 by 100 m grid cell size, the RoG model captures the river network and flow paths quite well compared to the digitized river network from the Norwegian Water Administration database.

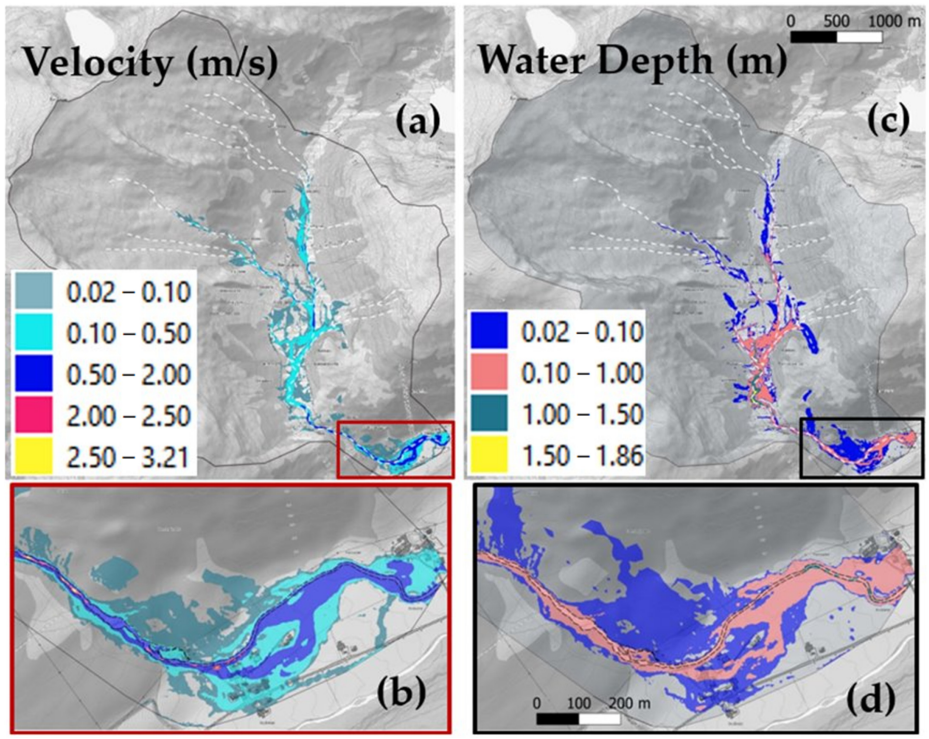

Figure 7. (**a**) Digitized river network from Norwegian Water Administration database (white dotted river lines) and flow velocity in the entire catchment. (**b**) Velocities in populated areas (red rectangle). (**c**) Water depths in entire catchment and (**d**) in the populated area (black rectangle) for the event shown in Figure 5A.

4. Discussion

This study analyses flash flood events caused by RoS events in small and steep snow-covered mountainous catchments using the RoG version of TELEMAC-2D combined with snowmelt calculation from the HBV model. The resulting RoG simulations for the investigated events indicate that the approach used in this study satisfactorily reproduces single peak flows, the inflow sources, and tributaries. However, as the hydraulic model is not calibrated towards observed water depths due to a lack of such information, the simulated water velocities and water depth are only indicative. Flood data from past flood events should be used for calibration and verifying the application of this technique in future studies. Nevertheless, the results of the current study provide crucial information for flood protection at any point along the river system in the catchment (Figure 7). High water levels and velocity locations are identified using the current technique, which is important information for contingency planners. Critical locations and risk levels in the catchment can be determined using the product of water depths and water velocity in terms of pedestrian, vehicle, and building safety [44–46].

An NSE of 0.70 for the period from 2018 to 2022 indicates that the HBV model is also able to reproduce the floods for Sleddalen. An average NSE for the seven events of

0.84 in HBV compared to 0.71 for the RoG in TELEMAC-2D shows that the HBV model demonstrates a more accurate reproduction of the flood events in this study. However, the HBV model does not provide information on velocities, flooded areas, and water depths and is, therefore, not a sufficient tool for flood mitigation or preparedness. This is, nevertheless, an indication of a better hydrological approach in the HBV model than in the RoG TELEMAC-2D.

The good fit between the observed runoff and HBV-simulated runoff for the selected events shows that the calculated snowmelt for these events is a reliable input to the RoG model. In addition, the results, when combined with the rain from the RadPro data, show that the RadPro data represent true precipitation satisfactorily. The RoG model worked well for single peak events, whereas it did not give satisfactory results in the case of longer flood events with multiple peaks. In complex mountainous areas such as in western Norway, it is difficult to capture the correct spatial distribution of the precipitation either by gauge stations, radar datasets, or high-resolution interpolated data sets because the pattern is strongly influenced by the complex terrain [47]. Hence, the model results are subject to uncertainty due to the input data. However, the good fit achieved via the HBV model indicates that the input is probably not the cause of the poor simulation via RoG in TELEMAC-2D for events lasting over longer periods. It is also important to mention that the results from the hydrologic and hydraulic models are subjected to various uncertainties in the models themselves [48] and in the input data such as precipitation, digital elevation model, bathymetry of the river, and roughness [49].

The calibration results of TELEMAC-2D for CN values show decreasing CN values and thus a higher infiltration as the rainfall depth increases, which is a contradiction to an expected higher saturation and less infiltration during longer events [50]. However, this finding is coherent with the results from the study by Krvavica and Rubinić [51]. A possible explanation for this is that since RoG TELEMAC-2D does not simulate the subsurface drainage of infiltrated water, which, in nature, comes back to the river system, TELEMAC-2D compensates by a higher surface runoff using low infiltration capacity (high CN). For a longer duration flood, a low infiltration (high CN) gives a good fit in the initial stage but gives too high discharge at later stages. Vice versa, a high infiltration rate used to fit the model to a later peak in a longer flood event gives too low discharge in the early stage. This can explain why the first small peak in Figure 6a is not correctly reproduced via TELEMAC-2D, but the later peak flows are well captured via the TELEMAC-2D as well as HBV. Since the HBV model includes soil storage and runoff from infiltrated water, it performs better for longer events and events with multiple rain peaks as the case in the event in Figure 6b,c. For the same reasons, it better handles the increase in the discharge in situations with saturated conditions prior to the event and also the recession part of the flow as illustrated in the event in Figure 6a. However, in contrast to the HBV model, TELEMAC-2D with RoG technique gives the hydraulic conditions, such as water levels, velocities, and inundated areas along the watercourses in the catchment. As TELEMAC-2D, in contradiction to the HBV model, does not include water storages, the infiltered water will not return and contribute as subsurface drainage to the base flow in a later stage of the flood. Another consequence of this, which is apparent in all the cases, is a steeper recession limb compared to the observed.

Similarly, in Figure 6b, TELEMAC-2D is not able to maintain a high discharge during the entire event because even after the catchment is completely saturated, the continuing abstractions kept occurring based on the CN value selected. A solution to this can be a time-varying CN value in a single simulation, as illustrated in Figure 6c. A simulation with an average CN value of 41, which captured the first peak, was combined with a simulation with a lower CN to capture the last peak. Here, only two CN values were used, but this indicates that a continuous transition of curve numbers from high to low during the event can possibly enable RoG TELEMAC-2D to reconstruct the longer, multi-peaked floods. The CN value is used as a calibration parameter in this study, and the results are sensitive to the CN values in determining the runoff volume [40]. Each flood event from the same

catchment needs to be calibrated against a CN value. Therefore, further investigation is necessary to better understand the factors influencing CN values and to develop a methodology for selecting an appropriate CN value for specific storm events. A sensitivity analysis in the previous study [40] has shown that CN values and antecedent moisture conditions (AMCs) in the catchment are very crucial factors that influence the output runoff volume. Nevertheless, the analysis did not reveal any distinct correlation between CN and cumulative rainfall over the preceding five days, base flow, or the flow peak. Since CN is a calibration parameter in this study, the proposed integrated HDRRM model cannot be used as a forecasting model but can be used satisfactorily for the identification and post-analysis of the consequences of flood events. In order to employ this approach as a predictive model, the variability of the CN values among various events needs to be further investigated. The varying CN value is an issue here, and further work is needed to understand why CN value varies for each event. However, the multiple CN values calibrated for each flood event can be utilized to conduct an ensemble analysis of outputs for predictive analysis.

Since the CN method is a lumped conceptual approach that was originally developed for single storm events [52], the results for the sustained flow events align with what could be expected. However, it is important to examine the consequences of such events. A solution to satisfactorily simulate multi-peak flood events can either be to include variable CN values in RoG T2D or implement another hydrological model allowing for storage and subsurface drainage back to the river system as in the HBV model. Such a combination can also be used to integrate the snowmelt and rain with hydraulic simulations in rain-on-grid models as demonstrated in this study.

5. Conclusions

The main objective of this study was to examine the effects of the snowmelt contribution in flash flood events and to see how snowmelt calculations can be combined with the rain-on-grid method in an HDRRM model. Since a snowmelt routine is not available in the HDRRM T2D model, an external snowmelt algorithm from the HBV model was used and integrated with the rain-on-grid technique in the TELEMAC-2D model. This study's purpose and objectives have been successfully fulfilled as evidenced by generated flood maps and depth and velocity maps. Significantly, this study demonstrated that these analyses could be executed without using the conventional methodology of using a separate hydrological model for discharge computation, followed by its use as input in a hydraulic routing model. The implementation of a soil and snow storage routine in the RoG hydraulic models would give a valuable contribution to flash flood mitigation and contingency work because such a combination gives both the hydrology and the hydraulics in the river and catchment in a continuous operational simulation model.

Author Contributions: Conceptualization, N.G., O.B. and K.A.; methodology, N.G., O.B. and K.A.; software, N.G.; validation, N.G.; formal analysis, N.G.; investigation: N.G. and resources, N.G., O.B. and K.A.; data curation, N.G.; writing—original draft preparation, N.G.; writing—review and editing, N.G. and O.B.; visualization, N.G. and O.B.; supervision, O.B. and K.A.; project administration, O.B.; funding acquisition, O.B. All authors have read and agreed to the published version of the manuscript.

Funding: This publication is part of the World of Wild Waters (WoWW) project number 949203100, which falls under the umbrella of the Norwegian University of Science and Technology (NTNU)'s Digital Transformation initiative.

Data Availability Statement: The data that support the findings of this study are available from the corresponding author, N.G., upon reasonable request.

Conflicts of Interest: The authors declare no conflict of interest. The funders had no role in the design of this study; in the collection, analyses, or interpretation of data; in the writing of the manuscript, or in the decision to publish the results.

References

1. Sweeney, T.L. Modernized Areal Flash Flood Guidance. NOAA Technical Memorandum NWS HYDRO. 1992. Available online: https://repository.library.noaa.gov/view/noaa/13498 (accessed on 20 October 2023).
2. Zhang, Y.; Wang, Y.; Chen, Y.; Xu, Y.; Zhang, G.; Lin, Q.; Luo, R. Projection of changes in flash flood occurrence under climate change at tourist attractions. *J. Hydrol.* **2021**, *595*, 126039. [CrossRef]
3. Zhang, Y.; Wang, Y.; Chen, Y.; Liang, F.; Liu, H. Assessment of future flash flood inundations in coastal regions under climate change scenarios—A case study of Hadahe River basin in northeastern China. *Sci. Total Environ.* **2019**, *693*, 133550. [CrossRef] [PubMed]
4. Modrick, T.M.; Georgakakos, K.P. The character and causes of flash flood occurrence changes in mountainous small basins of Southern California under projected climatic change. *J. Hydrol. Reg. Stud.* **2015**, *3*, 312–336. [CrossRef]
5. Swanston, D.N. *Slope Stability Problems Associated with Timber Harvesting in Mountainous Regions of the Western United States*; Pacific Northwest Research Station, US Department of Agriculture, Forest Service: Washington, DC, USA, 1974.
6. Johnson, J.P.L.; Whipple, K.X.; Sklar, L.S. Contrasting bedrock incision rates from snowmelt and flash floods in the Henry Mountains, Utah. *Geol. Soc. Am. Bull.* **2010**, *122*, 1600–1615. [CrossRef]
7. Sandersen, F.; Bakkehøi, S.; Hestnes, E.; Lied, K. The influence of meteorological factors on the initiation of debris flows, rockfalls, rockslides and rockmass stability. *Publ.-Nor. Geotek. Inst.* **1997**, *201*, 97–114.
8. Heyerdahl, H.; Høydal, Ø.A. Geomorphology and Susceptibility to Rainfall Triggered Landslides in Gudbrandsdalen Valley, Norway. *Adv. Cult. Living Landslides* **2017**, *4*, 267–279. [CrossRef]
9. Pall, P.; Tallaksen, L.M.; Stordal, F. A climatology of rain-on-snow events for Norway. *J. Clim.* **2019**, *32*, 6995–7016. [CrossRef]
10. Hansen, B.B.; Isaksen, K.; Benestad, R.E.; Kohler, J.; Pedersen, Å.Ø.; Loe, L.E.; Coulson, S.J.; Larsen, J.O.; Varpe, Ø. Warmer and wetter winters: Characteristics and implications of an extreme weather event in the High Arctic. *Environ. Res. Lett.* **2014**, *9*, 114021. [CrossRef]
11. Krug, A.; Primo, C.; Fischer, S.; Schumann, A.; Ahrens, B. On the temporal variability of widespread rain-on-snow floods. *Meteorol. Z.* **2020**, *29*, 147–163. [CrossRef]
12. Schmocker-Fackel, P.; Naef, F. Changes in flood frequencies in Switzerland since 1500. *Hydrol. Earth Syst. Sci.* **2010**, *14*, 1581–1594. [CrossRef]
13. Sui, J.; Koehler, G. Rain-on-snow induced flood events in southern Germany. *J. Hydrol.* **2001**, *252*, 205–220. [CrossRef]
14. Uhlemann, S.; Thieken, A.H.; Merz, B. A consistent set of trans-basin floods in Germany between 1952–2002. *Hydrol. Earth Syst. Sci.* **2010**, *14*, 1277–1295. [CrossRef]
15. Gvoždíková, B.; Müller, M. Evaluation of extensive floods in western/central Europe. *Hydrol. Earth Syst. Sci.* **2017**, *21*, 3715–3725. [CrossRef]
16. Musselman, K.N.; Lehner, F.; Ikeda, K.; Clark, M.P.; Prein, A.F.; Liu, C.; Barlage, M.; Rasmussen, R. Projected increases and shifts in rain-on-snow flood risk over western North America. *Nat. Clim. Chang.* **2018**, *8*, 808–812. [CrossRef]
17. Marks, D.; Kimball, J.; Tingey, D.; Link, T. The sensitivity of snowmelt processes to climate conditions and forest cover during rain-on-snow: A case study of the 1996 Pacific Northwest flood. *Hydrol. Process.* **1998**, *12*, 1569–1587. [CrossRef]
18. McCabe, G.J.; Clark, M.P.; Hay, L.E. Rain-on-snow events in the western United States. *Bull. Am. Meteorol. Soc.* **2007**, *88*, 319–328. [CrossRef]
19. Pomeroy, J.W.; Fang, X.; Marks, D.G. The cold rain-on-snow event of June 2013 in the Canadian Rockies—Characteristics and diagnosis. *Hydrol. Process.* **2016**, *30*, 2899–2914. [CrossRef]
20. Kattelmann, R. Flooding from rain-on-snow events in the Sierra Nevada. *IAHS-AISH Publ.* **1997**, *239*, 59–65.
21. Seneviratne, S.I.; Zhang, X.; Adnan, M.; Badi, W.; Dereczynski, C.; Di Luca, A.; Ghosh, S.; Iskandar, I.; Kossin, J.; Ewitson, B.; et al. *IPCC—Climate Change 2021: The Physical Science Basis*; Chapter 11: Weather and Climate Extreme Events in a Changing Climate; Cambridge University Press: Cambridge, UK; New York, NY, USA, 2021; p. 1610. [CrossRef]
22. Førland, E.J.; Skaugen, T.E.; Benestad, R.E.; Hanssen-Bauer, I.; Tveito, O.E. Variations in thermal growing, heating, and freezing indices in the Nordic Arctic, 1900–2050. *Arct. Antarct. Alp. Res.* **2004**, *36*, 347–356. [CrossRef]
23. Rantanen, M.; Karpechko, A.Y.; Lipponen, A.; Nordling, K.; Hyvärinen, O.; Ruosteenoja, K.; Vihma, T.; Laaksonen, A. The Arctic has warmed nearly four times faster than the globe since 1979. *Commun. Earth Environ.* **2022**, *3*, 168. [CrossRef]
24. Singh, P.; Spitzbart, G.; Hübl, H.; Weinmeister, H. Hydrological response of snowpack under rain-on-snow events: A field study. *J. Hydrol.* **1997**, *202*, 1–20. [CrossRef]
25. Sati, V.P. Glacier bursts-triggered debris flow and flash flood in Rishi and Dhauli Ganga valleys: A study on its causes and consequences. *Nat. Hazards Res.* **2022**, *2*, 33–40. [CrossRef]
26. Roald, L.A. Floods in Norway. In *Changes in Flood Risk in Europe*; CRC Press: Boca Raton, FL, USA, 2019.
27. Yang, Z.; Yuan, X.; Liu, C.; Nie, R.; Liu, T.; Dai, X.; Ma, L.; Tang, M.; Xu, Y.; Lu, H. Meta-Analysis and Visualization of the Literature on Early Identification of Flash Floods. *Remote Sens.* **2022**, *14*, 3313. [CrossRef]
28. Merz, R.; Blöschl, G. A process typology of regional floods. *Water Resour. Res.* **2003**, *39*, 1340. [CrossRef]
29. Surfleet, C.G.; Tullos, D. Variability in effect of climate change on rain-on-snow peak flow events in a temperate climate. *J. Hydrol.* **2013**, *479*, 24–34. [CrossRef]

30. Blöschl, G.; Bierkens, M.F.P.; Chambel, A.; Cudennec, C.; Destouni, G.; Fiori, A.; Kirchner, J.W.; McDonnell, J.J.; Savenije, H.H.G.; Sivapalan, M.; et al. Twenty-three unsolved problems in hydrology (UPH)–a community perspective. *Hydrol. Sci. J.* **2019**, *64*, 1141–1158. [CrossRef]
31. Li, D.; Lettenmaier, D.P.; Margulis, S.A.; Andreadis, K. The Role of Rain-on-Snow in Flooding Over the Conterminous United States. *Water Resour. Res.* **2019**, *55*, 8492–8513. [CrossRef]
32. Costabile, P.; Costanzo, C.; Ferraro, D.; Barca, P. Is HEC-RAS 2D accurate enough for storm-event hazard assessment? Lessons learnt from a benchmarking study based on rain-on-grid modelling. *J. Hydrol.* **2021**, *603*, 126962. [CrossRef]
33. David, A.; Schmalz, B. A systematic analysis of the interaction between rain-on-grid-simulations and spatial resolution in 2d hydrodynamic modeling. *Water* **2021**, *13*, 2346. [CrossRef]
34. Norwegian Directorate for Civil Protection (DSB). *Analyses of Crisis Scenarios 2019*; DSB Skien: Porsgrunn, Norway, 2019; pp. 1–228. Available online: https://www.dsb.no/rapporter-og-evalueringer/analyses-of-crisis-scenarios-2019/ (accessed on 20 October 2023).
35. Bergström, S.; Forsman, A. Development of a conceptual deterministic rainfall-runoff model. *Nord. Hydrol.* **1973**, *4*, 240–253. [CrossRef]
36. Ligier, P. Implementation of a rainfall-runoff model in TELEMAC-2D. In Proceedings of the XXIIIrd TELEMAC-MASCARET User Conference 2016, Paris, France, 11–13 October 2016.
37. Engeland, K.; Abdella, S.Y.; Azad, R.; Arrturi Elo, C.; Lussana, C.; Tadege Mengistu, Z.; Nipen, T.; Randriamampianina, R. Use of precipitation radar for improving estimates and forecasts of precipitation estimates and streamflow. In Proceedings of the 20th EGU General Assembly, EGU2018, Vienna, Austria, 4–13 April 2018; 2018; p. 12207.
38. Killingtveit, A.; Sælthun, N.R. *Hydropower Development: Hydrology*; NTNU: Trondheim, Norge, 1995.
39. Bruland, O. Snow processes, modeling, and impact. In *Precipitation*; Elsevier Inc.: Amsterdam, The Netherlands, 2021; pp. 107–143. [CrossRef]
40. Godara, N.; Bruland, O.; Alfredsen, K. Simulation of flash flood peaks in a small and steep catchment using rain-on-grid technique. *J. Flood Risk Manag.* **2023**, *16*, e12898. [CrossRef]
41. Broich, K.; Pflugbeil, T.; Disse, M.; Nguyen, H. Using TELEMAC-2D for Hydrodynamic Modeling of Rainfall-Runoff. In Proceedings of the 26th TELEMAC-MASCARET User Conference, Toulouse, France, 15–17 October 2019.
42. The ASCE/EWRI Curve Number Hydrology Task Committee. *Curve Number Hydrology*; Hawkins, R.H., Ward, T.J., Woodward, D.E., Van Mullem, J.A., Eds.; American Society of Civil Engineers: Reston, VA, USA, 2008; ISBN 9780784410042.
43. Barton, A.J. Blue Kenue Enhancements from 2014 to 2019. In Proceedings of the 26th TELEMAC-MASCARET User Conference, Toulouse, France, 15–17 October 2019. [CrossRef]
44. Shand, T.; Smith, G.; Cox, R.; Blacka, M. Development of Appropriate Criteria for the Safety and Stability of Persons and Vehicles in Floods. In Proceedings of the 34th World Congress of the International Association for Hydro—Environment Research and Engineering: 33rd Hydrology and Water Resources Symposium and 10th Conference on Hydraulics in Water Engineering, Brisbane, Australia, 26 June–1 July 2011; p. 9.
45. Direktoratet for Byggkvalitet. Veiledning om Tekniske Krav Til Byggverk; TEK17. 2017. Available online: http://www.jurpc.de/jurpc/show?id=20140073 (accessed on 20 September 2023).
46. Skrede, T.I.; Muthanna, T.M.; Alfredesen, K. Applicability of urban streets as temporary open floodways. *Hydrol. Res.* **2020**, *51*, 621–634. [CrossRef]
47. Li, L.; Pontoppidan, M.; Sobolowski, S.; Senatore, A. The impact of initial conditions on convection-permitting simulations of a flood event over complex mountainous terrain. *Hydrol. Earth Syst. Sci.* **2020**, *24*, 771–791. [CrossRef]
48. McMillan, H.K.; Westerberg, I.K.; Krueger, T. Hydrological data uncertainty and its implications. *WIREs Water* **2018**, *5*, e1319. [CrossRef]
49. Annis, A.; Nardi, F.; Volpi, E.; Fiori, A. Quantifying the relative impact of hydrological and hydraulic modelling parameterizations on uncertainty of inundation maps. *Hydrol. Sci. J.* **2020**, *65*, 507–523. [CrossRef]
50. Hjelmfelt, A.T. Investigation of Curve Number Procedure. *J. Hydraul. Eng.* **1991**, *117*, 725–737. [CrossRef]
51. Krvavica, N.; Rubinić, J. Evaluation of design storms and critical rainfall durations for flood prediction in partially urbanized catchments. *Water* **2020**, *12*, 2044. [CrossRef]
52. USDA-SCS. Part 630 Hydrology National Engineering Handbook. Chapter 10 Estimation of Direct Runoff from Storm Rainfall. 2004. Available online: https://directives.sc.egov.usda.gov/OpenNonWebContent.aspx?content=17752.wba (accessed on 20 October 2023).

Paper 3

Comparison of two hydrodynamic models for their rain-on-grid technique to simulate flash floods in steep catchment

Nitesh Godara, Oddbjørn Bruland, Knut Tore Alfredsen

Published: Frontiers in Water (6 May 2024).

frontiers | Frontiers in Water

TYPE Original Research
PUBLISHED 06 May 2024
DOI 10.3389/frwa.2024.1384205

OPEN ACCESS

EDITED BY
Simone Schauwecker,
Catholic University of the North, Chile

REVIEWED BY
Shiblu Sarker,
Virginia Department of Conservation and Recreation, United States
Tomasz Dysarz,
Poznan University of Life Sciences, Poland

*CORRESPONDENCE
Nitesh Godara
✉ Nitesh.godara@ntnu.no

RECEIVED 08 February 2024
ACCEPTED 12 April 2024
PUBLISHED 06 May 2024

CITATION
Godara N, Bruland O and Alfredsen K (2024) Comparison of two hydrodynamic models for their rain-on-grid technique to simulate flash floods in steep catchment.
Front. Water 6:1384205.
doi: 10.3389/frwa.2024.1384205

Comparison of two hydrodynamic models for their rain-on-grid technique to simulate flash floods in steep catchment

Nitesh Godara*, Oddbjørn Bruland and Knut Alfredsen

Department of Civil and Environmental Engineering, Norwegian University of Science and Technology (NTNU), Trondheim, Norway

In this study, two hydrodynamic models, TELEMAC-2D and HEC-RAS 2D, were compared for their Rain-on-Grid (RoG) technique with a particular focus on runoff generation processes in a small and steep catchment. Curve number (CN) method was applied in both the models to simulate two single storm events up to 20 h of duration, whereas the Green-Ampt Redistribution (GAR) method was additionally applied in HEC-RAS 2D for a multi-peak flood event with sustained flow between the peaks. CN and GAR methods were compared for this flood event, and a sensitivity analysis of the GAR parameters was also done. Moreover, the two models were compared for their calibration process, computational time, mesh size and shape, and model availability, in general, as well as the results including inundated areas, water depth, and velocity. The results indicate that both the models are capable of reproducing short duration single storm floods. NSE and R^2 for both models ranged from 0.70 to 0.90 and from 0.93 to 0.95. However, the models struggled to reproduce the long- duration multi-peak flood event. The sensitivity analysis showed that the results are not very sensitive to the two GAR parameters which are responsible to influence the flow of the second peak in the flood event. Neither the CN nor the GAR infiltration method successfully replicated such events because the hydraulic models permanently lose infiltrated water from the domain. The returned sub-surface flow significantly contributes to river flow during these flood events; however, none of the model incorporates a return flow algorithm.

KEYWORDS

small catchments, TELEMAC-2D, HEC-RAS 2D, rainfall-runoff modeling, HDRRM, hydrology, hydraulics

1 Introduction

Frequency of extreme rainfall events has been increasing in recent years leading to extreme floods. The frequency and magnitude of such events are likely to increase in the future because of global warming and changing climate (Seneviratne et al., 2021), urbanization, land use, and infrastructure development (Feng et al., 2021). When there is a sudden, violent rise in water level and high peak flows within less than 6 h, it is referred as a flash flood (Sweeney, 1992; Marchi et al., 2010; Kishore and Rishi, 2014; Zhang et al., 2019). Floods of this nature can occur due to factors such as extreme precipitation and temperatures, rain-on-snow events, snowmelt,

glacial lake outbursts (Jha and Khare, 2016), volcanic eruptions (Basso-Báez et al., 2020), or dam breaks.

The adverse environmental impacts of flash floods can include soil erosion, riverbank and bed erosion (Swanston, 1974), and debris flow (Borga et al., 2014) and may lead to sedimentation and river overflow (Johnson et al., 2010) and even landslides (Lin et al., 2021). Floodwater can also harm vegetation, whereas pollutants transported by it may adversely affect water quality, habitats, and flora and fauna. A case study by Vázquez Conde et al. (2001) describes that huge amount of fine and coarse sediments was transported by flash flood in Mexico. These sediments not only reduced the discharge capacity of the river but also contributed to the rise of the water level and eventually killed more than 800 people. Flash floods have been one of the most damaging natural hazards throughout the world (Maatar et al., 2015) in terms of loss of lives, property, and environmental damage (Liu et al., 2022). Furthermore, flash floods have contributed to 40% of the total casualties in Europe from 1950 to 2006 (Barredo, 2007). Thus, it is crucial to analyze flash flood events and the consequences in an efficient way using the hydrologic and hydraulic characteristics of such events.

Flash floods in small and steep mountainous catchments can be particularly dangerous as they lead to a rapid rise in discharge and water velocities (Bruland, 2020; Moraru et al., 2021). Complex topography and meteorological complexity in such catchments make it even more difficult to model flash floods (Li et al., 2020; Maqtan et al., 2022). Usually, flood scenarios are modeled using hydrological and hydraulic models separately. Hydrological models are used to calculate the discharge (hydrograph) at a point in the catchment, whereas the hydrodynamic models are used to simulate the hydraulic characteristics with given inflows to the water course. Such characteristics include flow velocity, water depth, submerged area, shear stress, erosion, and sedimentation. An output hydrograph from a hydrological model or an observed hydrograph is usually used as input or boundary condition to the hydrodynamic model. The two types of models can be integrated manually, but that is a laborious process due to the need for separate calibration and running simulations in the two models. Additionally, both establishing the boundary conditions and determining their placement along the water course in the hydrodynamic model can be challenging. Thus, the boundary condition is usually not set for small tributaries, resulting in inaccurate discharge predictions along the main river. Hence, to address these issues, this study has used a Rain-on-Grid technique implementation in hydrodynamic models (HDRRM-Hydrodynamic Rainfall-Runoff Models). This technique defines the river network in the catchment and provides the inflow to any point along the rivers and streams.

The Rain-on-Grid (RoG) technique or the direct rainfall method (DRM) is a method in which precipitation is used directly as input over the grid cells in a hydrodynamic model. This method integrates both hydrological and hydrodynamic calculations within a single model, eliminating the need for manual integration of the two model types. Thus, in contrast to traditional 1D/2D hydraulic modeling, the inflow to the water courses is fed continuously along the rivers and the tributaries rather than through defined boundaries. Even though hydrodynamic routing between all grid cells across the entire catchment is computationally more demanding than restricting it to grid cells within the water course, it was observed to be more efficient compared with the offline coupling of the two model types (Rangari et al., 2019; David and Schmalz, 2021; Zeiger and Hubbart, 2021).

In this study, we compare the performance of two hydrodynamic models, TELEMAC-2D (Ligier, 2016) and HEC-RAS 2D (Brunner, 2002) for their Rain-on-Grid (RoG) technique in a steep catchment to find out their limitations and strengths. RoG implementation in TELEMAC-2D (T2D hereafter) has been tested before to model flash floods in a steep and small snow-covered catchment (Godara et al., 2023b), and it was found that the model was able to reproduce single storm flood events but struggled to reproduce all peaks in a sustained flow event with multiple peaks. Therefore, the first objective of this study is to check if HEC-RAS 2D (HR2D hereafter) can achieve equally good results as T2D for simulating single storm flood events. The second objective of this comparison is to check if HR2D is able to reproduce long duration of flood events better than T2D. A particular focus for the second objective has been on how they handle the hydrology, i.e., infiltration and generation of rainfall excess and the long duration of multi-storm events. T2D uses the Curve-Number (CN) method to determine the infiltration rate and the remaining portion of the rainfall from each cell goes to runoff (Ligier, 2016). HEC-RAS 2D (HR2D hereafter) has three optional methods for calculating the infiltration: Deficit and Constant Loss method, CN method, and Green-Ampt Redistribution (GAR) method (Brunner, 2020), where CN and GAR are the two methods used in this study. Moreover, the two models are compared for their calibration process, computational time, mesh size and shape, and model availability, in general, as well as the inundated areas, water depths, and velocity of water after a rainfall event. The current study is one of the first to compare these two hydrodynamic models for their rain-on-grid rainfall-runoff modeling.

2 Materials and methods

2.1 Study area and input data

The Sleddalen catchment in Møre og Romsdal county in western Norway was selected for this study. This catchment is selected because it is steep and has the potential of disastrous flash floods and a discharge measurement station. It is a steep mountainous catchment with an area of 10.5 km^2 and average slope of 0.5 m/m with highest and lowest elevations at 1,379 and 77 m, respectively. The catchment is mostly covered by open land, forest, bare rock, and scarce vegetation, as shown in Figure 1 (generated using QGIS version 3.34).

The input data used for this study are digital terrain model (DTM), observed discharge, and temperature and precipitation data. DTM data with a resolution of 0.5 m by 0.5 m were downloaded from the Norwegian mapping authority database.[1] The observed discharge data with 15 min of resolution and temperature data with 1 h of resolution were taken from the measurement station (Sleddalen station ID: 97.5.0) inside the catchment, as shown in Figure 1. Precipitation data with 1 km by 1 km spatially distribution and 1 h temporal resolution were extracted from the RadPro dataset which is a merged product of gridded precipitation point observations and

1 www.hoydedata.no

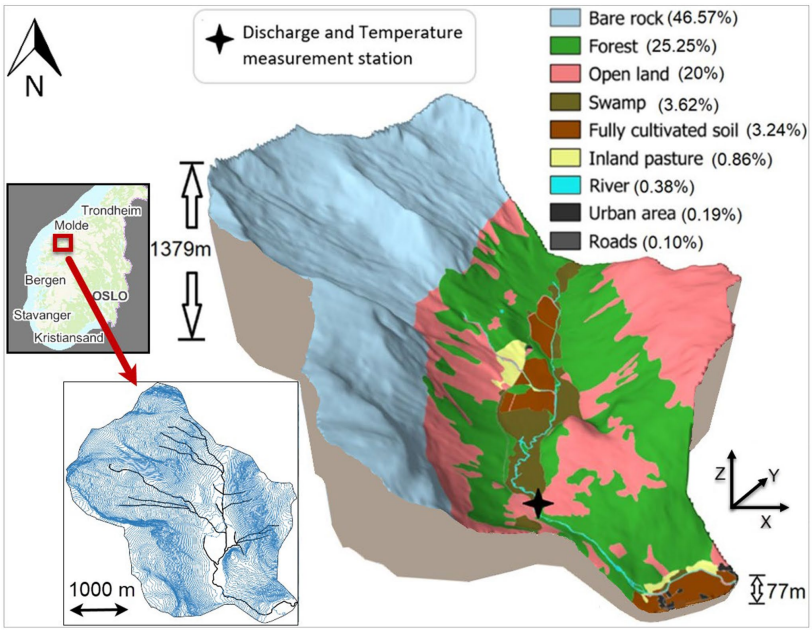

FIGURE 1
Study area showing steepness and land cover-land use information with the percentage of each type, maximum and minimum elevation levels in the catchment, and the location of discharge and temperature measurement stations. Small figure in bottom left shows the DTM of the area with contour lines at 10 m vertical distance along with a digitized river network from the Norwegian Water Administration database.

precipitation radar data (Engeland et al., 2018). Land use–land cover data were downloaded from Geonorge[2] which is a Norwegian national website for maps and other geographical information in Norway. Two high flow events up to 20 h of duration induced by single storm rainfall events and one longer duration event with sustained flow between the storms induced by a multi-storm rain-on-snow event were selected for this study.

2.2 Models and methods

2.2.1 Model concepts, availability, installation, and input file preparation

In this study, two hydraulic models, T2D and HR2D, are used for the hydrodynamic rainfall-runoff modeling (HDRRM). These models have an option to use the precipitation data directly as input to the model grid cells also called the rain-on-grid (RoG) technique (David and Schmalz, 2021). Both the models are based on solving the Shallow Water Equations (SWE), which are derived from the Navier–Stokes equations. T2D is a freely available and open-source model. The users can change and implement new methods themselves in the source code of this model. On the other hand, HR2D is freely available but not open source. RoG was recently introduced in HR2D (Zeiger and Hubbart, 2021; Hariri et al., 2022) and it has a graphical user interface (GUI) which makes its use and installation easier than T2D. For the same reason, preparation of the input files is also less time-consuming for HR2D. RAS-mapper alone was used for pre- and post-processing and visualization of the results, whereas in T2D, various software and programs such as Bluekenue, QGIS, R, and Python were used.

2.2.2 TELEMAC-2D

T2D calculates water depth and the components of velocity in two dimensions of horizontal space using a computational mesh of triangular elements (Figure 2). Various numerical methods are available in T2D for solving shallow water equations such as the finite-volume and finite-element method (Sarker, 2022), but finite-volume is utilized in this study. T2D can work on up to eight parallel core processers in a CPU computer. T2D version v8p2 was used in this research study. Main input files required are the boundary condition file (*cli), precipitation file (*.slf), simulation file (CAS file), and geometry file (*.slf) containing information about watershed characteristics, grid cells, Manning's roughness, and CN values. Python and R were used for preprocessing and converting the precipitation file from netCDF file into a SELAFIN (*.slf) file. Bluekenue (Barton, 2019) was used for preparing the other input files. PostTelemac plugin in QGIS (3.34) was used for visualization of T2D results, creating inundation maps. Mesh size varies from a maximum of 100 meter triangle edges in the drainage area to a refined grid down to 5 meter edge in the vicinity of the river network and 3 meter edge inside the river downstream of the measurement stations. Steep slope

2 www.geonorge.no

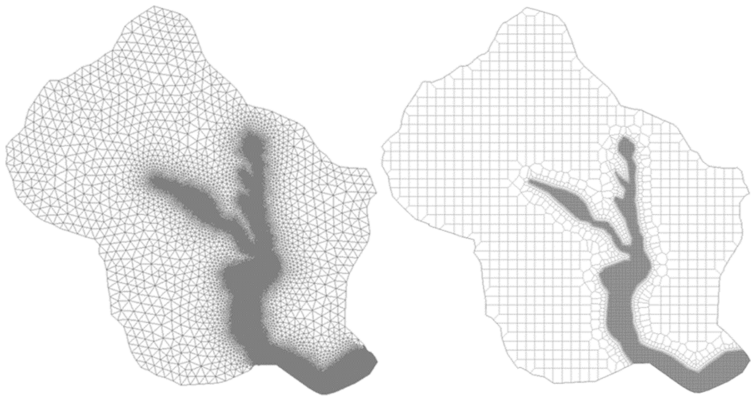

FIGURE 2
Triangle shaped mesh in T2D (104,566 cells) (left) and square shaped mesh in HR2D (56,106 cells) (right) with 5 m*5 m around and 3 m*3 m resolution in the river and 100 m*100 m resolution in rest of the catchment.

correction for CN values was applied in the T2D simulations considering the mountainous catchment. The code in T2D model simultaneously solves the following hydrodynamic equations:

(a) Continuity equation:

$$\frac{\partial h}{\partial t} + u \cdot \nabla(h) + h div(u) = S_h \tag{1}$$

(b) Momentum equation along x:

$$\frac{\partial u}{\partial t} + u \cdot \nabla(u) = -g \frac{\partial Z}{\partial x} + S_x + \frac{1}{h} div(h\, v_t \nabla u) \tag{2}$$

(c) Momentum equation along y:

$$\frac{\partial v}{\partial t} + u \cdot \nabla(v) = -g \frac{\partial Z}{\partial y} + S_y + \frac{1}{h} div(h\, v_t \nabla v) \tag{3}$$

where the equations are given here in Cartesian coordinates, and
h (m) = water depth;
u, v (m/s) = velocity components;
g (m/s^2) = gravity acceleration;
v_t (m^2/s) = momentum coefficient;
Z (m) = free surface elevation;
t (s) = time;
x, y (m) = horizontal space coordinates;
S_h (m/s) = source or sink of fluid; and
h, u, and v are the unknowns

2.2.3 HEC-RAS 2D

The Hydrologic Engineering Center's River Analysis System (HEC-RAS) version 6.3.1 was used in the current study. Input data required are similar to T2D except their formats. The precipitation file was used directly in netCDF format. Since HR2D has a user interface, the simulations can run directly from the main window of the HR2D unlike T2D. The model was run with the SWE-ELM (Eulerian–Lagrangian Method) equation set. HR2D uses a computational mesh of square shaped elements (Figure 2), and it allows for mesh refinement to increase the computational points to ensure numerical stability and increase the simulation precision in hydraulically complex regions. The initial mesh resolution used was similar to T2D (Figure 2), but later, the mesh was refined at various places by introducing more computational points (Figure 3B) due to the reasons explained in detail in the "Results" section. For both the models, Manning's roughness and CN values were used in spatially distributed format (Table 1) based on the land cover types in the catchment (Figure 1).

HR2D solves the following shallow water equations for its 2D modeling approach (Brunner, 2020):

(a) Continuity equation:

$$\frac{\partial h}{\partial t} + \frac{\partial (hu)}{\partial x} + \frac{\partial (hv)}{\partial y} = q \tag{4}$$

(b) Momentum equations:

$$\frac{\partial u}{\partial t} + u\frac{\partial u}{\partial x} + v\frac{\partial u}{\partial y} - f_c v = -g\frac{\partial Z_S}{\partial x} + \frac{1}{h}\frac{\partial}{\partial x}\left(v_{t,xx} h \frac{\partial u}{\partial x}\right) + \frac{1}{h}\frac{\partial}{\partial y}\left(v_{t,yy} h \frac{\partial u}{\partial y}\right) - \frac{\tau_{b,x}}{\rho R} + \frac{\tau_{s,x}}{\rho h} - \frac{1}{\rho}\frac{\partial p_a}{\partial x} \tag{5}$$

$$\frac{\partial v}{\partial t} + u\frac{\partial v}{\partial x} + v\frac{\partial v}{\partial y} - f_c u = -g\frac{\partial Z_S}{\partial y} + \frac{1}{h}\frac{\partial}{\partial x}\left(v_{t,xx} h \frac{\partial v}{\partial x}\right) + \frac{1}{h}\frac{\partial}{\partial y}\left(v_{t,yy} h \frac{\partial v}{\partial y}\right) - \frac{\tau_{b,y}}{\rho R} + \frac{\tau_{s,y}}{\rho h} - \frac{1}{\rho}\frac{\partial p_a}{\partial y} \tag{6}$$

where u, v = velocity components in the Cartesian directions [L/T],
q = Water source/sink;
g = gravity acceleration [L/T^2];
z_s = Water surface elevation [L];

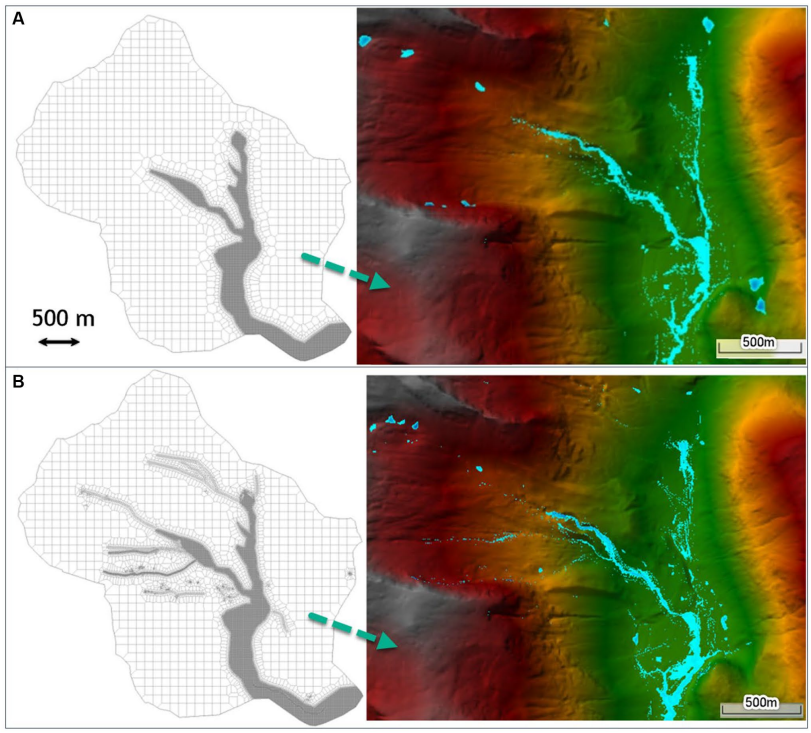

FIGURE 3
(A) Some of the artificial sinks where water was trapped at the end of the HR2D simulation for 100 m grid size, **(B)** Finer mesh breaklines to remove the artifact locations (approximately 56,000 cells).

TABLE 1 **Calibrated CN and Manning's roughness values used for various land covers for both the models.**

↓Land-cover	CN (T2D)		CN (HR2D)		Roughness (T2D)	Roughness (HR2D)
Events from Figure 5→	A	B	A	B		
Bare rock and scarce vegetation	89	85	99	98	0.02	0.1
Forest	88	80	95	96	0.2	0.2
Open land	80	75	94	95.5	0.05	0.15
Marsh	90	90	95	92	0.2	0.2
Fully cultivated soil	90	90	94	90	0.04	0.04
Inland pasture	89	89	95	89	0.259	0.259
River	100	100	100	100	0.04	0.055
Urban area	89	89	95	96	0.1	0.1
Roads	91	91	99	91	0.02	0.02

$\nu_{t,xx}, \nu_{t,yy}$= horizontal eddy viscosity coefficients in the x and y directions [L^2/T];

$\tau_{b,x}, \tau_{b,y}$ = Bottom shear stresses on the x and y directions [L^2/T];

$\tau_{s,x}, \tau_{s,y}$= Surface wind stresses in the x and y directions, respectively [M/L/T^2];

R= Hydraulic radius [L];

h = water depth [L];

p_a= Atmospheric pressure [M/L/T^2]; and

f_c= Coriolis parameter [1/T]

2.2.4 Models' setup and input data

Raw RadPro precipitation dataset does not distinguish between rainfall and snowfall. Input precipitation to the HDRR models was therefore preprocessed according to a previous study by Godara et al.

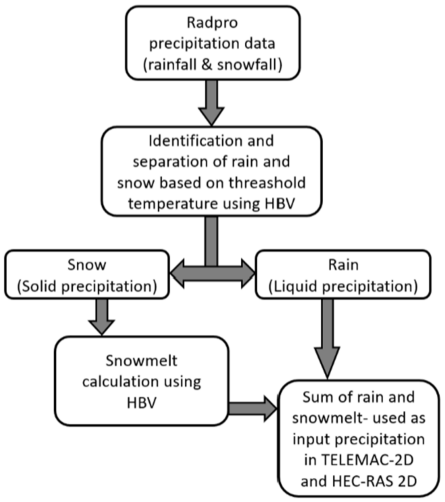

FIGURE 4
Flow chart for the methodology used in this research study.

(2023a), where snowmelt was calculated using a hydrological model HBV (Bergström and Forsman, 1973). Sum of the calculated snowmelt and rain per timestep was used as input precipitation to the grid cells in T2D and HR2D. A flow chart for this methodology is shown in Figure 4. Base flow in the river was set based on the observed discharge using two internal boundary conditions with a constant discharge in the hydraulic models. One external boundary condition was set at the outlet of the catchment to a normal depth with a friction slope calculated using RAS-mapper close to the outlet. The computational-interval for the simulations was controlled by the courant number which was set as 0.9 for T2D which is the recommended value for steep slopes (TELEMAC-2D User Manual v8p2, 2020), whereas, in HR2D, the minimum and maximum courant number were set as 0.4 and 1, respectively. The initial computational time interval was set as 1 s in both the models, and the output hydrographs were extracted for 15 min.

2.2.5 Curve number method

The CN method is an empirical method which is commonly used to estimate the infiltration or direct runoff from rainfall excess in a particular catchment. The equation to calculate the direct runoff depth is as follows:

$$Q = \begin{cases} 0 & for\ P \le I_a \\ \dfrac{(P - I_a)^2}{P - I_a + S} & for\ P > I_a \end{cases} \quad (7)$$

where Q (mm) is the direct runoff depth, P (mm) is the event rainfall depth, S (mm) is the potential maximum retention, and I_a is the initial abstraction or the amount of water lost before the runoff starts. In the current study, it is assumed as $I_a = 0.2S$. Curve number is a dimensionless parameter which depends on catchment's hydrologic soil group, moisture condition, and land use. It is related to the above equation in the following way:

$$S = 24.5\left(\frac{100}{CN} - 10\right) \quad (8)$$

CN varies from 30 to 100, where CN = 100 indicates no infiltration (high runoff) and lower CN values indicate higher infiltration (lower runoff). As shown in the CN equation, the runoff is generated only after the initial abstraction has been completed. Nonetheless, this method does not anticipate infiltration rate; instead, it predicts cumulative infiltration. In addition, time and rainfall intensity are not considered. As a result, this method is not the best for the areas in karst topography and for the areas containing the type of soils where a significant proportion of the flow is subsurface flow rather than direct runoff. Spatially distributed Manning's roughness and CN values were used (Table 1) in both the models which were based only on the land cover data because soil information was not available for the catchment. Steep slope correction for CN values was applied in the T2D simulations considering the mountainous catchment using the following formula (Huang et al., 2006):

$$CN(II)_\alpha = CN(II)\left(\frac{322.79 + 15.63\alpha}{\alpha + 323.52}\right) \quad (9)$$

Here, $CN(II)$ represents the CN value corresponding to a $AMC(II)$, the normal antecedent moisture condition, while α denotes the terrain slope in m/m, ranging from 0.14 to 1.4 m/m. The $CN(II)$ values may experience an increase of up to 6% for α = 1.4 (Ligier, 2016).

2.2.6 Green-Ampt and green-Ampt redistribution method

In contrast to the CN method, the GA method is a physically based model. The rate of infiltration varies with time depending on the soil properties (Ogden and Saghafian, 1997). The CN method assumes an initial abstraction before the runoff starts, the GA model assumes that the runoff starts only when the rainfall rate is more than the infiltration rate. The GA approach assumes a sharp boundary between wet and dry soil, and the water potential varies with water content on the wetting front in the dry soil (Green and Ampt, 1911). To calculate the infiltration rate (f), the basic GA equation is as follows:

$$f = K_S\left(1 + \frac{\psi\theta_d}{F}\right) \quad (10)$$

Here, K_S is the saturated hydraulic conductivity, Ψ is the suction head, θ_d is the difference between the saturated water content (θ_s) and the initial soil water content (θ_i), and F is the cumulative infiltration. The depth of the wetting front (Z) is presented as F/θ_d. It is important to notice that the actual infiltration rate is the minimum of the rainfall intensity, and the infiltration rate calculated in the above equation.

The GA approach is suitable for reproducing single peak flow events where the effects of evapotranspiration and unsaturated gravity-driven flow are negligible. On the other hand, it is crucial to consider the soil moisture redistribution to accurately model sustained flow flood events caused by multi-storm rainfall. Two wetting fronts

may be considered for such events and the Green-Ampt Redistribution (GAR) method is used to simulate the soil moisture recovery during a rainfall hiatus period. The basic GA method depends on four parameters, namely, saturated hydraulic conductivity (K_S), suction head (Ψ), initial (θi) moisture content, and saturated (θs) moisture content, whereas the GAR method considers two additional parameters, namely, residual moisture content (θ_r) and the pore size distribution index (λ). A rainfall hiatus period starts when the saturated hydraulic conductivity K_s is more than the rainfall. During this hiatus period, the soil moisture content starts to decrease and this change in the moisture content (θ_0) for the redistribution process is calculated as follows:

$$\frac{d\theta_d}{dt} = \frac{1}{Z_0}\left\{ f - E_{v,0} - K_i - \left[K_0 + \frac{K_S G(\theta_i,\theta_0)}{Z_0} \right] \right\} \quad (11)$$

where Z_0 is the depth to the wetting front given as $F_0/(\theta_0 - \theta_i)$, $E_{v,0}$ is the evapotranspiration rate, K_i, K_S, and K_0 are the unsaturated hydraulic conductivities corresponding to initial θ_i, the saturated θ_S, and a moisture content of θ_0, respectively. G (θ_i, θ_0) is integral of the capillary drive through the saturated front which is computed as follows:

$$G(\theta_i,\theta_0) = \psi \frac{\Theta_0^{3+\frac{1}{\lambda}} - \Theta_i^{3+\frac{1}{\lambda}}}{1 - \Theta_i^{3+\frac{1}{\lambda}}} \quad (12)$$

where Θ is the relative water content. The main benefit of using the GAR method is that it takes into account the variation of rainfall excess intensity over time, a feature which is absent in the CN method. However, the calibration of GAR method depends on the availability of soil data, and it is a tedious and time-consuming process because of the large number of parameters and long simulation run-time in the hydrodynamic models. Therefore, to test the influence of the GAR parameters, a sensitivity analysis was done on a smaller model of only two cells.

2.2.7 Measures of accuracy

Pearson's correlation coefficient (Pearson, 1897) and Nash–Sutcliffe Efficiency Index (Nash and Sutcliffe, 1970) were used as the measures of accuracy for the model results. The formulas for both are described below:

(a) Pearson's correlation coefficient (R^2)

It is the ratio of the mean square error to the potential error. The value ranges from 0 to 1, where 1 represents a perfect fit and 0 represents no fit. It is calculated using the following formula:

$$R^2 = \frac{\sum_{i=1}^{n}\left(Q_{obs} - Q_{obs_m}\right)\left(Q_{sim} - Q_{sim_m}\right)}{\sqrt{\sum_{i=1}^{n}\left(Q_{obs} - Q_{obs_m}\right)^2 \cdot \sum_{i=1}^{n}\left(Q_{sim} - Q_{sim_m}\right)^2}} \quad (13)$$

In this equation:
R^2 represents the Nash–Sutcliffe Efficiency Index;
n is the total number of observations;
Q_{obs} denotes the observed values;
Q_{sim} represents the predicted values;
Q_{obs_m} signifies the mean of the observed values; and
Q_{sim_m} signifies the mean of the simulated values.

(b) Nash–Sutcliffe Efficiency Index (NSE)

Nash–Sutcliffe Efficiency (NSE) Index is the absolute difference between observed and simulated values, which is then normalized by the variance of the observed discharge to remove any bias. In case of a perfect model, the estimated error value is 0, and hence, the NSE is 1. On the contrary, the NSE is 0 if the model produces an estimation error-variance equal to the observed time series. It is calculated using the following formula:

$$NSE = 1 - \frac{\sum_{i=1}^{n}\left(Q_{obs} - Q_{sim}\right)^2}{\sum_{i=1}^{n}\left(Q_{obs} - Q_{obs_m}\right)^2} \quad (14)$$

In this equation:
NSE represents the Nash–Sutcliffe Efficiency Index;
n is the total number of observations;
Q_{obs} denotes the observed values;
Q_{sim} represents the predicted values; and
Q_{obs_m} signifies the mean of the observed values.

3 Results and discussion

3.1 Calibration and single-storm flood events

The models are calibrated by varying the CN values and the roughness for different land covers (Table 1) to fit the simulated hydrograph for single storm events to the observations from the measurement station in the river (Figure 1). During the calibration process, when the same roughness and CN values were used in HR2D as in T2D, the runoff was lower (Pilotti et al., 2020), and the peak flow was not captured for event A by HR2D, as shown in Figure 5. Hence, the CN values were increased, and roughness was decreased to reproduce the peak flow in HR2D. Consequently, the time to the peak flow was earlier for HR2D. Moreover, it was also observed in a study by Zeiger and Hubbart (2021), where the Manning roughness was adjusted and decreased with 25% and down to 75% which was not physically realistic for their study area. To reproduce the peak in HR2D, more flow volume and a delayed peak were needed. Since the mesh size also controls the runoff volume (Godara et al., 2023b), the cell size for the catchment was decreased to 50 m, which increased the runoff volume. Afterward, Manning's roughness values were increased to delay the peak which resulted in a good calibration of peak flow and timing for event A (Figure 5). One reason for different results from the two models for the same CN and Manning's n values may be the steep slope correction applied in T2D as per the formula given in Equation (9), which increases the CN value based on the slope at the location. For event B in the same Figure 5, the mesh resolution was the same (5 m by 5 m and 100 m by 100 m); as in T2D (except the breaklines in HR2D), only the CN and roughness values were adjusted to reproduce the peak flow. These two flow events were induced by only single-storm rainfall events without any contribution of snowmelt.

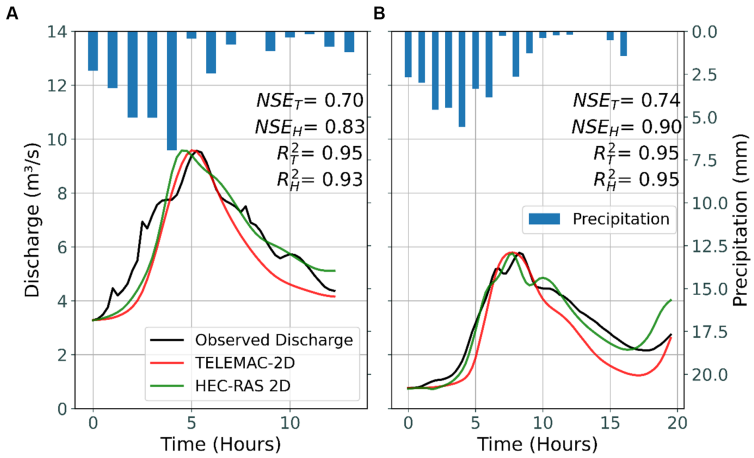

FIGURE 5
Observed discharge (black) and results from T2D (red) and HR2D (green) simulations. Both the models struggled to capture the initial rising part of the flood hydrograph in event A, but the recession part was better simulated by HR2D than by T2D in both the events.

The results show that the recession part is better simulated by HR2D than T2D in both the events, but both the models are struggled to capture the initial rising part of the flood hydrograph in event A. Similar results were observed in a study by Vu et al. (2015) for T2D flood inundation modeling, where the highest agreement between the modeled results and observations is for the peak flow conditions, not for pre- and post- flood conditions even for the flood extent. Reason behind a higher and therefore a better recession limb in HR2D can be the finer mesh in HR2D, which influence the overall volume under the curve of a hydrograph and a higher roughness, delaying and distributing the flow and keeping the volume higher until the end of simulations. A dam-break wave propagation study in a moderately steep valley was done by Pilotti et al. (2020) using HR2D version 5.0.7 and then compared the results with T2D version 7.0. They observed a slightly steeper rising limb and an early peak of the hydrograph in both models, which aligns with the findings of this study. However, they observed a milder recession limb compared to the observed one. However, the NSE values were quite similar. For this study, Nash–Sutcliffe efficiency and Pearson Correlation Coefficient values for T2D and HR2D are shown in Figure 5.

3.2 Mesh grid cells and simulation run-times

HR2D uses square shaped grid cells while T2D uses triangular shaped grid cells in the mesh. For the same length of the cell edges in the catchment, T2D gave more stable results as compared with HEC-RAS. One possible explanation for this can be the triangular shape of the grid cells instead of the square shape in HR2D which makes almost double the number of grid cells in T2D than in HR2D (Figure 2). Furthermore, HR2D took approximately five times longer simulation run-time as compared with T2D for the same set of parameters. T2D can run the simulation on eight core processors at the same time, showing the usage of 100% CPU capacity of the computer in task manager. HR2D also has an option to select the number of cores to be used (Goodell, 2016). Simulation run-time was tested by using 8, 16 and all available cores, but still, the task manager shows only approximately 60% of the CPU capacity usage during the simulations. This could be the reason for longer simulation times in HR2D. However, we refer to an article by Kleinschmidt Group (Goodell, 2016), to understand the utilization of a computer's CPU by HR2D. Another reason for a longer simulation run-time in HR2D is the irregular shape of the grid cells along the steep sections in the catchments (Figure 3A, right).

Some artificial sinks were observed at the end of the HR2D simulations (David and Schmalz, 2021) and a significant amount of water was trapped in there (Figure 3A, right), which resulted in a lower runoff volume in the initial stages of the calibration. Unlike HR2D, T2D did not have any such problem of discontinuous flow or artifacts at extreme steep slopes. To remove these artifacts in HR2D, the mesh was refined in those particular areas by introducing breaklines (Figure 3B, left), which resulted in an increased runoff volume, peak flow, and simulation run-time. Even after the refined mesh in these areas, water was still trapped in very small point locations with extremely steep slopes (Figure 3B, right), which was difficult to remove.

The resulting flow did not seem continuous for the steeper sections of the river. One possible reason for the flow discontinuity in HR2D could be the way in which the model fills the grid cells with water. The cells are filled according to a stage–volume relationship and it starts filling up the cell from the deepest part of the cell. Low flow or long time-steps can lead to a visual impression of discontinuity even if the wetted areas of the cells are continuous (Goodell, 2015). Moreover, the acceleration term in the full momentum equation cannot be neglected in such a steep terrain. Therefore, full momentum shallow water equation set was used which gave a more continuous flow and stable results for these steeper sections in HR2D. Even after

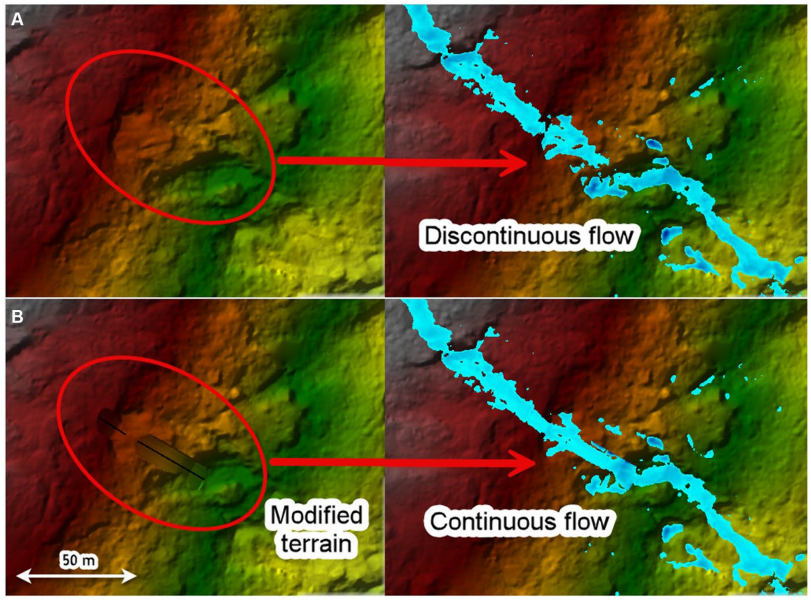

FIGURE 6
Original **(A)** and the modified river **(B)** at the steep sections.

using the SWE-ELM with 1 s of computation interval, the flow was discontinuous at a small section of the river where there was a sudden vertical drop. The channel was modified at this location to smoothen the drop (Figure 6) and the flow became continuous. On the other hand, there was not such a discontinuity problem in T2D results because T2D calculates the values at the nodes of the triangular mesh elements and distributes evenly inside the grid cell. Hence, no discontinuity problem was observed inside the cells.

3.3 Multi-storm flood events with sustained flow

Figure 7 shows results from HBV hydrological model and T2D and HR2D HDRRM models for a flood event occurred by multiple storms. T2D simulations were run using the CN method, and HR2D simulations were run using CN and GAR methods. The results from the GAR method in HR2D (green curve in Figure 7) show that the flow between the two peaks was not reproduced, and the second peak is way higher than that of the observed flow.

Hydraulic conductivity (K_s) affects the resulting runoff volume throughout the entire event. When the conductivity is less than the rainfall rate throughout the event, the infiltration rate decreases exponentially to reach the infiltration rate equal to the hydraulic conductivity. During the rainfall hiatus period (when $K_s >$ rainfall rate), the infiltration rate is approximately equal to the K_s (which is higher than the rainfall). As explained in section 2.2.6, the actual infiltration will be minimum of the infiltration rate [f(t)] and the rainfall rate. Hence, most of the rain infiltrates and the sustained flow between the two storms are not reproduced. For the event as shown in Figure 7, the minimum precipitation rate between the two rainstorms is approximately 5 mm/h; so, to maintain the non-hiatus period and the flow between the two storms, the K_s should always be less than 5 mm/h. However, such a low value of hydraulic conductivity results in higher peak flows for both the storms. Hence, a higher value of the hydraulic conductivity, 10 mm/h is used to calibrate the model at least for the first peak. Consequently, this high value of conductivity leads to a lower flow between the peaks.

The simulated extremely high peak flow for the last storm in this event is because even though the infiltration rate decreases with the time, the soil moisture recovery was not enough prior to the following heavy rainfall. Attempts were made to calibrate this peak, but the model results were not very sensitive to the two GAR parameters, which are responsible for the recovery of the infiltration rate. A sensitivity analysis for all the GAR parameters was done to better understand the effect of these parameters. The results are shown in the subsequent section. The GAR parameters used for the event, as shown in Figure 7, are:

Wetting Front Suction = 100 mm;
Saturated Hydraulic Conductivity = 10 mm/h;
Initial Soil Water Content = 0.1;
Saturated Soil Water Content = 0.8;
Residual Soil Water Content = 0.02;
Pore-size Distribution Index = 0.7;

Additionally, there always exists a return flow component. In such a steep catchment with shallow soils, the contributing return flow is even higher to the river. The water which is infiltrated into the shallow soils is permanently lost from the T2D and HR2D models because a groundwater model is not incorporated into these HDRR models, and thereby, the infiltrated water does not contribute to the runoff flow in

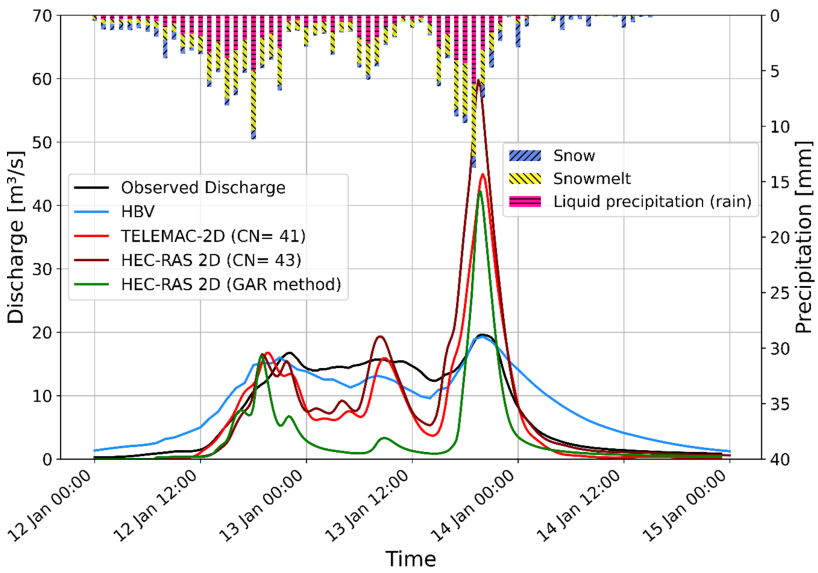

FIGURE 7
Multi-storm flood event with two peaks induced by a rain-on-snow event. Observed discharge (black) and results from the hydrologic model HBV (blue) and hydrodynamic rainfall-runoff models T2D (red) and HR2D from CN (maroon) and GAR methods (green).

the river. However, it is well established that in reality, the infiltrated water significantly contributes to the runoff in thin soils with steep slopes. Therefore, this problem of low flow between the storms can be resolved by introducing a delay mechanism that enables the infiltrated water to resurface and contribute to the runoff between the two precipitation events. This is precisely what is implemented in the soil routine of the HBV model, where the release of water from the soil routine to the runoff is followed by a retention delay that mimics the subsurface water dynamic. In the HBV model, the sub-surface water that is withheld by the soil routine is available for the model for future time-steps, which ensures continued runoff generation during the entire events with sustained flow. This contrasts with the T2D and HR2D models, where the infiltrated water is lost and not included in the runoff at later stages.

Furthermore, it is also shown in Figure 7 that CN method and GAR method did not give similar result for the flow between two peaks. The reason behind this is that the CN method has a constant infiltration rate, but in the GAR method, the infiltration rate varies with time based on the relationship between precipitation rate and hydraulic conductivity. The actual infiltration rate in the GAR method is the minimum out of the precipitation rate and the infiltration rate as calculated by Equation (10). Since the precipitation rate is lower than the hydraulic conductivity, most of the precipitation infiltrates, in contrast to the CN method, which has a constant infiltration. Therefore, the flow between the two peaks is higher for the CN method than for GAR method, as shown in Figure 7.

Figure 8 shows the cumulative precipitation, infiltration, and excess depth for a grid cell from the HR2D simulation using both CN and GAR infiltration methods for the event, as shown in Figure 7. The results show that the difference between the precipitation depth and the excess depth is equal to the infiltration depth, which means if the infiltrated water could contribute to the runoff as a return flow, the flow between the storms would have been higher and sustained. Figure 8 also shows how the infiltration rate in the GAR method varies and confirms that it is higher in the GAR method than in the CN method for the period between the two storms (roughly between 12 January 20:00 and 13 January 08:00) as claimed in the previous paragraph.

3.4 Sensitivity analysis of GAR method parameters

Based on the experience from the multipeak event (Figure 7) and the application of the CN method in T2D in the earlier study (Godara et al., 2023a), it is evident that the CN method has limitations to produce satisfactory results for flood events with multiple peak flows. Therefore, the HR2D model with the GAR infiltration method was tested to simulate such events because GAR has a variable infiltration rate unlike the CN method. In theory, the GA model should be able to recover the infiltration capacity during dry periods (Brunner, 2020), as also explained in the methods section, and should overcome the limitations of the CN method in T2D. However, this was not the case as shown in the previous section. Hence, sensitivity analysis of the GAR method parameters was done to understand why this method is not be able to reproduce multi-peak floods and understand the effect of each parameter. The analysis was done on a smaller area with two cells for faster simulations.

The parameters for original GA method are Wetting Front Suction (Ψ), Saturated Hydraulic Conductivity (K_s), Initial Soil Moisture Content (θi), and the Saturated Soil Moisture Content also called the

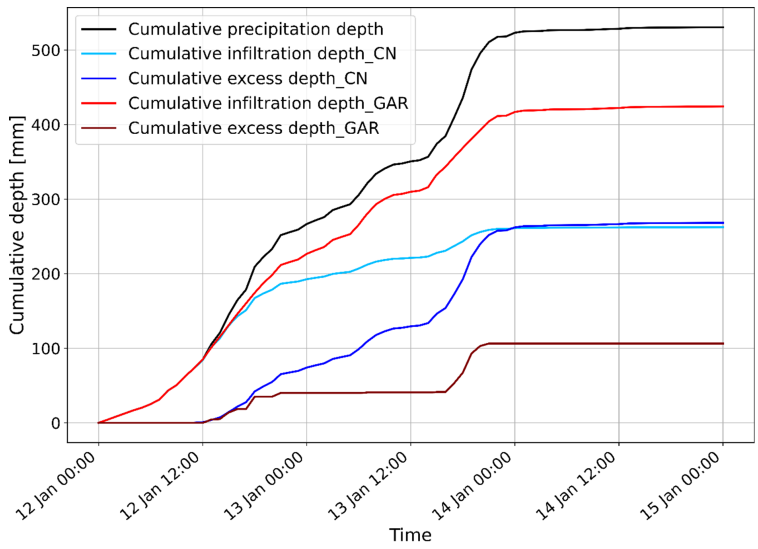

FIGURE 8
Cumulative precipitation, infiltration depths, and excess depths for a grid cell from HR2D simulation using CN and GAR methods for the event, shown in Figure 7.

Porosity (θs). Two additional parameters making it the GAR method are Residual Soil Moisture Content (θr) and Pore-size Distribution Index (λ). These six parameters were used for the flood events triggered by multi-storm precipitations. The analysis shows that the results are most sensitive to the four parameters that are used in the basic GA method, whereas the additional two parameters from the GAR method do not have a large effect on the results. The subsequent sub-sections show the effect of each parameter in detail.

3.4.1 Saturated hydraulic conductivity (K_S)

Three values of hydraulic conductivity $K_S = 2$, 5 and 10 mm/h were used in a smaller model to check the sensitivity using a constant precipitation rate of 10 mm/h. All the other parameters were kept constant. The results in Figures 9A,B show that if the hydraulic conductivity is more than or equal to the precipitation rate (10 mm/h in this case), all the water infiltrates and there is no excess water left as surface runoff. Additionally, as the difference between conductivity and precipitation rate increases, infiltration decreases exponentially to reach an infiltration rate equal to the hydraulic conductivity.

3.4.2 Suction head (Ψ)

A constant precipitation rate of 10 mm/h was used over two cells to check the sensitivity of suction head for three values $\Psi = 100$, 400, and 700 mm keeping the other parameters constant. The results in Figures 9C,D show that the higher the suction head, the higher the infiltration rate. Consequently, the excess flow rate is lower, and runoff starts later in time for a higher suction head.

3.4.3 Moisture deficit (θd = θs − θi)

Various values of initial (θi) and saturated (θs) moisture content were tested, and it was found that the results were sensitive to the difference between the two moisture contents (moisture deficit (θd)), instead of the initial and saturated moisture contents separately. Constant precipitation rate of 10 mm/h, $K_S = 5$ mm/h, and $\Psi = 700$ mm was used over the cells to check the sensitivity. Figures 10A,B shows that the higher the moisture deficit, the larger the infiltration rate, and the surface runoff start later in time. The results also show the same curves for the scenarios, where the value of moisture deficit is same, even though the initial and saturated moisture content values are changed.

3.4.4 Residual water content (θr)

Residual moisture content θr is the one of the parameters that affects the shape of the hydrograph after the rainfall hiatus period (GAR method). Therefore, a rainfall event with varying intensities 10 mm/h, 5 mm/h and 15 mm/h was used in this case as shown in Figure 11A. Keeping the initial and saturated moisture contents constant along with the rest of the parameters, residual moisture content was varied from minimum 0.01 to maximum 0.1 (as per the Table 4 in Brunner, 2020). Figures 11B,C shows that the higher the residual moisture content, the lower the infiltration rate after the rainfall hiatus period and the higher the second peak, but the results are not very sensitive to this GAR parameter.

Different combinations of the initial and saturated moisture contents were also tested for sensitivity (Figures 11D,E), keeping the same values for residual moisture content and moisture deficit. The results in Figure 11 show that the effect is only on the second peak, but overall, the results are not very sensitive.

3.4.5 Pore size distribution index (λ)

Keeping all the parameters constant and using the same varying precipitation as above, the pore size infiltration index was changed to

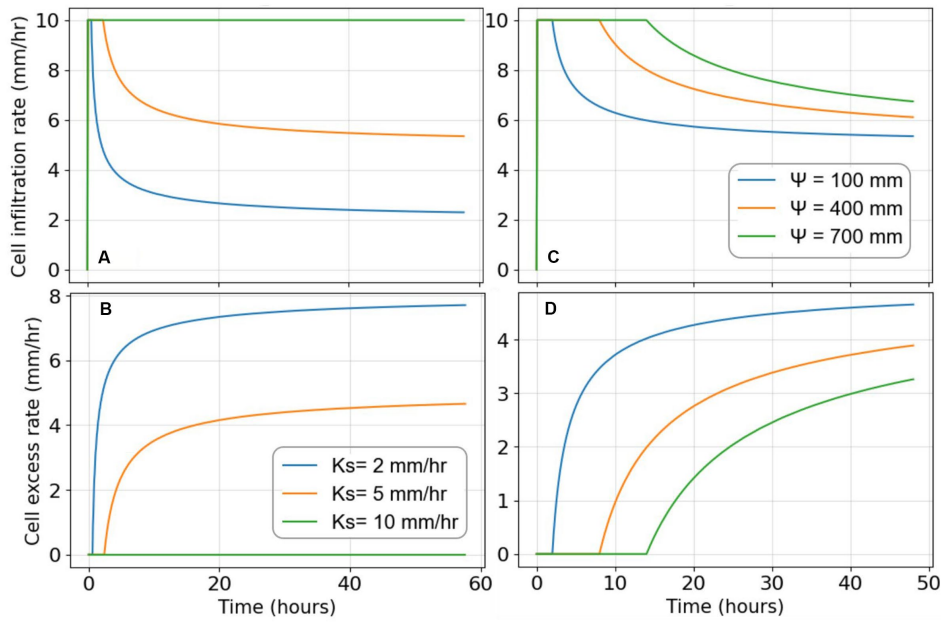

FIGURE 9
Cell infiltration and excess rate for different saturated hydraulic conductivity **(A,B)** and suction heads **(C,D)** using precipitation rate of 10 mm/h.

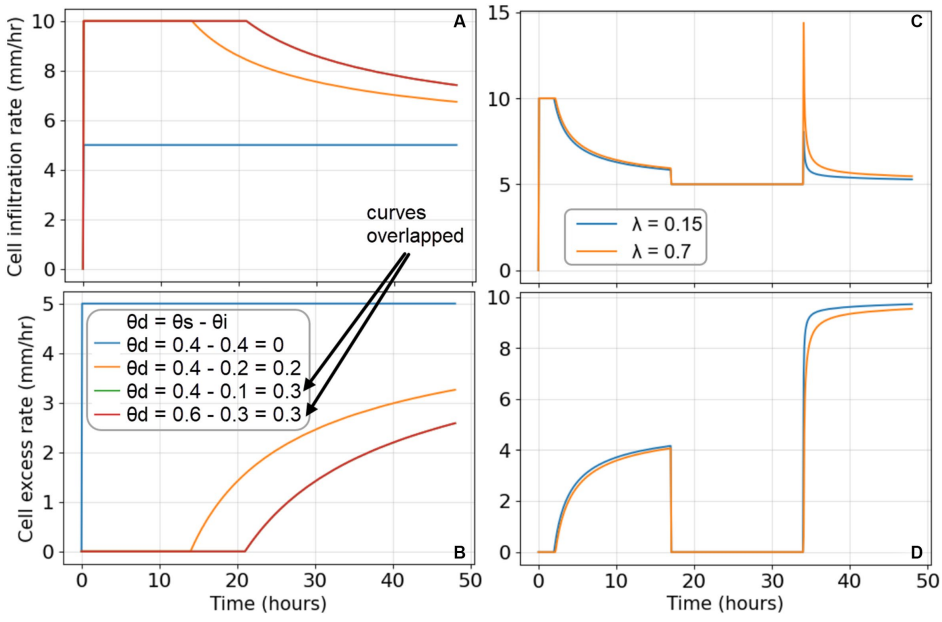

FIGURE 10
Cell infiltration and excess rate for different moisture deficit values **(A,B)** and the maximum and minimum values of pore size distribution index **(C,D)**.

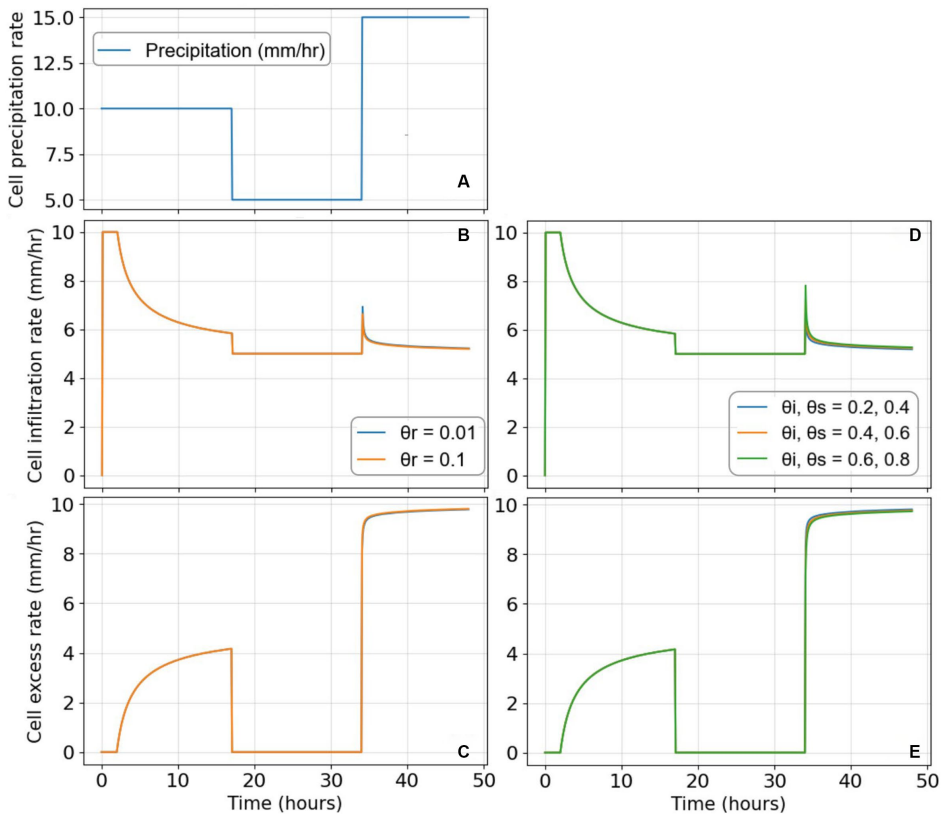

FIGURE 11
Precipitation **(A)** used for the sensitive analysis of redistribution parameters, **(B,C)** show cell infiltration and excess rate for the various values of the residual moisture contents. **(D,E)** Show the same for various combinations of initial and saturated moisture contents, keeping the same value of moisture deficit.

the maximum and minimum values of λ (0.7 and 0.15) (Brunner, 2020). The results in Figures 10C,D show that higher the pore size index, the lower the first and second peak flows, but the second peak is influenced more, although the overall results are not very sensitive to the value of pore size distribution index.

The outcomes of the sensitivity analysis reveal that the GAR method behaves as anticipated and produces the expected results. Nevertheless, it is still not be able to simulate longer flood events correctly. This discrepancy suggests that the probable cause for the inability to reproduce multi-storm and prolonged flood events lies in the loss of infiltrated water and the absence of a subsurface water module in HDRR models (T2D and HR2D).

3.5 Velocity and inundation maps

Figures 12, 13 show velocity and inundation maps from the models T2D and HR2D for event B, as shown in Figure 5. Finer mesh (3 m × 3 m) was introduced along the steep section of the river in both the models to capture the terrain with better accuracy. The results show that the inundation areas are approximately the same from both the models except that T2D shows continuous regions, whereas HR2D shows that it scattered at some locations outside the river reach. This discrepancy in the results was also observed in a study (Orozco et al., 2023), where the two models were compared for levee breach analysis. This difference is because T2D distributes the water evenly across each grid cell calculated from the values at nodes of the grid cell. In contrast, HR2D has sub-grid technology, preserving the detailed information of topography within the grid cells, resulting in partially wet cells and more distinctly defined floodplain areas. This feature enhances result precision, providing a more comprehensive understanding of the area and water behavior during both modeling and post-processing stages. Because of this difference, the extent of the inundation seems more continuous from T2D simulations as compared with that from HR2D simulations.

Furthermore, the results show that maximum water depth and maximum velocity values are higher in HR2D than T2D. The reason behind excessively high maximum values can be the steep slope of the catchment, in which HR2D probably is not designed to accommodate. Some locations in the catchment have vertical drops, and even after refining the mesh, tiny ponds were formed similar to the ones shown

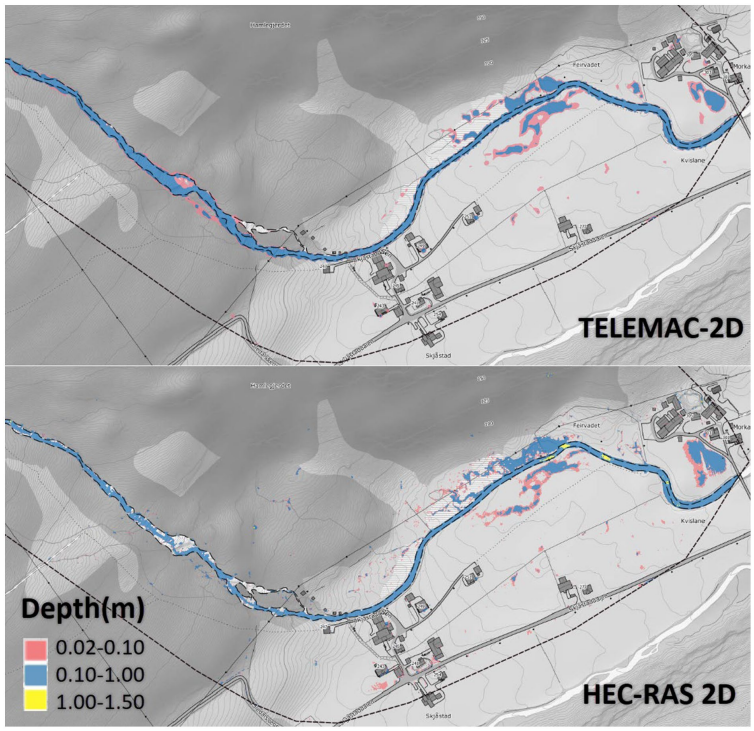

FIGURE 12
Water depth results from T2D and HR2D simulation results for event B in Figure 5.

in Figure 3A, with a high value of depth at the location and velocity at these vertical drops.

In general, higher values of velocity were calculated by HR2D, as shown in Figure 13. Figure 14 shows the velocity distribution along the centerline of the river stretch shown in depth and velocity maps, along with the slope in the same river stretch. The figure shows that HR2D calculates higher velocities than T2D along the steeper sections, especially when the slope is more than approximately 20 degrees which is way above the suggested maximum slope values for HR2D (Brunner, 2016). However, velocities at the flatter sections were mostly similar from both the models, as shown in the most right and the most left river sections in Figures 13, 14.

4 Conclusion

The goal of this study was to compare the two hydrodynamic rainfall-runoff models TELEMAC-2D and HEC-RAS 2D for their rain-on-grid technique and, especially, to reproduce long-duration flood events with sustained flow between flow peaks. Sensitivity analysis of the GAR infiltration method parameters was also done to understand the behavior of models to simulate such events. The study has also explored their strengths and weaknesses in terms of calibration process, simulation run-time, input file preparation, and post-processing of results. Use of CN infiltration method in T2D and HR2D was compared, as well as the GAR infiltration method in HR2D was tested in the RoG technique.

Peak flow for single storm flood events was reproduced by both the models. The results show that this fully integrated hydrodynamic rainfall-runoff modeling with RoG tool can only be used for flash floods in small rivers not for a big river flood with long duration floods, where significant amount of water infiltrates. The plots from this study and our previous studies on this topic conclude that this type of models is good to simulate single-storm flood events limited to 10–15 h of duration or to the flood events where it is sure that the infiltrated water percolates to the deep groundwater flow, and there is no chance of subsurface return flow. For the longer duration single-storm floods, the recession part is not simulated well. Similarly, for multi-storm events, this tool fails to accurately capture the flow dynamics between the storms. Although, the sensitivity analysis of the GAR parameters on a multi-storm event gave expected results, but none of the HDRR models with CN or GAR infiltration method could simulate this. The main reason for this limitation is the lack of a soil routine module which can include the contribution of delayed subsurface water to resulting flow hydrograph. The addition of a subsurface water routine inside the HDRR models should be one of the future works. Furthermore, the resulting inundation maps from the models should be compared with the observed inundation maps, since

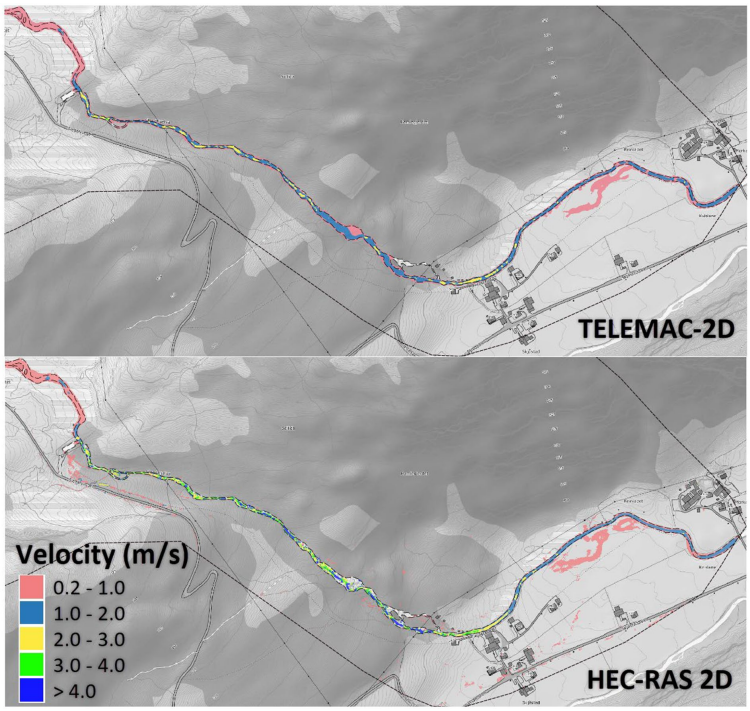

FIGURE 13
Velocity results from T2D and HR2D simulation results for event B in Figure 5.

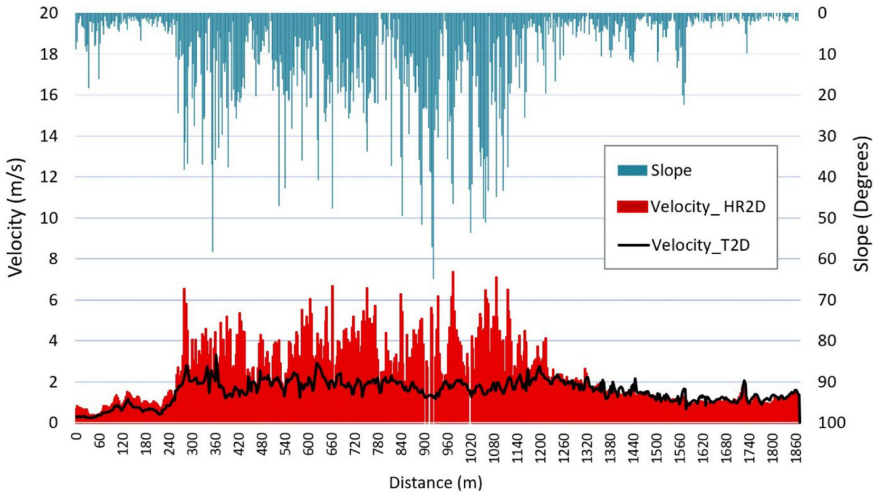

FIGURE 14
Slope (blue clustered columns on the secondary axis) and velocity distribution (red clustered columns from HR2D and black line from T2D) along the centerline of the river stretch shown in Figures 12, 13.

these were not available for the area and flood events used in this study.

Nonetheless, the tool developed in this research study is applicable for analyzing flash floods and their consequences in steep catchments. Since flash floods are expected to increase in future due to increased short-duration, high-intensity precipitation events, this model will hold direct relevance and significance in future assessments of climate change impacts in terms of flash floods. The results from this study may help the engineers and researchers to choose the suitable model for their purpose out of the two hydrodynamic rainfall-runoff models which have the option for modeling a steep catchment and river systems using rain-on-grid technique. Furthermore, these results can provide a useful tool for flood risk management, infrastructure planning, and risk and vulnerability analysis for flash floods using an appropriate rain-on-grid hydrodynamic model. The analysis can help the municipality and infrastructure planners to find critical locations in an area in terms of submergence, water depth, high velocities, and shear stresses.

Data availability statement

The raw data supporting the conclusions of this article will be made available by the authors, without undue reservation.

Author contributions

NG: Conceptualization, Data curation, Formal analysis, Investigation, Methodology, Software, Validation, Visualization, Writing – original draft, Writing – review & editing. OB: Conceptualization, Funding acquisition, Methodology, Project administration, Resources, Supervision, Writing – review & editing. KA: Conceptualization, Methodology, Supervision, Writing – review & editing.

Funding

The author(s) declare that financial support was received for the research, authorship, and/or publication of this article. This publication was part of the World of Wild Waters (WoWW) project number 949203100, which falls under the umbrella of the Norwegian University of Science and Technology (NTNU)'s Digital Transformation initiative.

Conflict of interest

The authors declare that the research was conducted in the absence of any commercial or financial relationships that could be construed as a potential conflict of interest.

Publisher's note

References

Barredo, J. I. (2007). Major flood disasters in Europe: 1950–2005. *Nat. Hazards* 42, 125–148. doi: 10.1007/s11069-006-9065-2

Barton, A. J. (2019). Blue Kenue enhancements from 2014 to 2019. 26th TELEMAC-MASCARET User Conference, 15th to 17th October 2019, Toulouse.

Basso-Báez, S., Mazzorana, B., Ulloa, H., Bahamondes, D., Ruiz-Villanueva, V., Sanhueza, D., et al. (2020). Unravelling the impacts to the built environment caused by floods in a river heavily perturbed by volcanic eruptions. *J. S. Am. Earth Sci.* 102:102655. doi: 10.1016/j.jsames.2020.102655

Bergström, S., and Forsman, A. (1973). Development of a conceptual deterministic rainfall - runoff model. *Nord. Hydrol.* 4, 147–170. doi: 10.2166/nh.1973.0012

Borga, M., Stoffel, M., Marchi, L., Marra, F., and Jakob, M. (2014). Hydrogeomorphic response to extreme rainfall in headwater systems: flash floods and debris flows. *J. Hydrol.* 518, 194–205. doi: 10.1016/j.jhydrol.2014.05.022

Bruland, O. (2020). How extreme can unit discharge become in steep Norwegian catchments? *Hydrol. Res.* 51, 290–307. doi: 10.2166/nh.2020.055

Brunner, G. W. (2002). Hec-ras (river analysis system). In North American water and environment congress & destructive water ASCE. 3782–3787.

Brunner, G. W. (2016). HEC-RAS river analysis system: hydraulic reference manual, version 5.0. Davis, CA, USA: US Army Corps of Engineers–Hydrologic Engineering Center. 547.

Brunner, G. W. (2020). HEC-RAS river analysis system: hydraulic reference manual, version 6.0 Beta. Davis, CA, USA: US Army Corps of Engineers–Hydrologic Engineering Center. 1–464.

David, A., and Schmalz, B. (2021). A systematic analysis of the interaction between rain-on-grid-simulations and spatial resolution in 2d hydrodynamic modeling. *Water (Switzerland)* 13:2346. doi: 10.3390/w13172346

Engeland, K., Abdella, S. Y., Azad, R., Arrturi Elo, C., Lussana, C., Tadege Mengistu, Z., et al. (2018). Use of precipitation radar for improving estimates and forecasts of precipitation estimates and streamflow. 20th EGU General Assembly, EGU2018, Proceedings from the Conference, 4–13 April, 2018, Vienna.

Feng, B., Zhang, Y., and Bourke, R. (2021). Urbanization impacts on flood risks based on urban growth data and coupled flood models. *Nat. Hazards* 106, 613–627. doi: 10.1007/s11069-020-04480-0

Godara, N., Bruland, O., and Alfredsen, K. (2023a). Modelling flash floods driven by rain-on-snow events using rain-on-grid technique in the hydrodynamic model TELEMAC-2D. *Water* 15:3945. doi: 10.3390/w15223945

Godara, N., Bruland, O., and Alfredsen, K. (2023b). Simulation of flash flood peaks in a small and steep catchment using rain-on-grid technique. *J. Flood Risk Manag.* 16, 1–14. doi: 10.1111/jfr3.12898

Goodell, C. (2015). *2D troubleshooting – fragmented inundation*. Available at: https://www.kleinschmidtgroup.com/ras-post/2d-troubleshooting-fragmented-inundation/

Goodell, C. (2016). *Optimizing your Computer for Fast HEC-RAS modeling*. Available at: https://www.kleinschmidtgroup.com/ras-post/optimizing-your-computer-for-fast-hec-ras-modeling/

Green, W. H., and Ampt, G. A. (1911). Studies on Soil Physics. *The Journal of Agricultural Science*, 4, 1–24. doi: 10.1017/S0021859600001441

Hariri, S., Weill, S., Gustedt, J., and Charpentier, I. (2022). A balanced watershed decomposition method for rain-on-grid simulations in HEC-RAS. *J. Hydroinf.* 24, 315–332. doi: 10.2166/hydro.2022.078

Huang, M., Gallichand, J., Wang, Z., and Goulet, M. (2006). A modification to the soil conservation service curve number method for steep slopes in the loess plateau of China. *Hydrol. Process.* 20, 579–589. doi: 10.1002/hyp.5925

Jha, L. K., and Khare, D. (2016). Glacial lake outburst flood (GLOF) study of Dhauliganga basin in the Himalaya. *Cogent Environ. Sci.* 2:1249107. doi: 10.1080/23311843.2016.1249107

Johnson, J. P. L., Whipple, K. X., and Sklar, L. S. (2010). Contrasting bedrock incision rates from snowmelt and flash floods in the Henry Mountains, Utah. *Geol. Soc. Am. Bull.* 122, 1600–1615. doi: 10.1130/B30126.1

Kishore, N., and Rishi, S. (2014). Morphometry and geomorphological investigations of the Neugal watershed, Beas River basin, Kangra District, Himachal Pradesh using GIS tools. *J. Environ. Earth Sci.* 4, 78–86.

Li, L., Pontoppidan, M., Sobolowski, S., and Senatore, A. (2020). The impact of initial conditions on convection-permitting simulations of a flood event over complex mountainous terrain. *Hydrol. Earth Syst. Sci.* 24, 771–791. doi: 10.5194/hess-24-771-2020

Ligier, P. (2016). Implementation of a rainfall-runoff model in TELEMAC-2D. In: *Bourban, Sébastien (Hg.): Proceedings of the XXIIIrd TELEMAC-MASCARET User Conference 2016, 11 to 13 October 2016*, Paris, France. Oxfordshire: HR Wallingford. S. 13–19.

Lin, Q., Lima, P., Steger, S., Glade, T., Jiang, T., Zhang, J., et al. (2021). National-scale data-driven rainfall induced landslide susceptibility mapping for China by accounting for incomplete landslide data. *Geosci. Front.* 12:101248. doi: 10.1016/j.gsf.2021.101248

Liu, T., Wang, Y., Yu, H., and Chen, Y. (2022). Using statistical functions and hydro-hydraulic models to develop human vulnerability curves for flash floods: the flash flood of the Taitou catchment (China) in 2016. *Int. J. Disast. Risk Reduct.* 73:102876. doi: 10.1016/j.ijdrr.2022.102876

Maatar, F. E., Domeneghetti, A., and Brath, A. (2015). HEC-RAS 5.0 vs. TELEMAC-2D: a model comparison for flood-hazard and flood-risk estimation. EGU General Assembly, Held 12–17 April, 2015, Vienna.

Maqtan, R., Othman, F., Wan Jaafar, W. Z., Sherif, M., and El-Shafie, A. (2022). A scoping review of flash floods in Malaysia: current status and the way forward. *Nat. Hazards* 114, 2387–2416. doi: 10.1007/s11069-022-05486-6

Marchi, L., Borga, M., Preciso, E., and Gaume, E. (2010). Characterisation of selected extreme flash floods in Europe and implications for flood risk management. *J. Hydrol.* 394, 118–133. doi: 10.1016/j.jhydrol.2010.07.017

Moraru, A., Pavlíček, M., Bruland, O., and Rüther, N. (2021). The story of a Steep River: causes and effects of the flash flood on 24 July 2017 in Western Norway. *Water* 13:1688. doi: 10.3390/W13121688

Nash, J. E., and Sutcliffe, J. V. (1970). River flow forecasting through conceptual models part I—a discussion of principles. *J. Hydrol.* 10, 282–290. doi: 10.1016/0022-1694(70)90255-6

Ogden, F. L., and Saghafian, B. (1997). Green and Ampt infiltration with redistribution. *Water Resour. Res.* 123, 386–393. doi: 10.1061/(ASCE)0733-9437(1997)123:5(386)

Orozco, A. N. R., Bertrand, N., Pheulpin, L., Migaud, A., and Abily, M. (2023). "Comparison between HEC-RAS and TELEMAC-2D hydrodynamic models of the Loire River, integrating levee breaches" in *SimHydro 2023: New Modelling Paradigms for Water Issues?*

Pearson, P. K. (1897). Mathematical contributions to the theory of evolution.—on a form of spurious correlation which may arise when indices are used in the measurement of organs. *Proc. R. Soc. Lond.* 60, 489–498. doi: 10.1098/rspl.1896.0076

Pilotti, M., Milanesi, L., Bacchi, V., Tomirotti, M., and Maranzoni, A. (2020). Dam-break wave propagation in Alpine Valley with HEC-RAS 2D: experimental Cancano test case. *J. Hydraul. Eng.* 146, 1–11. doi: 10.1061/(asce)hy.1943-7900.0001779

Rangari, V. A., Umamahesh, N. V., and Bhatt, C. M. (2019). Assessment of inundation risk in urban floods using HEC RAS 2D. *Model. Earth Syst. Environ.* 5, 1839–1851. doi: 10.1007/s40808-019-00641-8

Sarker, S. (2022). A short review on computational hydraulics in the context of water resources engineering. *Open J. Model. Simul.* 10, 1–31. doi: 10.4236/ojmsi.2022.101001

Seneviratne, S. I., Zhang, X., Adnan, M., Badi, W., Dereczynski, C., Di Luca, S. G., et al. (2021). *IPCC - climate change 2021: The physical science basis - chapter 11: Weather and climate extreme events in a changing climate*. Cambridge: Cambridge University Press.

Swanston, D. N. (1974). Slope stability problems associated with timber harvesting in mountainous regions of the Western United States. *USDA For. Serv. Gen. Tech. Rep.* PNW-21:21,

Sweeney, T. L. (1992). *Modernized areal flash flood guidance*. Springfield VA USA: NOAA technical memorandum NWS HYDRO, 44.

TELEMAC-2D User Manual v8p2. (2020). 1 December 2020. Last accessed: 12 January 2024. https://gitlab.pam-retd.fr/otm/telemac-mascaret/-/raw/v8p5r0/documentation/telemac2d/user/telemac2d_user_v8p2.pdf

Vázquez Conde, M. T., Lugo, J., and Guadalupe Matías, L. (2001). "Heavy rainfall effects in Mexico during early October 1999" in *Coping with flash floods* (Netherlands: Springer), 289–299.

Vu, T., Nguyen, P., Chua, L., and Law, A. (2015). Two-dimensional hydrodynamic modelling of flood inundation for a part of the Mekong River with TELEMAC-2D. *Br. J. Environ. Clim. Change* 5, 162–175. doi: 10.9734/bjecc/2015/12885

Zeiger, S. J., and Hubbart, J. A. (2021). Measuring and modeling event-based environmental flows: an assessment of HEC-RAS 2D rain-on-grid simulations. *J. Environ. Manag.* 285:112125. doi: 10.1016/j.jenvman.2021.112125

Zhang, G., Cui, P., Yin, Y., Liu, D., Jin, W., Wang, H., et al. (2019). Real-time monitoring and estimation of the discharge of flash floods in a steep mountain catchment. *Hydrol. Process.* 33, 3195–3212. doi: 10.1002/hyp.13551

Bibliography

M. Abily, N. Bertrand, O. Delestre, P. Gourbesville, and C.-M. Duluc. Spatial Global Sensitivity Analysis of High Resolution classified topographic data use in 2D urban flood modelling. *Environmental Modelling & Software*, 77:183–195, 3 2016. ISSN 13648152. doi: 10.1016/j.envsoft.2015.12.002. URL https://linkinghub.elsevier.com/retrieve/pii/S136481521530116X.

K. Ali, R. M. Bajracharyar, and N. Raut. Advances and Challenges in Flash Flood Risk Assessment: A Review. *Journal of Geography & Natural Disasters*, 07 (02), 2017. ISSN 21670587. doi: 10.4172/2167-0587.1000195. URL https://www.researchgate.net/publication/317821569_Advances_and_Challenges_in_Flash_Flood_Risk_Assessment_A_Review.

S. E. A. Ali. *Assessing the Performance of 2D HEC-RAS Rain-on-Grid Model: A Case Study in the Rainbow Creek Subwatershed*. PhD thesis, The University of Guelph, 2024. URL https://atrium.lib.uoguelph.ca/items/f0fef65c-e2b5-4a4b-b519-6767fe47b8b4.

H. Apel, G. T. Aronica, H. Kreibich, and A. H. Thieken. Flood risk analyses—how detailed do we need to be? *Natural Hazards*, 49(1):79–98, 4 2009. ISSN 0921-030X. doi: 10.1007/s11069-008-9277-8. URL http://link.springer.com/10.1007/s11069-008-9277-8.

J. G. Arnold, R. Srinivasan, R. S. Muttiah, and J. R. Williams. LARGE AREA HYDROLOGIC MODELING AND ASSESSMENT PART I: MODEL DEVELOPMENT 1. *JAWRA Journal of the American Water Resources Association*, 34(1):73–89, 2 1998. ISSN 1093-474X. doi: 10.1111/j.1752-1688.1998.tb05961.x. URL https://onlinelibrary.wiley.com/doi/10.1111/j.1752-1688.1998.tb05961.x.

A. Barattieri, P. Borda, A. Brugnoli, M. Pelli, and J. Tschopp. The short-run, dynamic employment effects of natural disasters: New insights from Puerto Rico. *Ecological Economics*, 205:107693, 3 2023. ISSN 09218009. doi: 10.1016/j.ecolecon.2022.107693. URL https://linkinghub.elsevier.com/retrieve/pii/S0921800922003548.

A. J. Barton. Blue Kenue enhancements from 2014 to 2019. In *26th TELEMAC-MASCARET User Conference, 15th to 17th October 2019, Toulouse.*, number October, 2019. doi: https://doi.org/10.5281/zenodo.3611511.

S. Bergström. THE DEVELOPMENT OF A SNOW ROUTINE FOR THE HBV-2 MODEL. *Nordic Hydrology*, 6(2):73–92, 1975. URL https://www.proquest.com/scholarly-journals/development-snow-routine-hbv-2-model/docview/1943669082/se-2.

S. Bergström and A. Forsman. Development of a conceptual deterministic rainfall - runoff model. *NORDIC HYDROLOGY*, 4:240–253, 1973.

K. Beven. *Rainfall-Runoff Modelling*. Wiley, 1 2012. ISBN 9780470714591. doi: 10.1002/9781119951001. URL https://onlinelibrary.wiley.com/doi/book/10.1002/9781119951001.

K. Beven and A. Binley. The future of distributed models: Model calibration and uncertainty prediction. *Hydrological Processes*, 6(3):279–298, 7 1992. ISSN 0885-6087. doi: 10.1002/hyp.3360060305. URL https://onlinelibrary.wiley.com/doi/10.1002/hyp.3360060305.

K. Broich, T. Pflugbeil, M. Disse, and H. Nguyen. Using TELEMAC-2D for Hydrodynamic Modeling of Rainfall-Runoff. *XXVIth Telemac & Mascaret User Club*, (October), 2019.

O. Bruland. How extreme can unit discharge become in steep Norwegian catchments? *Hydrology Research*, 51(2):290–307, 2020. ISSN 22247955. doi: 10.2166/nh.2020.055.

O. Bruland. Snow processes, modeling, and impact. In *Precipitation*, pages 107–143. Elsevier, 1 2021. doi: 10.1016/B978-0-12-822699-5.00006-9. URL https://linkinghub.elsevier.com/retrieve/pii/B9780128226995000069.

G. W. Brunner. HEC-RAS Hydraulic Reference Manual V6.3. *US Army Corps of Engineers*, (August):1–464, 2020.

G. W. Brunner. HEC-RAS River Analysis System. Hydraulic User's Manual, Version 6.0. 2021.

J. F. Burkhart, F. N. Matt, S. Helset, Y. Sultan Abdella, O. Skavhaug, and O. Silantyeva. Shyft v4.8: a framework for uncertainty assessment and distributed hydrologic modeling for operational hydrology. *Geoscientific Model Development*, 14(2):821–842, 2 2021. ISSN 1991-9603. doi: 10.5194/gmd-14-821-2021. URL https://gmd.copernicus.org/articles/14/821/2021/.

D. Caviedes-Voullième, P. García-Navarro, and J. Murillo. Influence of mesh structure on 2D full shallow water equations and SCS Curve Number simulation of rainfall/runoff events. *Journal of Hydrology*, 448-449:39–59, 2012. ISSN 00221694. doi: 10.1016/j.jhydrol.2012.04.006.

V. Chow. *Open Channel Hydraulics*. McGaw-Hill Classical Textbook Reissue, New York, 1988. ISBN ISBN 0-07-010810-2.

V. T. Chow, D. R. Maidment, and L. W. Mays. *Applied Hydrology*. McGaw-Hill, Singapore, 1988. ISBN 0-07-100174-3. URL http://ponce.sdsu.edu/Applied_Hydrology_Chow_1988.pdf.

X. Chu and A. Steinman. Event and Continuous Hydrologic Modeling with HEC-HMS. *Journal of Irrigation and Drainage Engineering*, 135(1):119–124, 2 2009. ISSN 0733-9437. doi: 10.1061/(ASCE)0733-9437(2009)135:1(119). URL https://ascelibrary.org/doi/10.1061/%28ASCE%290733-9437%282009%29135%3A1%28119%29.

K. Clark, J. Ball, and K. Babister. Can Fixed grid 2 Hydraulic Models be used as Hydrologic Models? In *Proceedings of Water Down Under 2008*, pages 2496 – 2507. 2008 Hydrology and Water resources Symposium, 2008.

P. Costabile, C. Costanzo, D. Ferraro, and P. Barca. Is HEC-RAS 2D accurate enough for storm-event hazard assessment? Lessons learnt from a benchmarking study based on rain-on-grid modelling. *Journal of Hydrology*, 603 (September):126962, 2021. ISSN 00221694. doi: 10.1016/j.jhydrol.2021.126962.

P. Costabile, C. Costanzo, C. Gandolfi, F. Gangi, and D. Masseroni. Effects of DEM Depression Filling on River Drainage Patterns and Surface Runoff Generated by 2D Rain-on-Grid Scenarios. *Water (Switzerland)*, 14(7), 2022. ISSN 20734441. doi: 10.3390/w14070997.

CRED. 2021 Disasters in numbers. *Centre for Research on the Epidemiology of Disasters*, 2022a. doi: 10.1787/eee82e6e-en. URL https://reliefweb.int/report/world/2021-disasters-numbers.

CRED. Natural Hazards & Disasters: an Overview of the First Half of 2022. *Archives of Public Health*, 80(1):1–2, 2022b. ISSN 20493258. doi: 10.1186/s13690.

A. David and B. Schmalz. A Systematic Analysis of the Interaction between Rain-on-Grid-Simulations and Spatial Resolution in 2D Hydrodynamic Modeling. *Water*, 13(17):2346, 8 2021. ISSN 2073-4441. doi: 10.3390/w13172346. URL https://www.mdpi.com/2073-4441/13/17/2346.

G. K. Devia, B. Ganasri, and G. Dwarakish. A Review on Hydrological Models. *Aquatic Procedia*, 4(Icwrcoe):1001–1007, 2015. ISSN 2214241X. doi: 10.1016/j.aqpro.2015.02.126. URL https://linkinghub.elsevier.com/retrieve/pii/S2214241X15001273.

Direktoratet for byggkvalitet. Veiledning om tekniske krav til byggverk. Technical Report July, 2017. URL http://www.jurpc.de/jurpc/show?id=20140073.

A. V. Dyrrdal, K. Isaksen, H. O. Hygen, and N. K. Meyer. Changes in meteorological variables that can trigger natural hazards in Norway. *Climate Research*, 55(2):153–165, 2012. ISSN 0936577X. doi: 10.3354/cr01125.

K. Engeland, S. Y. Abdella, R. Azad, C. Arrturi Elo, C. Lussana, Z. Tadege Mengistu, T. Nipen, and R. Randriamampianina. Use of precipitation radar for improving estimates and forecasts of precipitation estimates and streamflow. In *20th EGU General Assembly, EGU2018, Proceedings from the conference held 4-13 April, 2018 in Vienna, Austria*, page 12207, 2018. doi: 2018EGUGA..2012207E.

ESCAP. 2022 : A year when disasters compounded and cascaded by UN Economic and Social Commission for Asia and the Pacific, 2023. URL https://www.unescap.org/blog/2022-year-when-disasters-compounded-and-cascaded.

J. Garrote, F. Alvarenga, and A. Díez-Herrero. Quantification of flash flood economic risk using ultra-detailed stage–damage functions and 2-D hydraulic models. *Journal of Hydrology*, 541:611–625, 10 2016. ISSN 00221694. doi: 10.1016/j.jhydrol.2016.02.006. URL https://linkinghub.elsevier.com/retrieve/pii/S0022169416300312.

K. Glock, M. Tritthart, H. Habersack, and C. Hauer. Comparison of Hydrodynamics Simulated by 1D, 2D and 3D Models Focusing on Bed Shear Stresses. *Water*, 11(2):226, 1 2019. ISSN 2073-4441. doi: 10.3390/w11020226. URL http://www.mdpi.com/2073-4441/11/2/226.

W. H. Green and G. A. Ampt. Studies on Soil Physics. *The Journal of Agricultural Science*, 4(1):1–24, 5 1911. ISSN 0021-8596. doi: 10.1017/S0021859600001441. URL https://www.cambridge.org/core/product/identifier/S0021859600001441/type/journal_article.

S. Grimaldi, G. J. Schumann, A. Shokri, J. P. Walker, and V. R. Pauwels. Challenges, Opportunities, and Pitfalls for Global Coupled Hydrologic-Hydraulic Modeling of Floods. *Water Resources Research*, 55(7):5277–5300, 2019. ISSN 19447973. doi: 10.1029/2018WR024289.

J. Hall. Direct rainfall flood modelling: The good, the bad and the ugly. *Australian Journal of Water Resources*, 19(1):74–85, 2015. ISSN 13241583. doi: 10.7158/13241583.2015.11465458.

B. B. Hansen, K. Isaksen, R. E. Benestad, J. Kohler, Pedersen, L. E. Loe, S. J. Coulson, J. O. Larsen, and Varpe. Warmer and wetter winters: characteristics and implications of an extreme weather event in the High Arctic. *Environmental Research Letters*, 9(11):114021, 11 2014. ISSN 1748-9326. doi: 10.1088/1748-9326/9/11/114021. URL https://iopscience.iop.org/article/10.1088/1748-9326/9/11/114021.

I. Hanssen-Bauer, E. J. Førland, I. Haddeland, H. Hisdal, D. Lawrence, S. Mayer, A. Nesje, S. Sandven, A. B. Sandø, and A. Sorteberg. Climate in Norway 2100 – a knowledge base for climate adaptation. *Norwegian Environmental Agency, report no. 1/2017*, (1):1–47, 2017. URL www.miljodirektoratet.no/M741.

S. Hariri, S. Weill, J. Gustedt, and I. Charpentier. A balanced watershed decomposition method for rain-on-grid simulations in HEC-RAS. *Journal of Hydroinformatics*, 24(2):315–332, 2022. ISSN 14651734. doi: 10.2166/hydro.2022.078.

H. Heyerdahl and A. Høydal. Geomorphology and Susceptibility to Rainfall Triggered Landslides in Gudbrandsdalen Valley, Norway. *Advancing Culture of Living with Landslides*, 4:267–279, 2017. doi: 10.1007/978-3-319-53485-5.

R. Hinsberger, A. Biehler, and A. Yörük. Influence of Water Depth and Slope on Roughness—Experiments and Roughness Approach for Rain-on-Grid Modeling. *Water (Switzerland)*, 14(24), 2022. ISSN 20734441. doi: 10.3390/w14244017.

A. T. Hjelmfelt. Investigation of Curve Number Procedure. *Journal of Hydraulic Engineering*, 117(6):725–737, 6 1991. ISSN 0733-9429. doi: 10.1061/(ASCE)0733-9429(1991)117:6(725). URL http://ascelibrary.org/doi/10.1061/%28ASCE%290733-9429%281991%29117%3A6%28725%29.

A. Hope and R. Schulze. Improved estimates of stormflow volumes using the SCS curve number method. In *In: V.P. Singh (ed.), Rainfall-runoff relationships.Water Resources Publications, Littleton*, pages 419–431, 1982.

M. Huang, J. Gallichand, Z. Wang, and M. Goulet. A modification to the Soil Conservation Service curve number method for steep slopes in the Loess Plateau of China. *Hydrological Processes*, 20(3):579–589, 2 2006. ISSN 0885-6087. doi: 10.1002/hyp.5925. URL https://onlinelibrary.wiley.com/doi/10.1002/hyp.5925.

J. P. L. Johnson, K. X. Whipple, and L. S. Sklar. Contrasting bedrock incision rates from snowmelt and flash floods in the Henry Mountains , Utah. *Geological Society of America Bulletin*, 122(9/10):1600–1615, 2010. doi: 10.1130/B30126.1.

S. Khosh Bin Ghomash, D. Bachmann, D. Caviedes-Voullième, and C. Hinz. Impact of Rainfall Movement on Flash Flood Response: A Synthetic Study of a Semi-Arid Mountainous Catchment. *Water*, 14(12):1844, 6 2022. ISSN 2073-4441. doi: 10.3390/w14121844. URL https://www.mdpi.com/2073-4441/14/12/1844.

A. Killingtveit and N. R. Sælthun. *Hydropower development: hydrology*. 1995.

H. Kreibich, K. Piroth, I. Seifert, H. Maiwald, U. Kunert, J. Schwarz, B. Merz, and A. H. Thieken. Is flow velocity a significant parameter in flood damage modelling? *Natural Hazards and Earth System Science*, 9(5):1679–1692, 2009. ISSN 16849981. doi: 10.5194/nhess-9-1679-2009.

L. Li, M. Pontoppidan, S. Sobolowski, and A. Senatore. The impact of initial conditions on convection-permitting simulations of a flood event over complex mountainous terrain. *Hydrology and Earth System Sciences*, 24(2):771–791, 2020. ISSN 16077938. doi: 10.5194/hess-24-771-2020.

Z. Li, M. Chen, S. Gao, X. Luo, J. J. Gourley, P. Kirstetter, T. Yang, R. Kolar, A. McGovern, Y. Wen, B. Rao, T. Yami, and Y. Hong. CREST-iMAP v1.0: A fully coupled hydrologic-hydraulic modeling framework dedicated to flood inundation mapping and prediction. *Environmental Modelling and Software*, 141 (April):105051, 2021. ISSN 13648152. doi: 10.1016/j.envsoft.2021.105051. URL https://doi.org/10.1016/j.envsoft.2021.105051.

P.-l. Ligier. Implementation of a rainfall-runoff model in TELEMAC-2D. In *Proceedings of the XXIIIrd TELEMAC-MASCARET User Conference 2016, 11 to 13 October 2016*, Paris, France, 2016.

S. K. Mishra and V. P. Singh. A relook at NEH-4 curve number data and antecedent moisture condition criteria. *Hydrological Processes*, 20(13):2755–2768, 2006. ISSN 08856087. doi: 10.1002/hyp.6066.

T. M. Modrick and K. P. Georgakakos. The character and causes of flash flood occurrence changes in mountainous small basins of Southern California under projected climatic change. *Journal of Hydrology: Regional Studies*, 3:312–336, 3 2015. ISSN 22145818. doi: 10.1016/j.ejrh.2015.02.003. URL https://linkinghub.elsevier.com/retrieve/pii/S2214581815000075.

J. Nash and J. Sutcliffe. River flow forecasting through conceptual models part I — A discussion of principles. *Journal of Hydrology*, 10(3):282–290, 4 1970. ISSN 00221694. doi: 10.1016/0022-1694(70)90255-6. URL https://linkinghub.elsevier.com/retrieve/pii/0022169470902556.

P. Novak, V. Guinot, A. Jeffrey, and D. Reeve. *Hydraulic Modelling – an Introduction*. CRC Press, 10 2018. ISBN 9781315272498. doi: 10.1201/9781315272498. URL https://www.taylorfrancis.com/books/9781351988933.

F. L. Ogden and B. Saghafian. Green and Ampt Infiltration with Redistribution. 123(October):386–393, 1997.

P. Pall, L. M. Tallaksen, and F. Stordal. A climatology of rain-on-snow events for Norway. *Journal of Climate*, 32(20):6995–7016, 2019. ISSN 08948755. doi: 10.1175/JCLI-D-18-0529.1.

F. Pappenberger, K. Beven, M. Horritt, and S. Blazkova. Uncertainty in the calibration of effective roughness parameters in HEC-RAS using inundation and downstream level observations. *Journal of Hydrology*, 302(1-4):46–69, 2 2005. ISSN 00221694. doi: 10.1016/j.jhydrol.2004.06.036. URL https://linkinghub.elsevier.com/retrieve/pii/S0022169404003294.

M. Pilotti, L. Milanesi, V. Bacchi, M. Tomirotti, and A. Maranzoni. Dam-Break Wave Propagation in Alpine Valley with HEC-RAS 2D: Experimental Cancano Test Case. *Journal of Hydraulic Engineering*, 146(6):1–11, 2020. ISSN 0733-9429. doi: 10.1061/(asce)hy.1943-7900.0001779.

V. A. Rangari, N. V. Umamahesh, and C. M. Bhatt. Assessment of inundation risk in urban floods using HEC RAS 2D. *Modeling Earth Systems and Environment*,

5(4):1839–1851, 2019. ISSN 23636211. doi: 10.1007/s40808-019-00641-8. URL https://doi.org/10.1007/s40808-019-00641-8.

J. C. Refshaard and B. Storm. MIKE SHE. In V. P. Singh, editor, *Computer Models of Watershed Hydrology*, volume 1113, pages 809–846. Water Resources Publications, Colorado, 1995. URL https://cir.nii.ac.jp/crid/1572261549358869632.bib?lang=en.

L. A. Roald. Floods in Norway. In *Changes in Flood Risk in Europe*, number SPEC. ISS. 10, pages 304–318. CRC Press, 4 2019. ISBN 9788241020759. doi: 10.1201/b12348-16. URL https://www.taylorfrancis.com/books/9781136225468/chapters/10.1201/b12348-16.

F. Sandersen, S. Bakkehøi, E. Hestnes, and K. Lied. The influence of meteorological factors on the initiation of debris flows, rockfalls, rockslides and rockmass stability. 1997.

T. M. Scanlon, J. P. Raffensperger, G. M. Hornberger, and R. B. Clapp. Shallow subsurface storm flow in a forested headwater catchment: Observations and modeling using a modified TOPMODEL. *Water Resources Research*, 36(9):2575–2586, 9 2000. ISSN 0043-1397. doi: 10.1029/2000WR900125. URL https://agupubs.onlinelibrary.wiley.com/doi/10.1029/2000WR900125.

R. Schulze. The use of soil moisture budgeting to improve stormflow estimates by the SCS curve number method. Technical report, 1982.

Seneviratne, S.I., X. Zhang, M. Adnan, W. Badi, C. Dereczynski, A. Di Luca, S. Ghosh, I. Iskandar, J. Kossin, S. Lewis, F. Otto, I. Pinto, M. Satoh, S.M. Vicente-Serrano, M. Wehner, and B. Zhou. IPCC - Climate Change 2021: The Physical Science Basis - Chapter 11: Weather and Climate Extreme Events in a Changing Climate. (Cambridge University Press, Cambridge, United Kingdom and New York, NY, USA):1610, 2021. doi: 10.1017/9781009157896.013.

T. Shand, G. Smith, R. Cox, and M. Blacka. Development of Appropriate Criteria for the Safety and Stability of Persons and Vehicles in Floods. In *Proceedings of the 34th World Congress of the International Association for Hydro- Environment Research and Engineering: 33rd Hydrology and Water Resources Symposium and 10th Conference on Hydraulics in Water Engineering, Brisbane, Australia, 26 June 2011*, page 404, Brisbane, 2011.

Y. Shen, J. L. Goodall, and S. B. Chase. Method for Rapidly Assessing the Overtopping Risk of Bridges Due to Flooding over a Large Geo-

graphic Region. *JAWRA Journal of the American Water Resources Association*, 53(6):1437–1452, 12 2017. ISSN 1093-474X. doi: 10.1111/1752-1688.12583. URL https://onlinelibrary.wiley.com/doi/10.1111/1752-1688.12583.

R. E. Smith, C. Corradini, and F. Melone. Modeling infiltration for multistorm runoff events. *Water Resources Research*, 29(1):133–144, 1 1993. ISSN 00431397. doi: 10.1029/92WR02093. URL http://doi.wiley.com/10.1029/92WR02093.

Sunnmørsposten. Prislapp for flommen i Sogn og Fjordane: 120 millioner kroner . (Price tag for the flood in Sogn og Fjordane: NOK 120 million), 2017.

C. G. Surfleet and D. Tullos. Variability in effect of climate change on rain-on-snow peak flow events in a temperate climate. *Journal of Hydrology*, 479:24–34, 2013. ISSN 00221694. doi: 10.1016/j.jhydrol.2012.11.021. URL http://dx.doi.org/10.1016/j.jhydrol.2012.11.021.

D. Swanston. Slope Stability Problems Associated with Timber Harvesting in Mountainous Regions of the Western United States. *USDA Forest Service General Technical Report PNW-21*, 21, 1974.

J. Teng, A. J. Jakeman, J. Vaze, B. F. Croke, D. Dutta, and S. Kim. Flood inundation modelling: A review of methods, recent advances and uncertainty analysis. *Environmental Modelling and Software*, 90:201–216, 2017. ISSN 13648152. doi: 10.1016/j.envsoft.2017.01.006. URL http://dx.doi.org/10.1016/j.envsoft.2017.01.006.

USDA-SCS. Part 630 Hydrology National Engineering Handbook Chapter 10 Estimation of Direct Runoff from Storm Rainfall. *National Engineering Handbook*, 2004. URL https://directives.sc.egov.usda.gov/OpenNonWebContent.aspx?content=17752.wba.

K. Vormoor, D. Lawrence, M. Heistermann, and A. Bronstert. Climate change impacts on the seasonality and generation processes of floods – projections and uncertainties for catchments with mixed snowmelt/rainfall regimes. *Hydrology and Earth System Sciences*, 19(2):913–931, 2 2015. ISSN 1607-7938. doi: 10.5194/hess-19-913-2015. URL https://hess.copernicus.org/articles/19/913/2015/.

T. Vu, P. Nguyen, L. Chua, and A. Law. Two-Dimensional Hydrodynamic Modelling of Flood Inundation for a Part of the Mekong River with TELEMAC-2D. *British Journal of Environment and Climate Change*, 5(2):162–175, 2015. doi: 10.9734/bjecc/2015/12885.

I. Yoosefdoost, O. Bozorg-Haddad, V. P. Singh, and K. W. Chau. Hydrological Models. pages 283–329. 2022. doi: 10.1007/978-981-19-1898-8{_}8. URL https://link.springer.com/10.1007/978-981-19-1898-8_8.

S. J. Zeiger and J. A. Hubbart. Measuring and modeling event-based environmental flows: An assessment of HEC-RAS 2D rain-on-grid simulations. *Journal of Environmental Management*, 285(February):112125, 2021. ISSN 10958630. doi: 10.1016/j.jenvman.2021.112125. URL https://doi.org/10.1016/j.jenvman.2021.112125.

Y. Zhang, Y. Wang, Y. Chen, Y. Xu, G. Zhang, Q. Lin, and R. Luo. Projection of changes in flash flood occurrence under climate change at tourist attractions. *Journal of Hydrology*, 595:126039, 4 2021. ISSN 00221694. doi: 10.1016/j.jhydrol.2021.126039. URL https://linkinghub.elsevier.com/retrieve/pii/S002216942100086X.

ISBN 978-82-326-8114-3 (printed ver.)
ISBN 978-82-326-8113-6 (electronic ver.)
ISSN 1503-8181 (printed ver.)
ISSN 2703-8084 (online ver.)

NTNU

Norwegian University of
Science and Technology